Electronic Supplementary Information

Synthesis and properties of metal trifluoride complexes with novel amide-functionalised tacn macrocycles and radiofluorination of $[GaF_3(L^1)$ by $^{18}F/^{19}F$ isotopic exchange

Figure S1: Spectroscopic data for Ligand $\mathbf{L^1}$

S1a: ^{1}H NMR spectrum (CD_3OD)

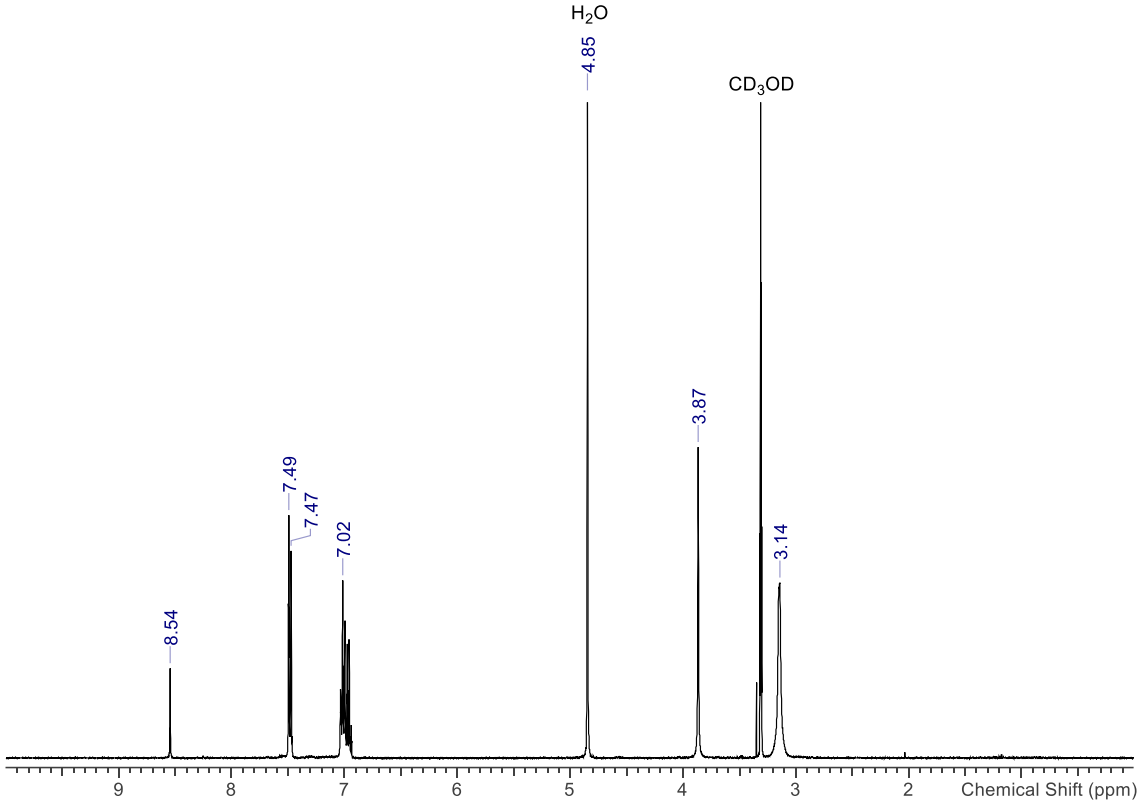

S1b: $^{13}C\{^{1}H\}$ NMR spectrum (CD_3OD)

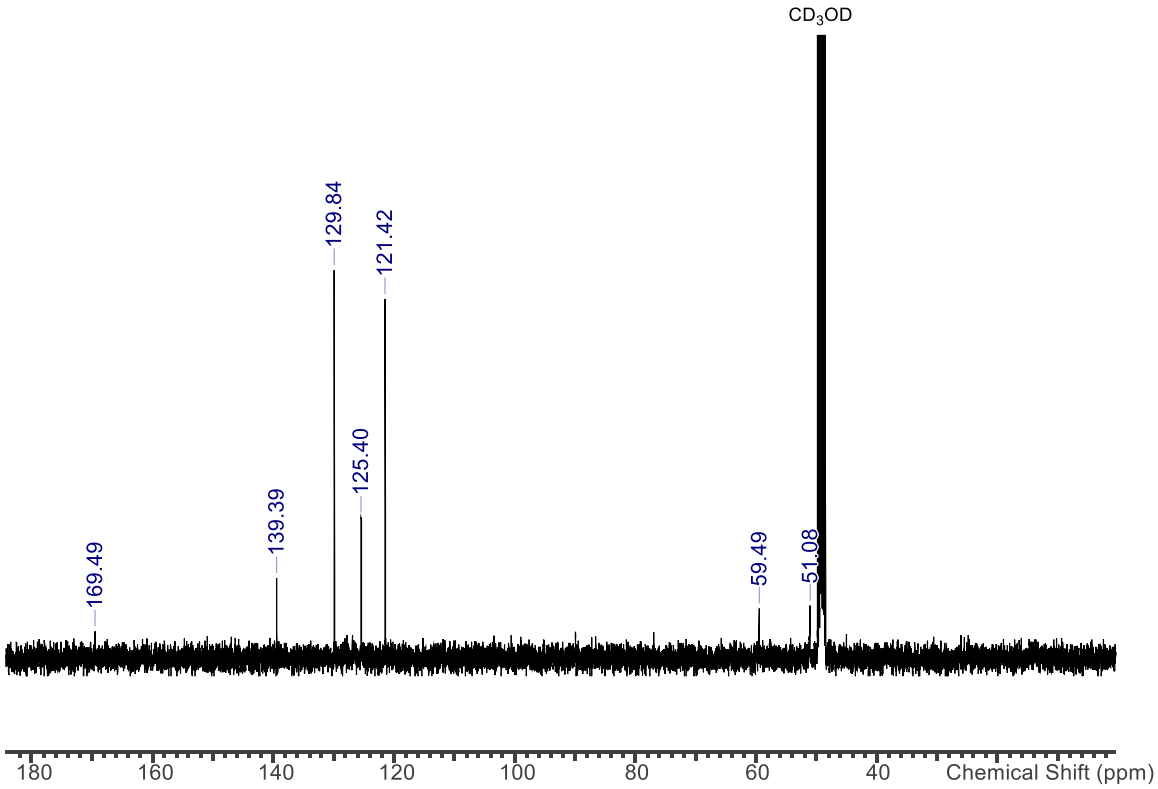

S1c: ^{13}C DEPT-135 NMR spectrum (CD_3OD)

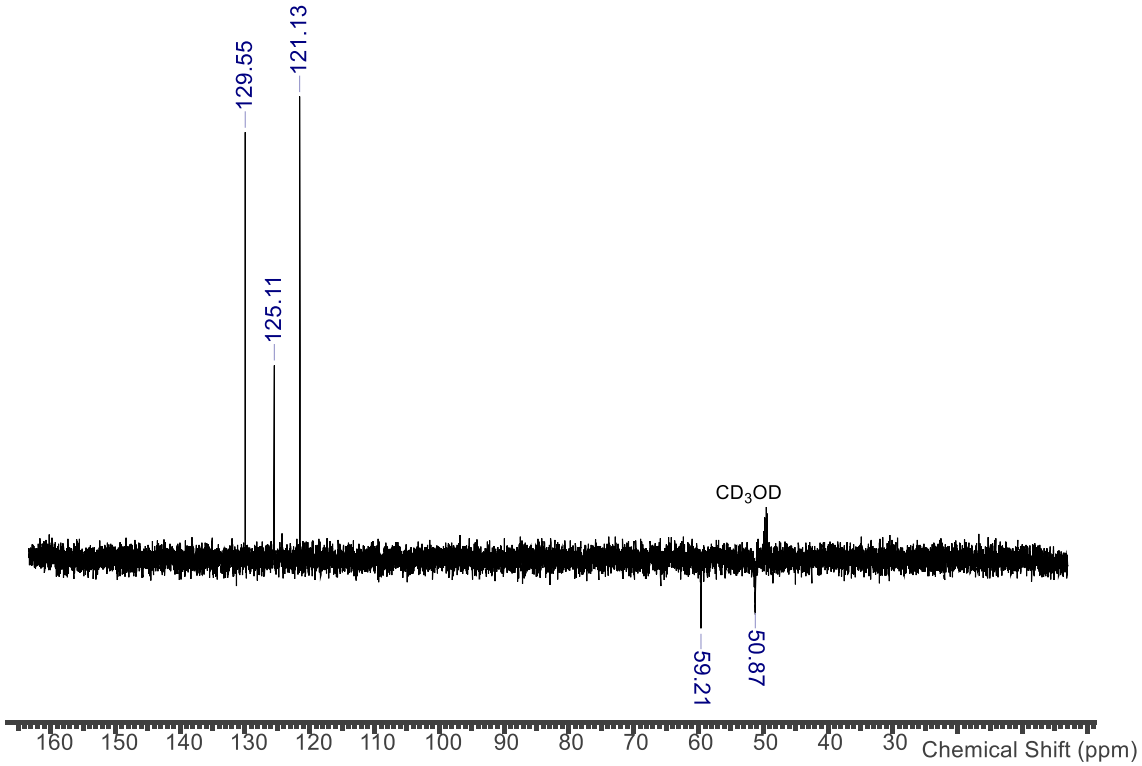

S1d: UV trace after purification *via* flash column chromatography

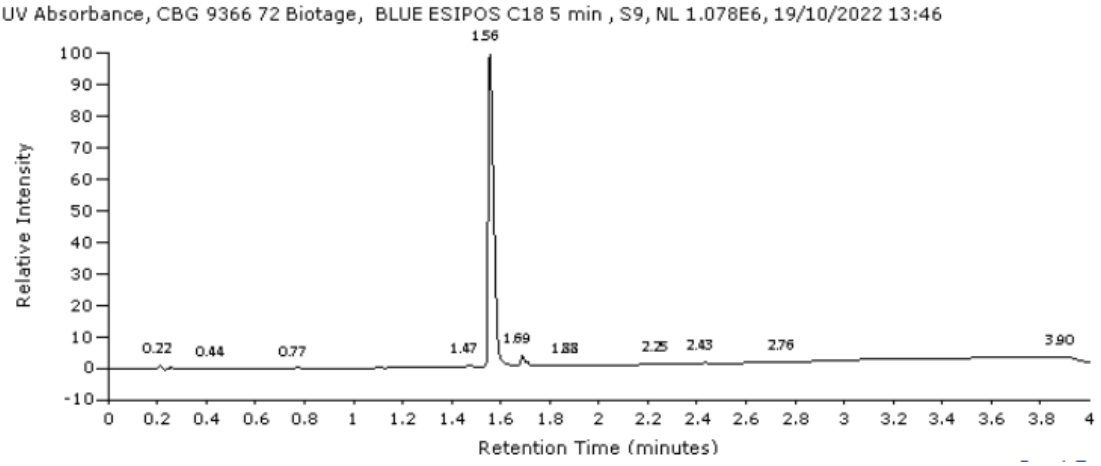

S1e: HR ESI$^+$ MS – experimental (MeOH) – top = experimental, bottom = calculated for [**L^1** + H]$^+$

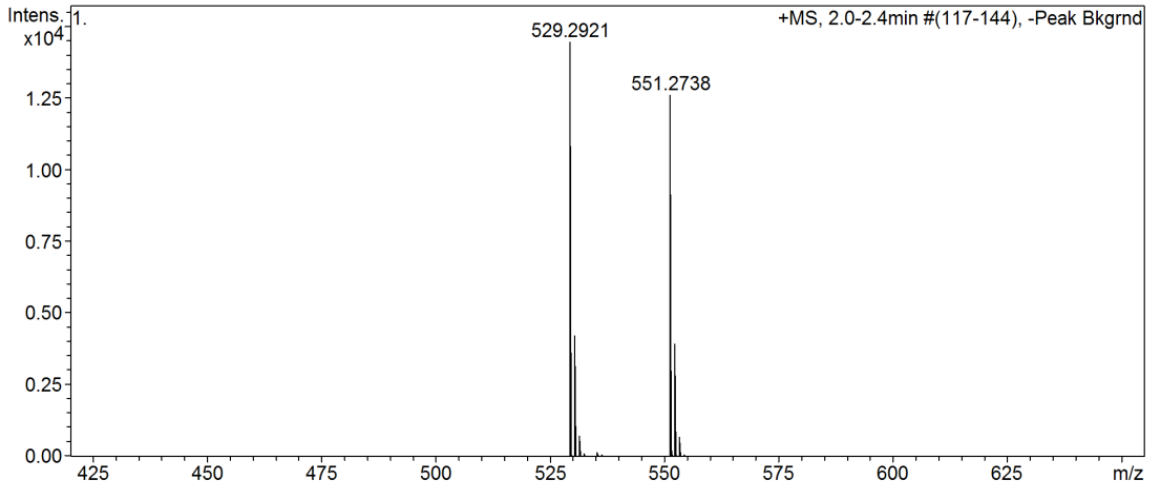

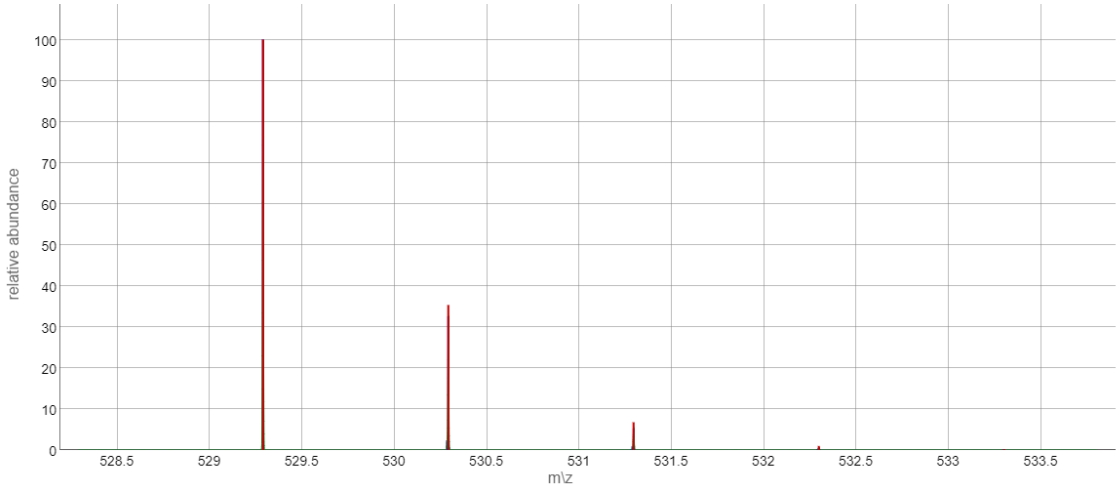

S1f: IR spectrum (Nujol)

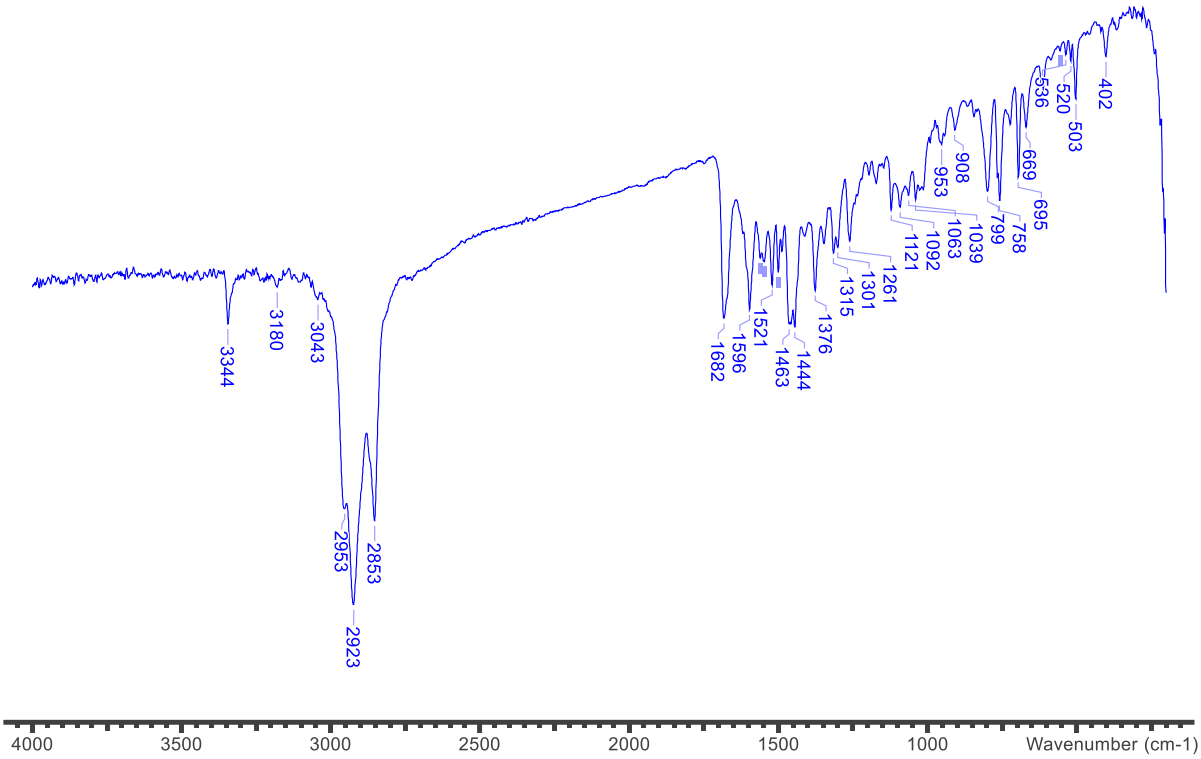

Figure S2 Spectroscopic data for **L^1**·HCl

S2a: ^{1}H NMR spectrum (CD_3OD)

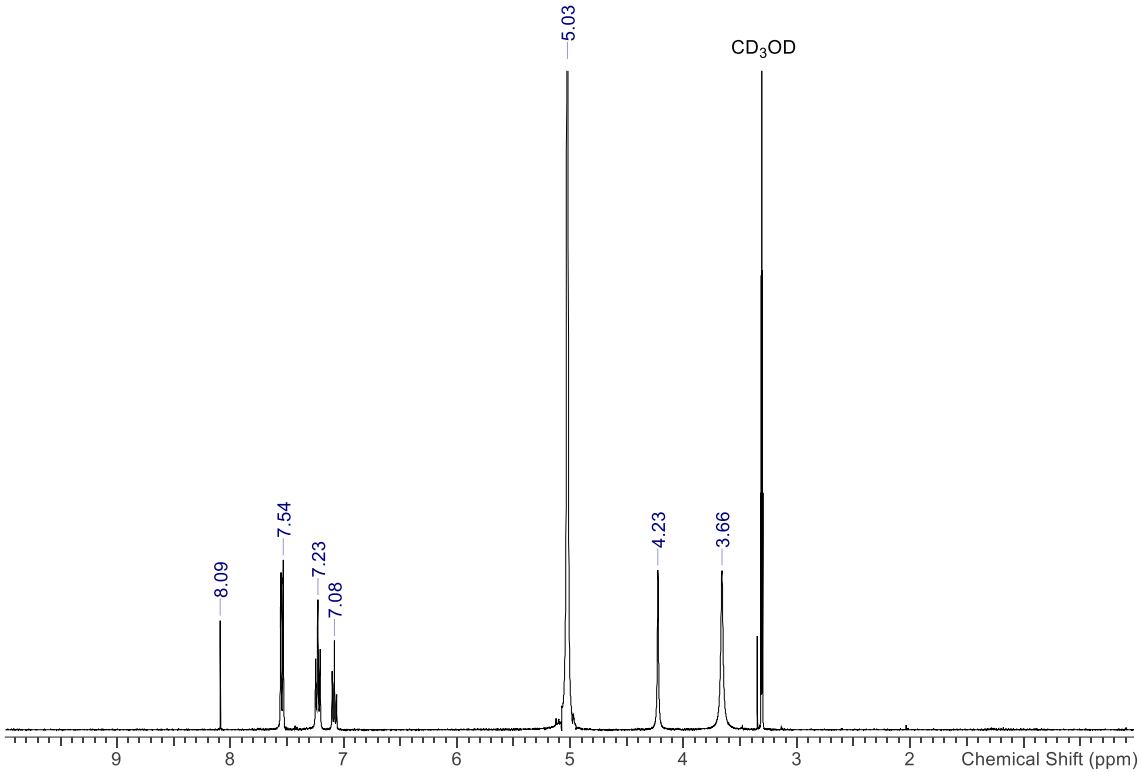

S2b: $^{13}C\{^1H\}$ NMR spectrum (CD_3OD)

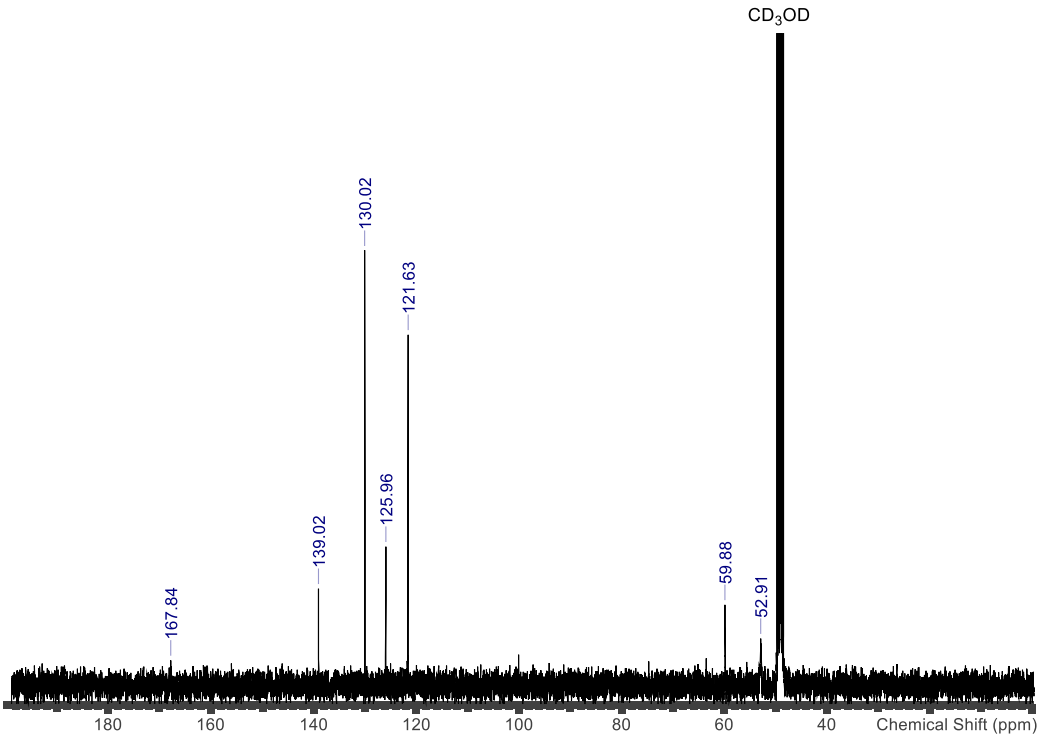

Figure S3 Spectroscopic data for Ligand **L²**

S3a: ^{1}H NMR spectrum (CD_3OD)

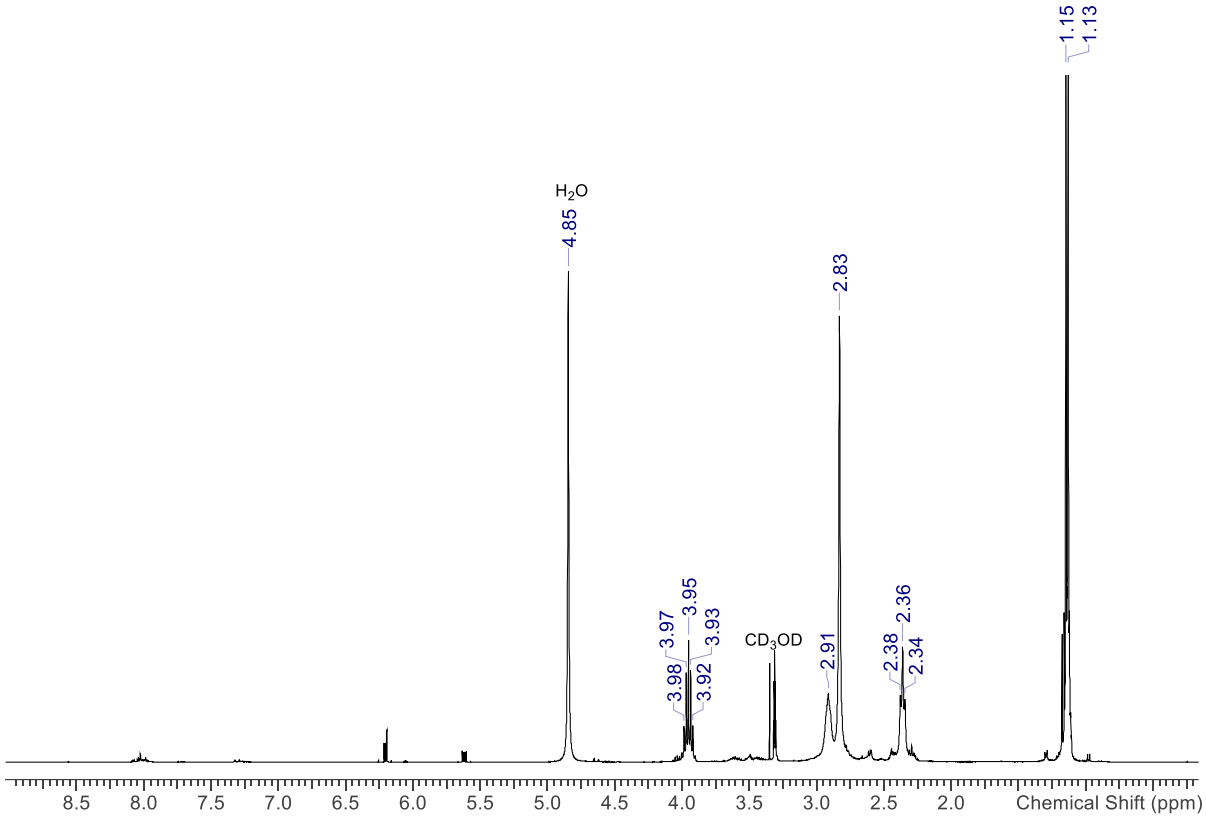

S3b: ^{1}H NMR spectrum ($CDCl_3$)

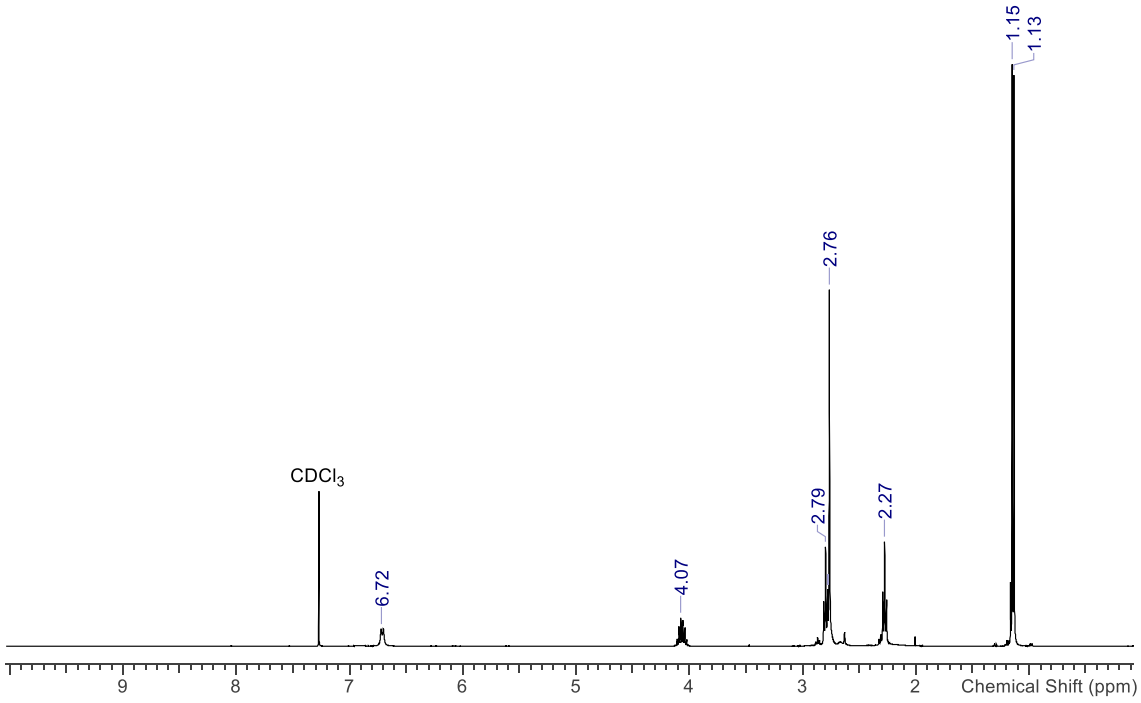

S3c: $^{13}C\{^{1}H\}$ NMR spectrum ($CDCl_3$)

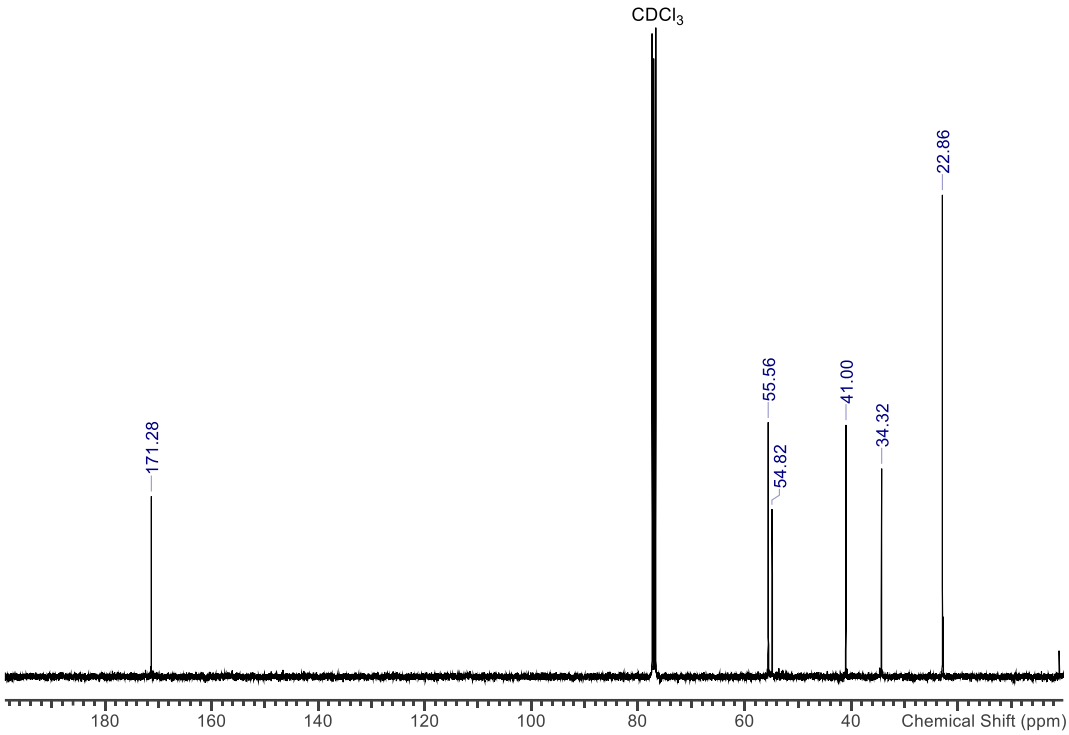

S3d: ^{13}C DEPT-135 NMR spectrum ($CDCl_3$)

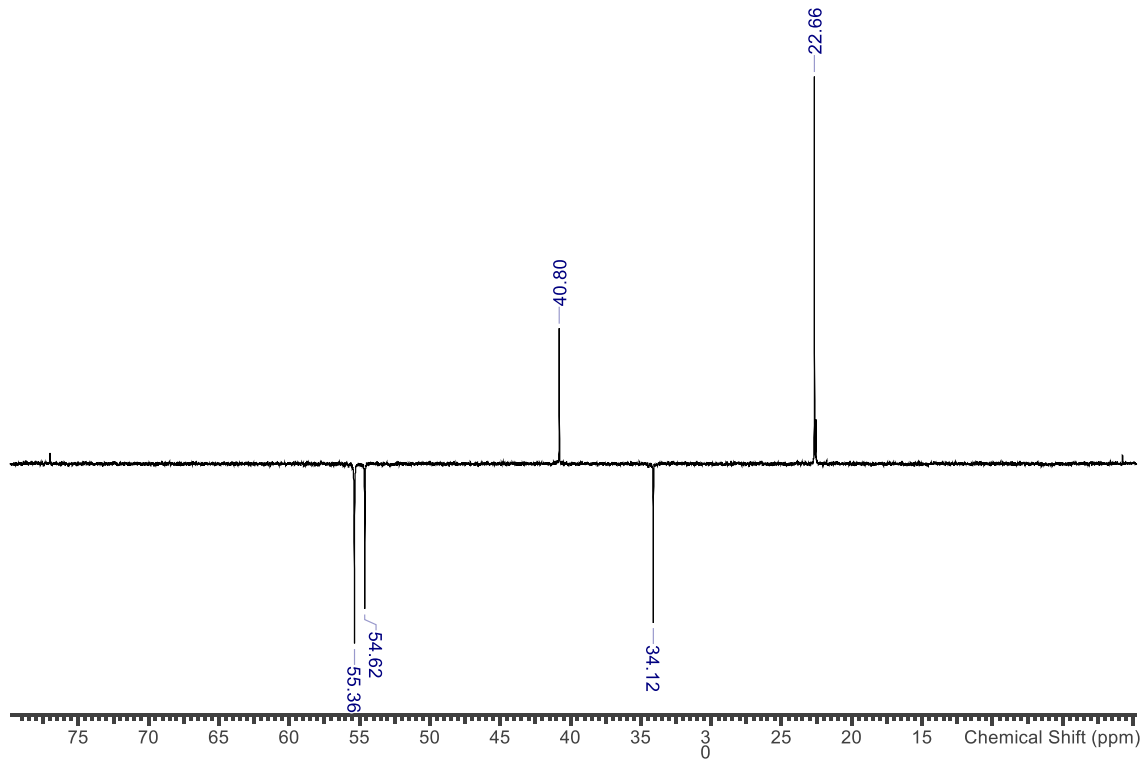

S3e: HR ESI^{+} MS (MeOH)

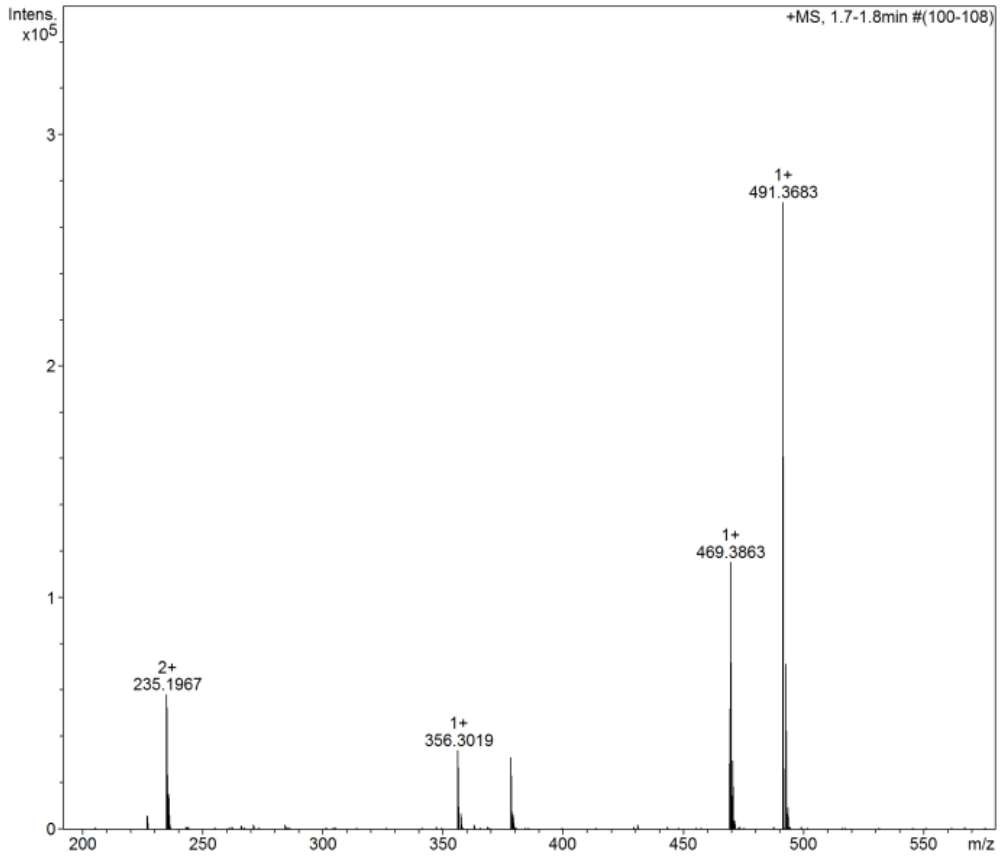

S3f: IR spectrum (neat thin film)

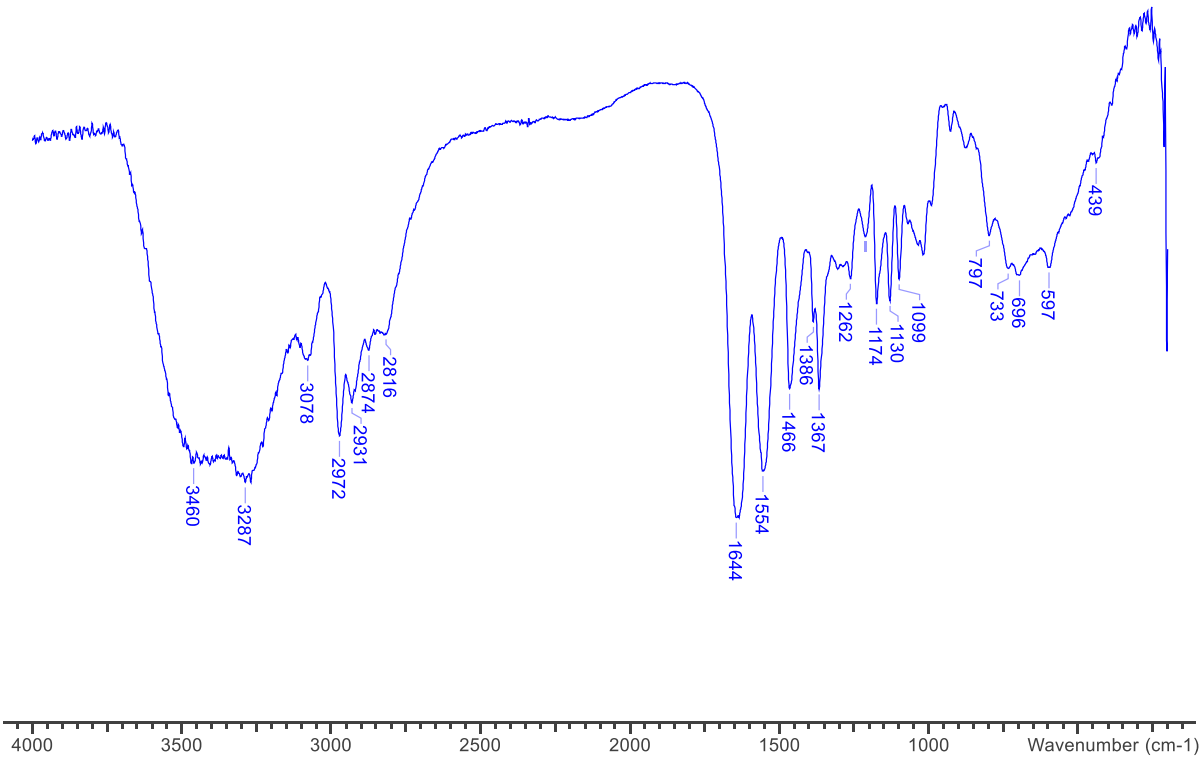

Figure S4 Spectroscopic data for **L^3**·HCl

S4a: ^{1}H NMR spectrum (CD_3OD)

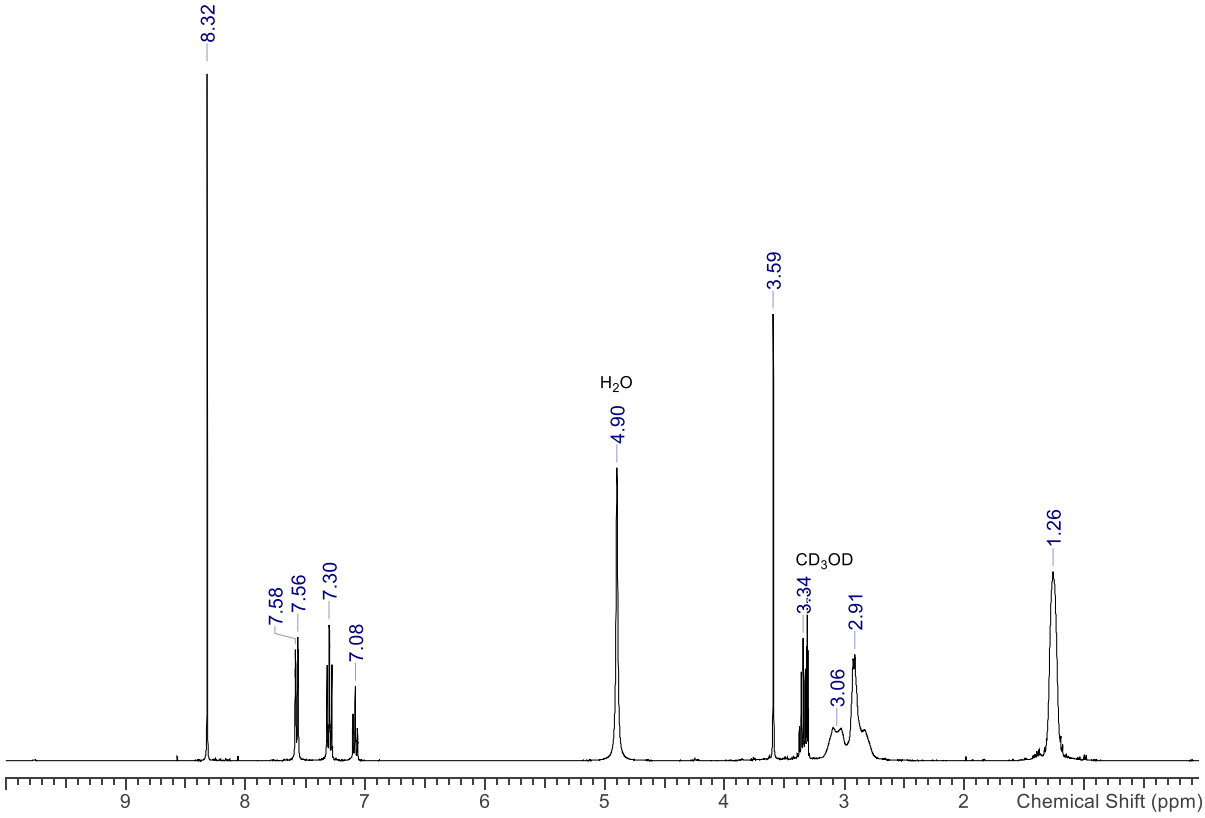

S4b: $^{13}C\{^1H\}$ NMR spectrum (CD_3OD)

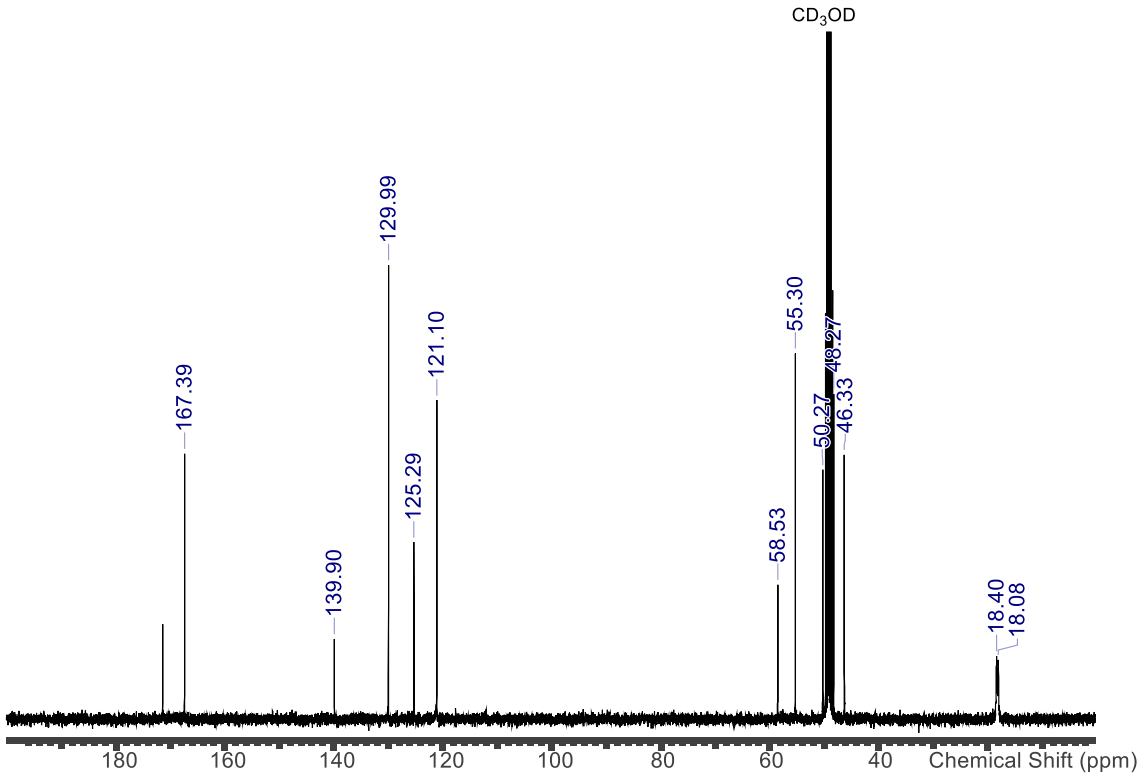

S4c: ^{13}C DEPT-135 NMR spectrum (CD_3OD)

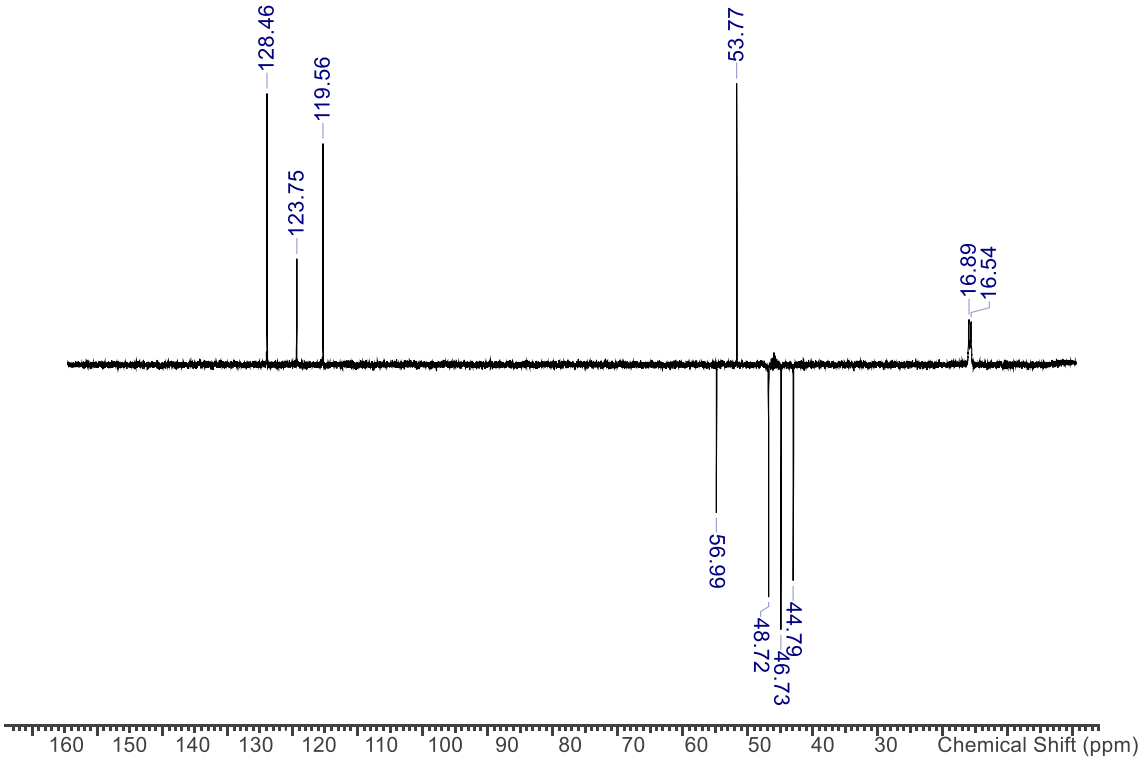

S4d: UV trace after purification *via* flash column chromatography

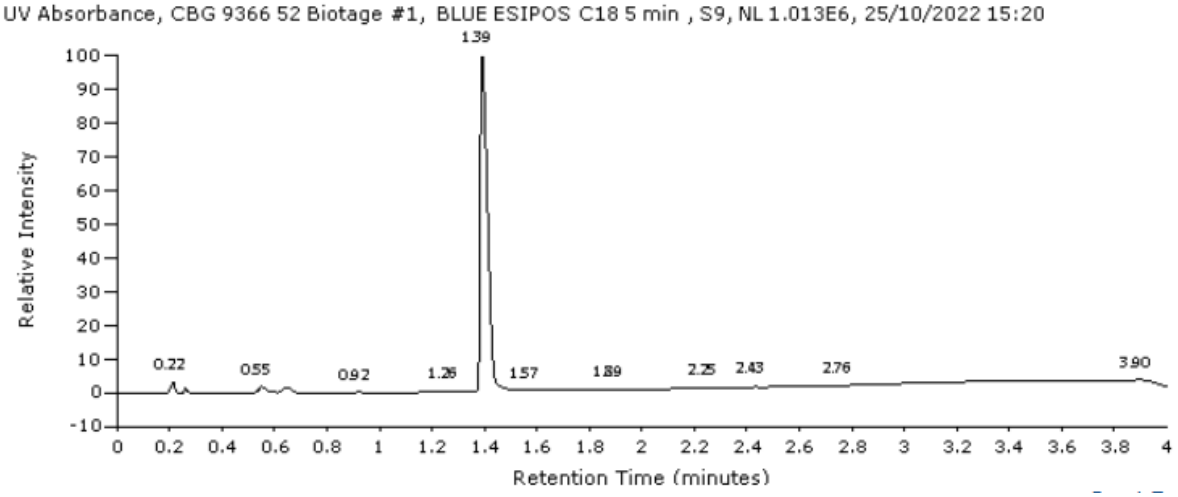

S4e: HR ESI^{+} MS (MeOH) – top = experimental spectrum, bottom = calculated for [**L**^{3} + H]$^{+}$

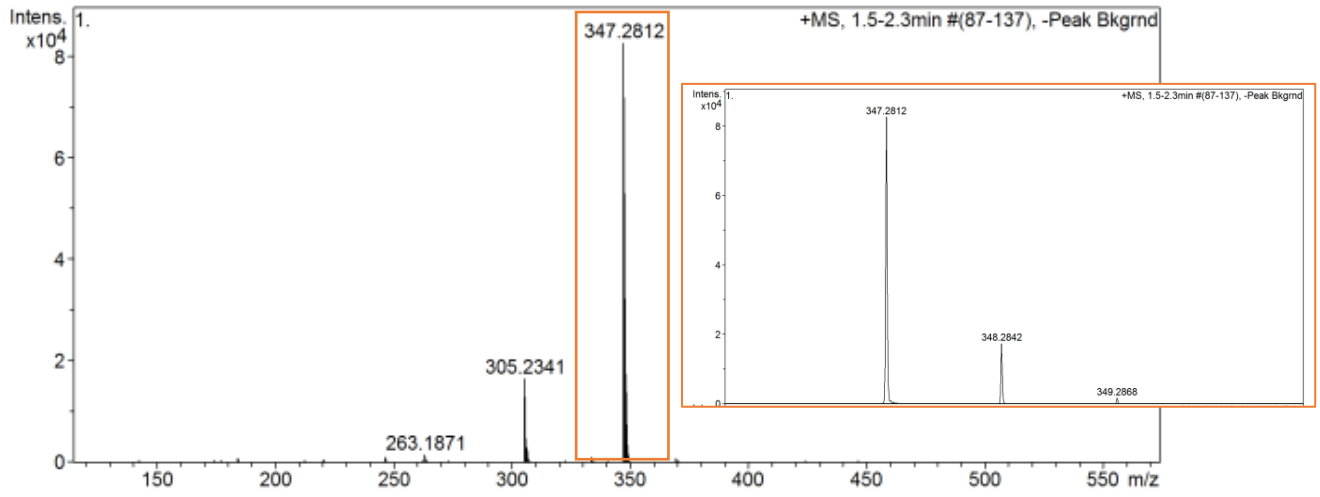

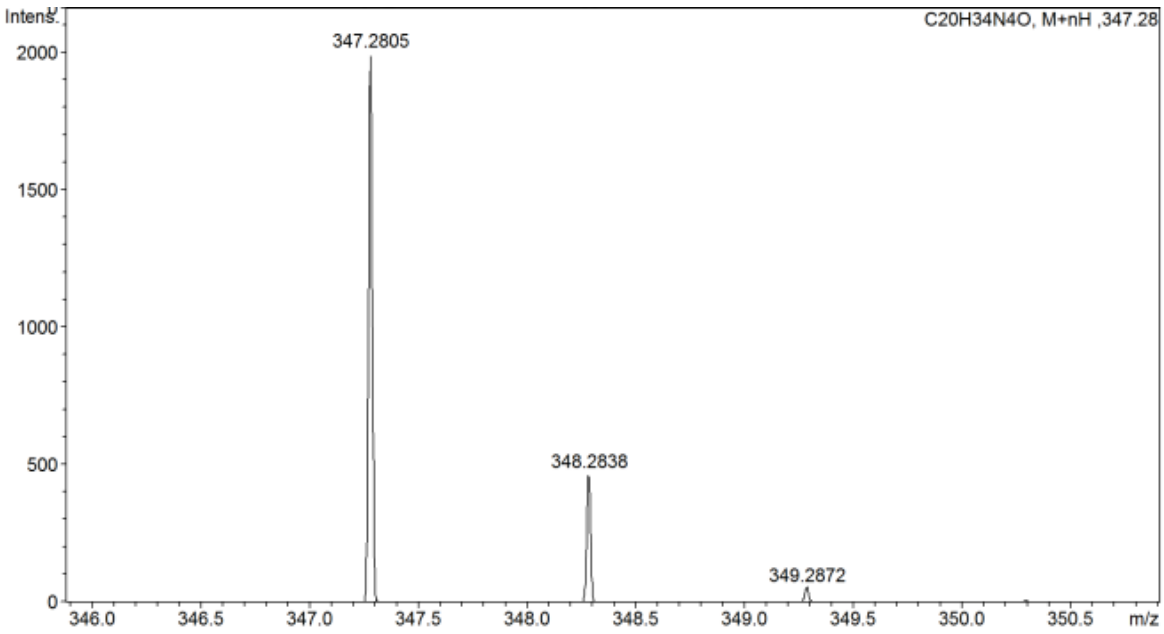

Figure S5 Spectroscopic data for **L^3**

S5a: ^{1}H NMR spectrum (CD_3OD)

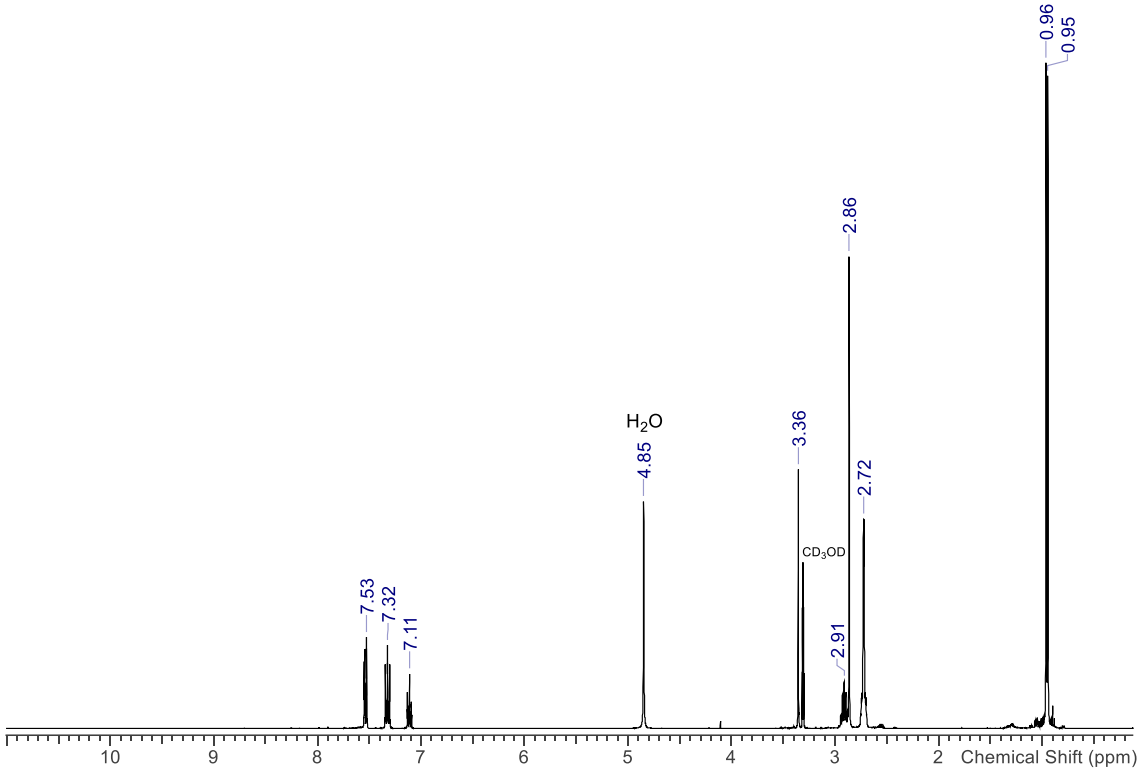

S5b: ^{1}H NMR spectrum ($CDCl_3$)

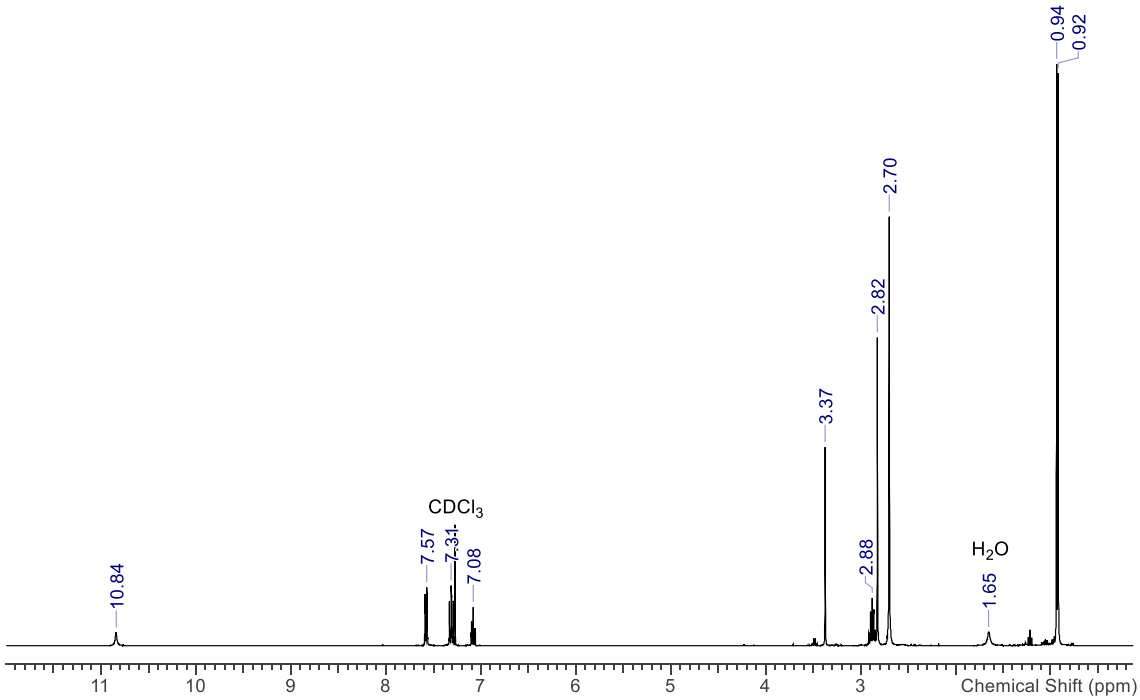

S5c: $^{13}C\{^{1}H\}$ NMR spectrum (CD_3OD)

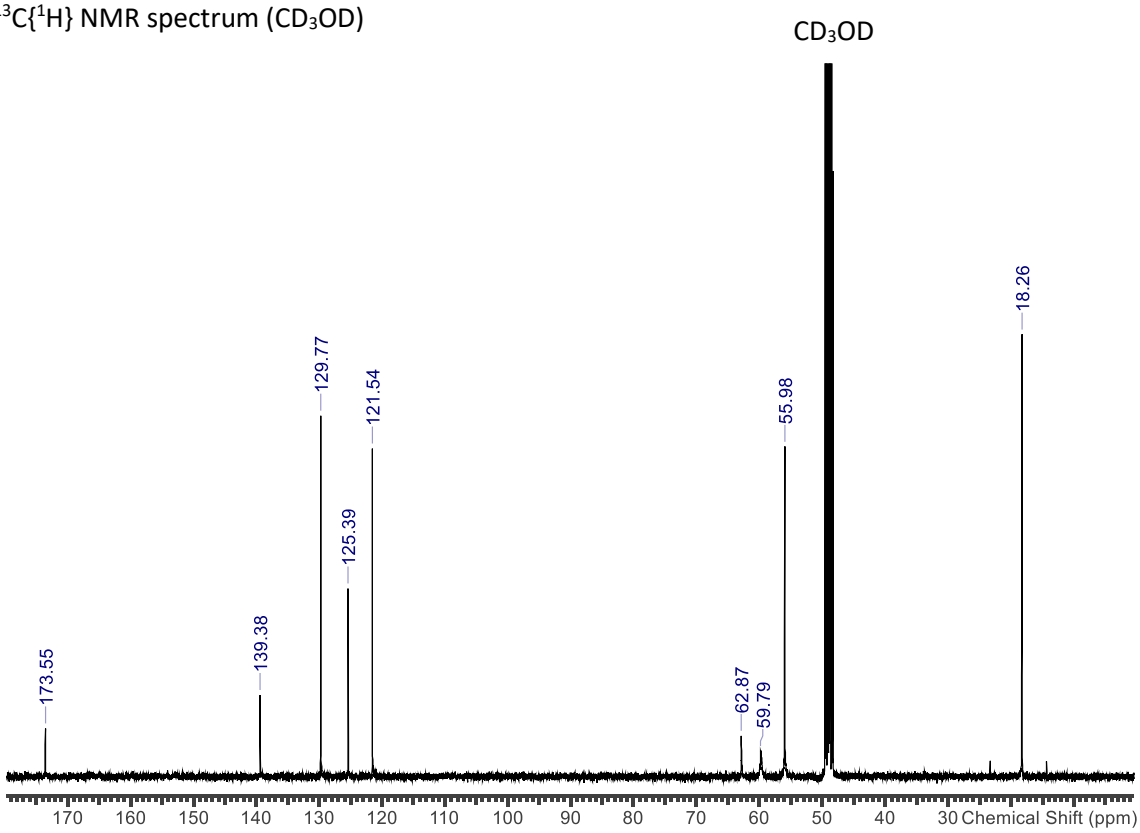

S5d: $^{13}C\{^{1}H\}$ NMR spectrum ($CDCl_3$)

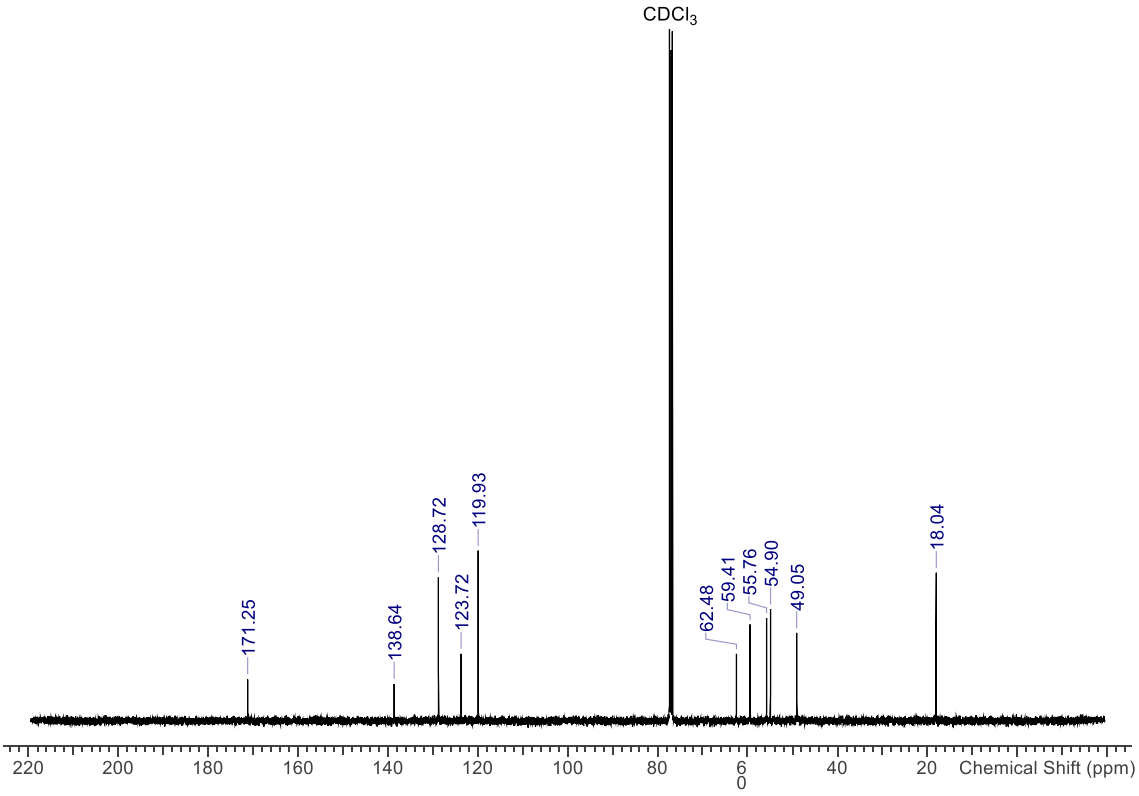

S5e: ^{13}C DEPT-135 NMR spectrum (CD_3OD)

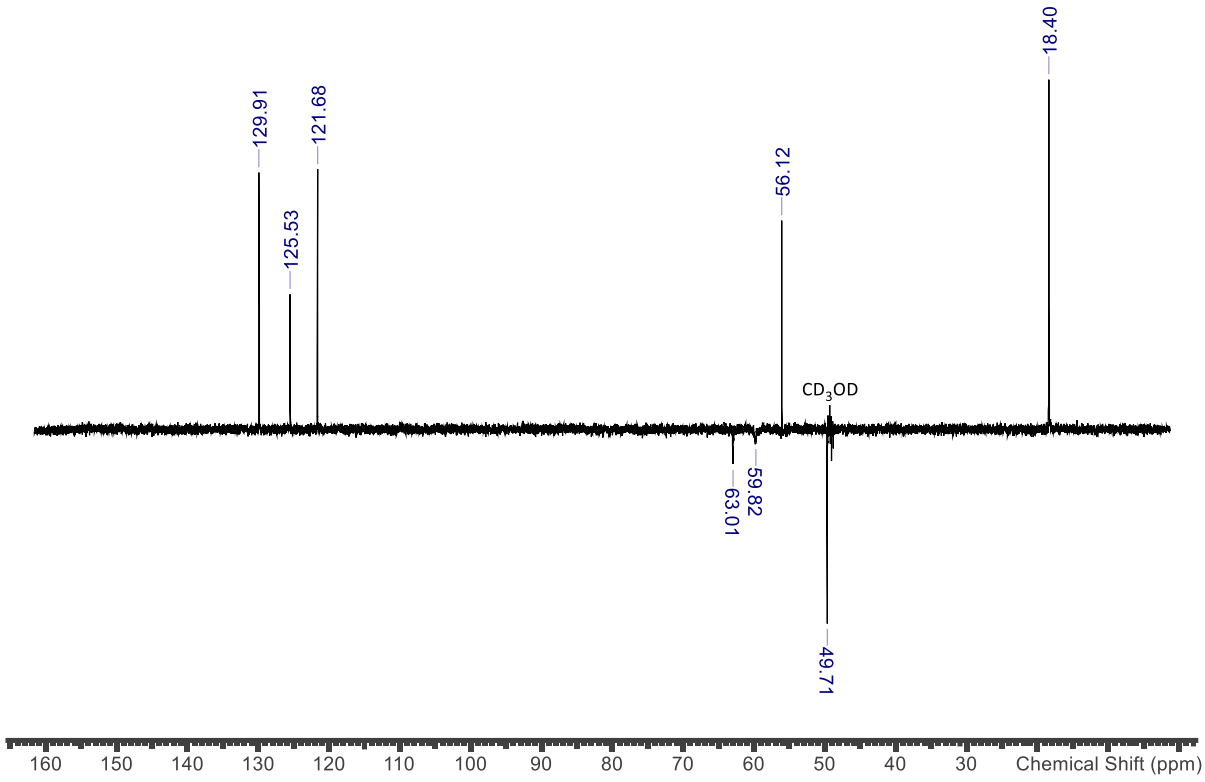

S5f: HR ESI MS (MeOH) showing $[\mathbf{L^3} + H]^+$

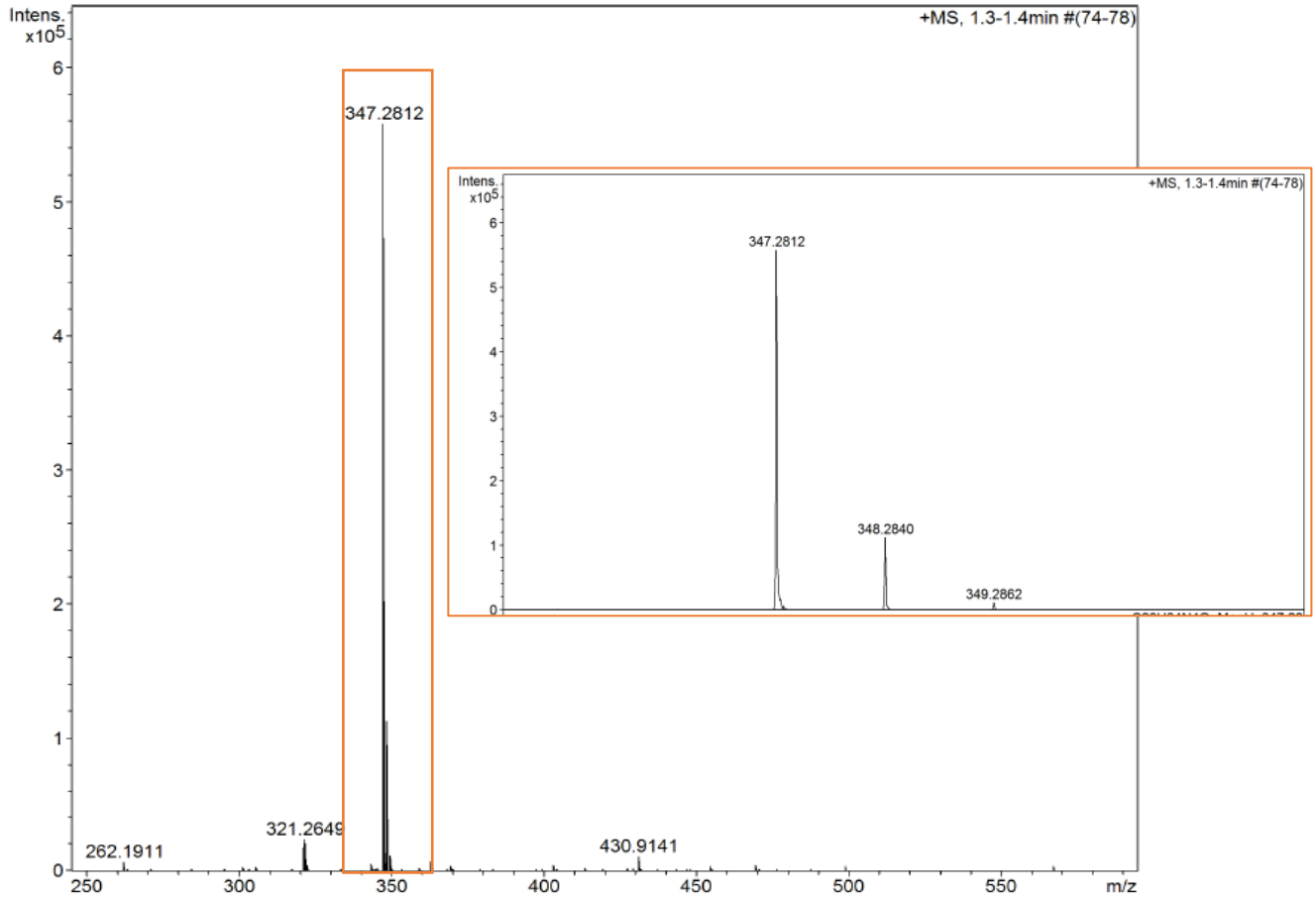

S5g: IR spectrum (neat thin film)

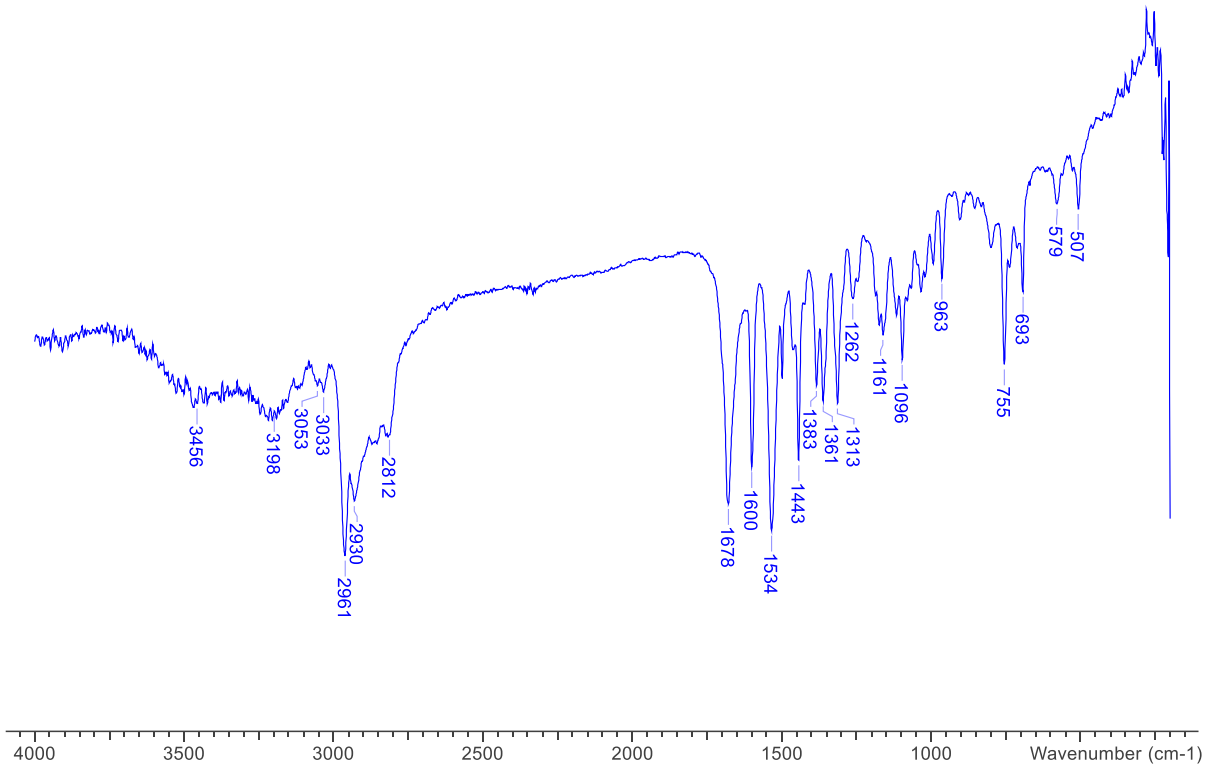

Figure S6 spectroscopic data for [AlF_3(**L**^{1})]

S6a: ^{1}H NMR spectrum (CD_3OD)

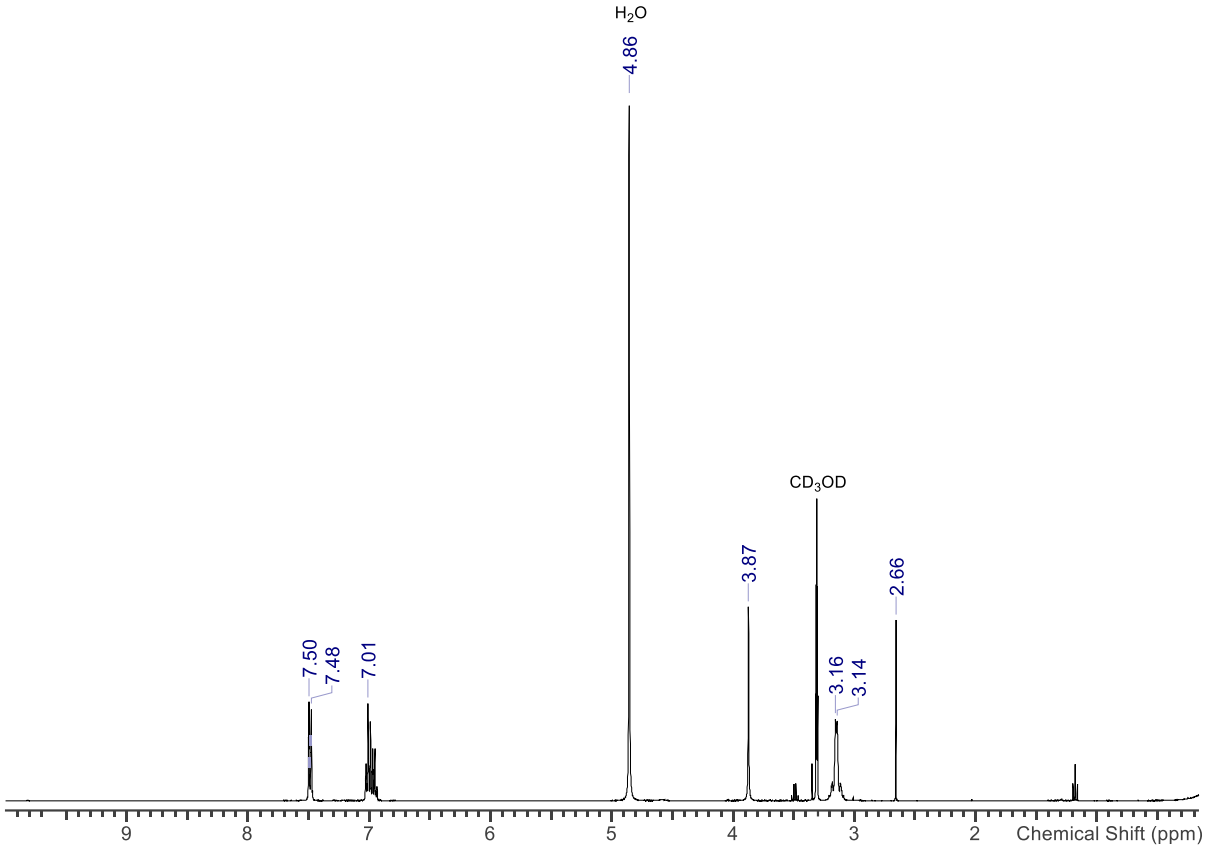

S6b: ^{18}F{^{1}H} NMR spectrum (CD_3OD) (the broad baseline is from the Teflon in the probe)

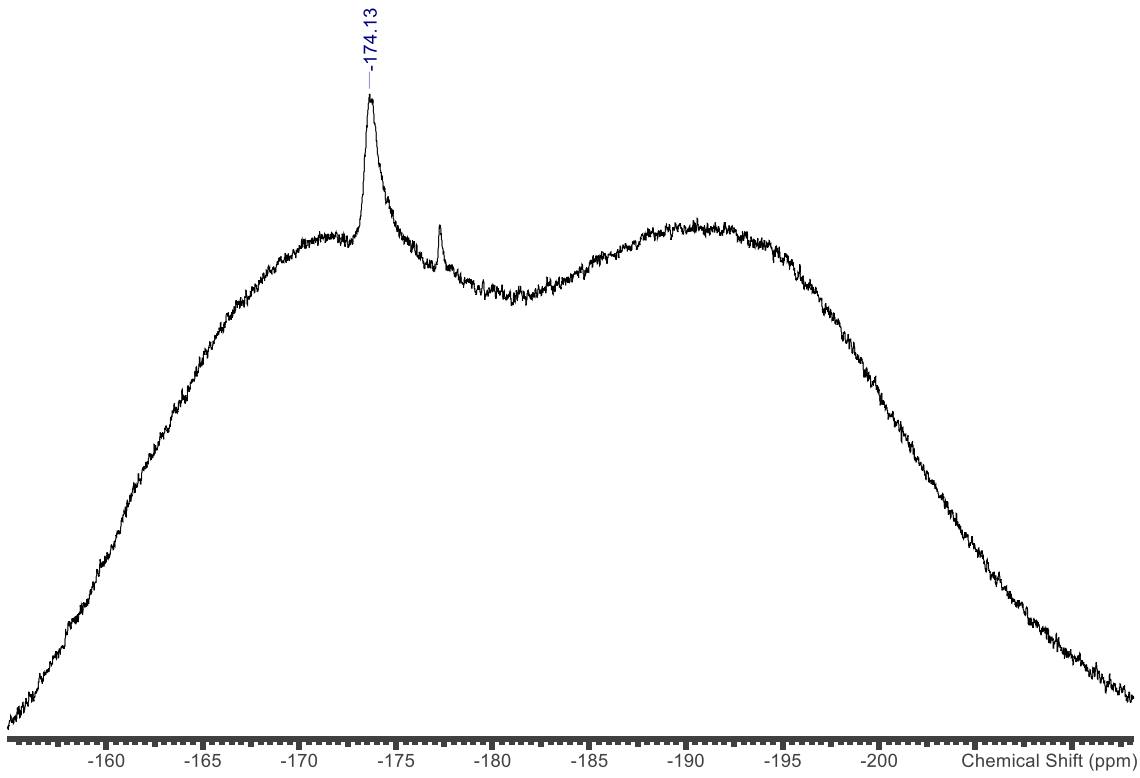

S6c: $^{13}C\{^{1}H\}$ NMR spectrum (CD_3OD)

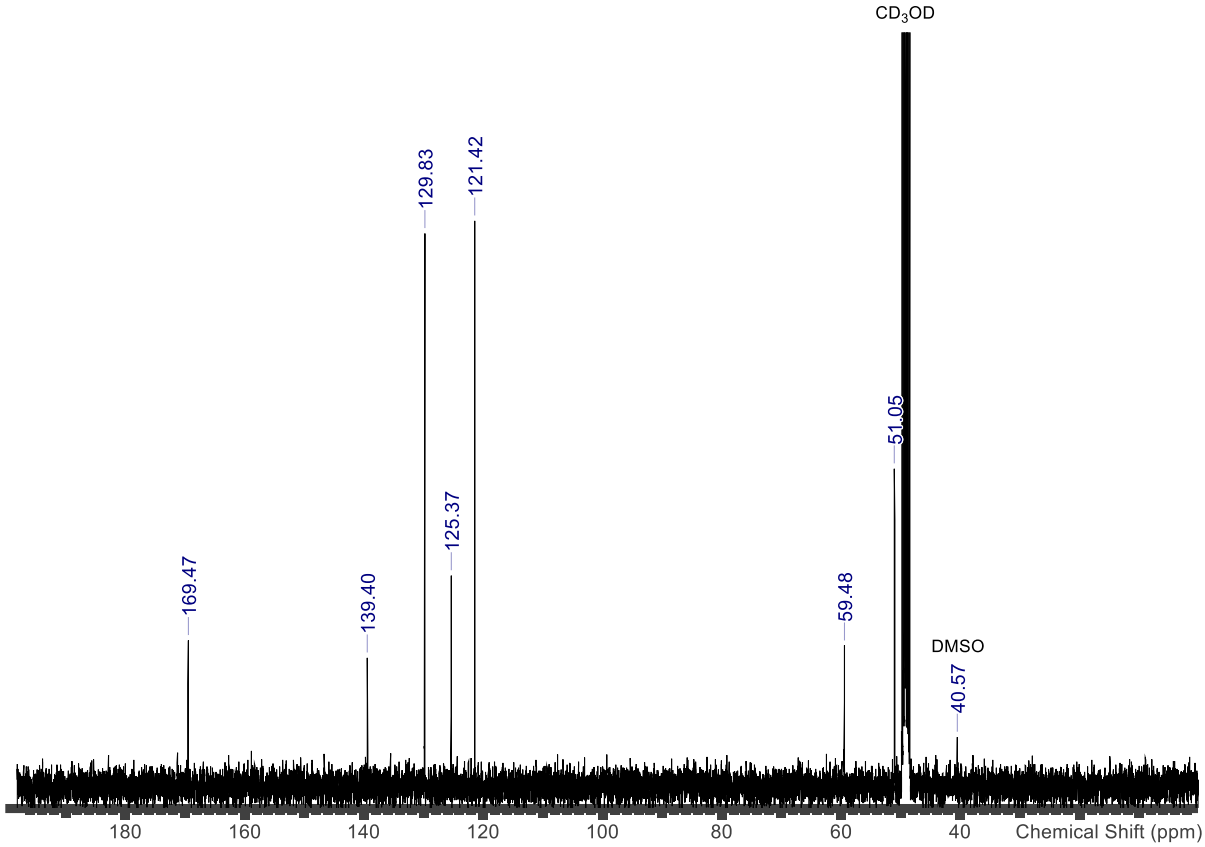

S6d: ESI MS (direct injection, MeOH) – top = experimental; bottom = calculated for $[AlF_3(\mathbf{L^1})][H]^+$

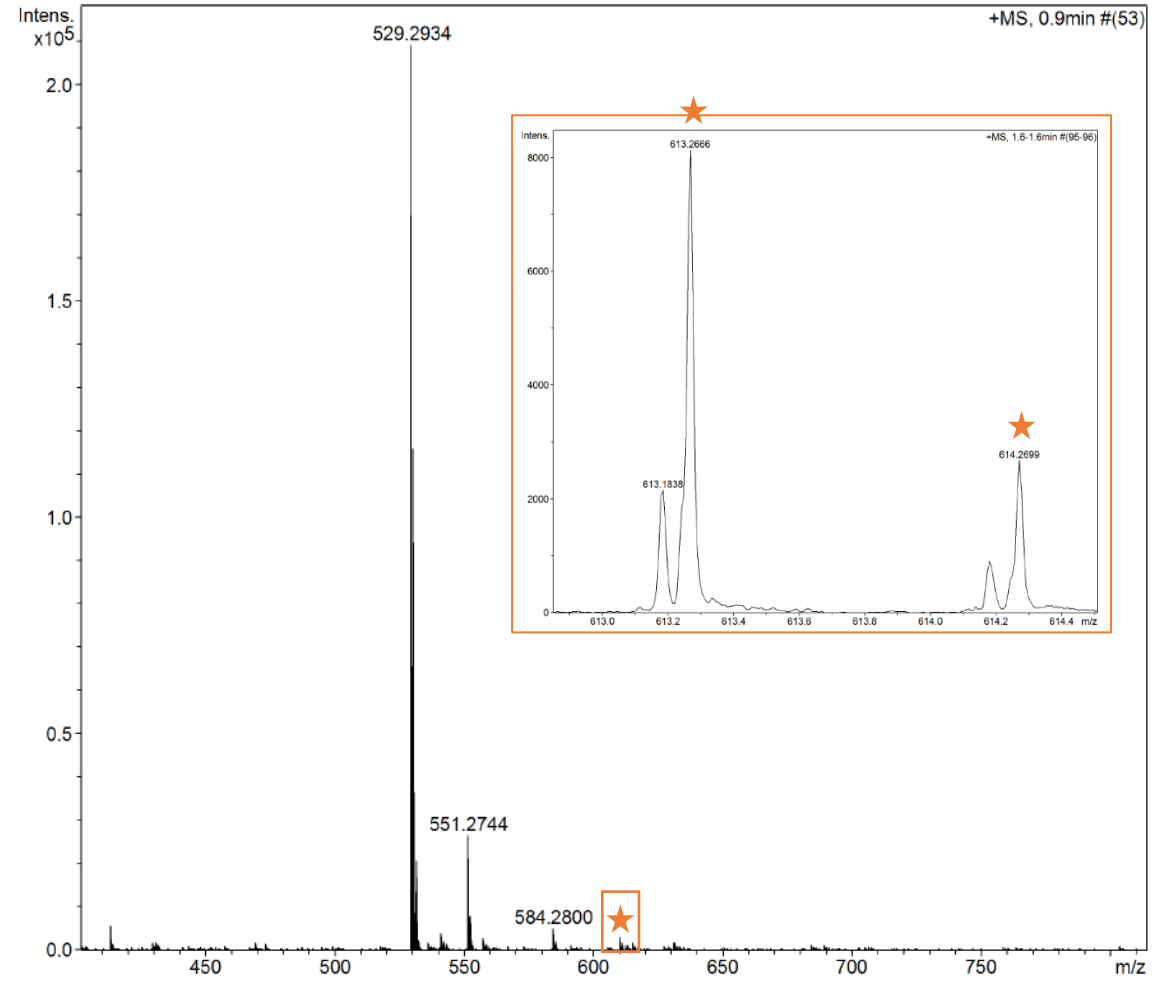

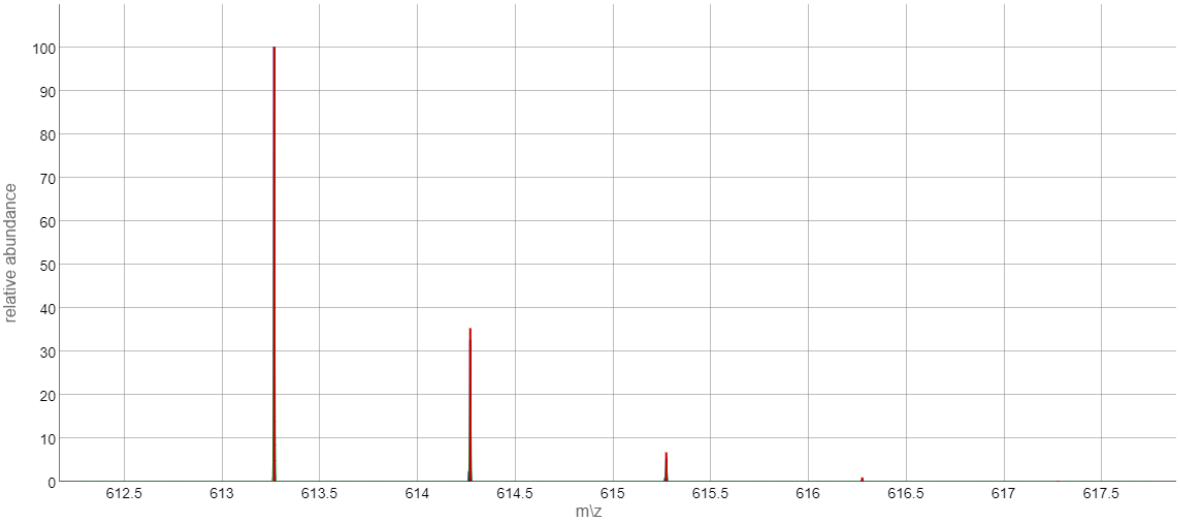

S6e: IR spectrum (Nujol)

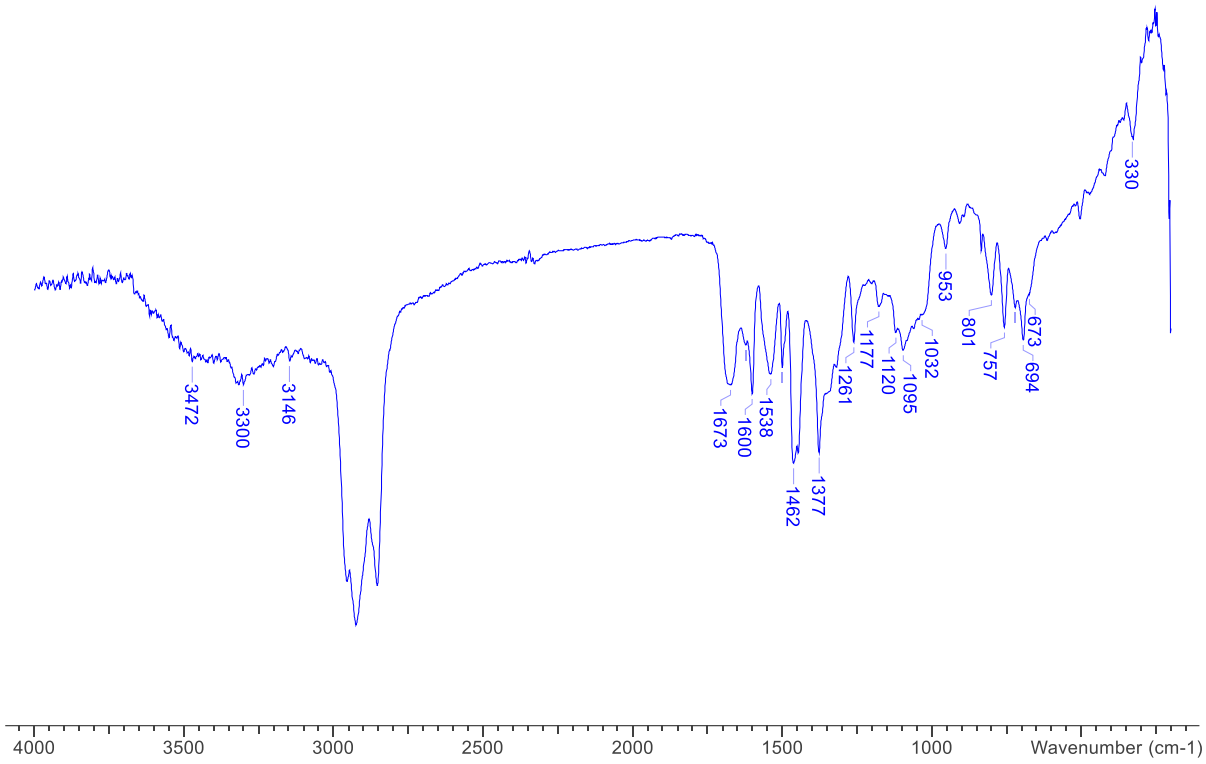

Figure S7 Spectroscopic data for [GaF_3(**L**^{1})]

S7a: ^{1}H NMR spectrum (CD_3OD)

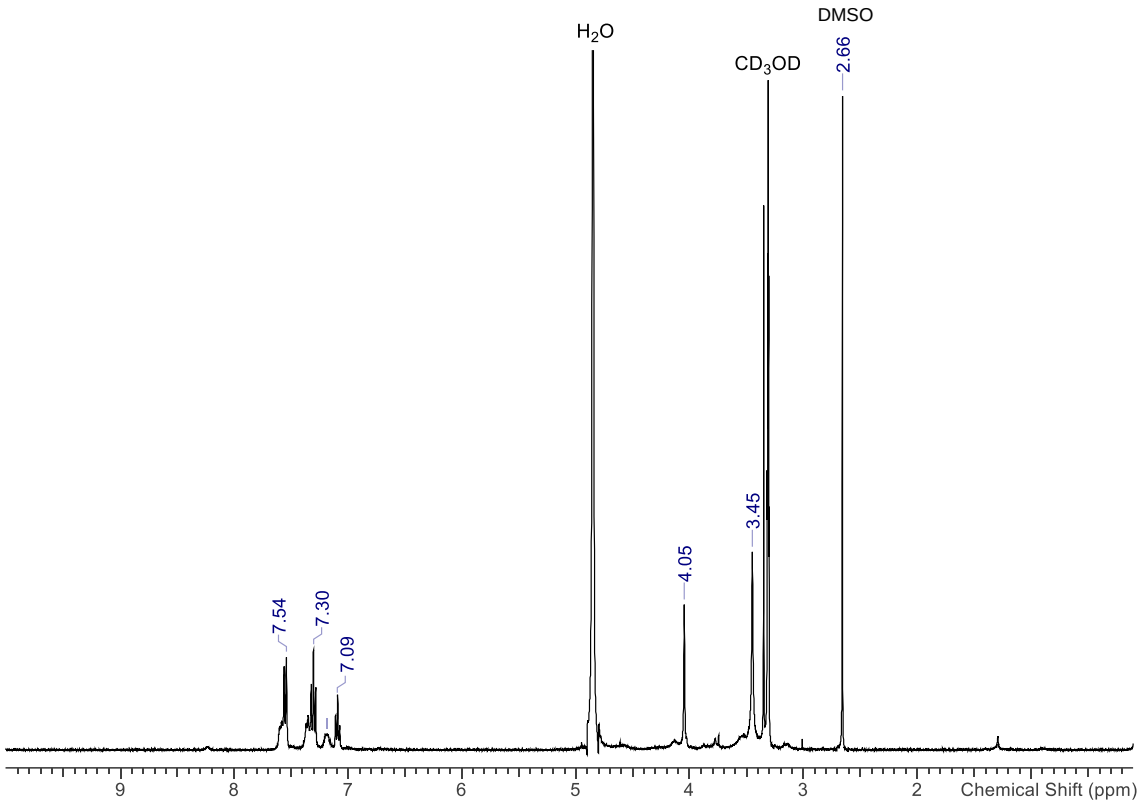

S7b: ^{13}C{^{1}H} NMR spectrum (CD_3OD)

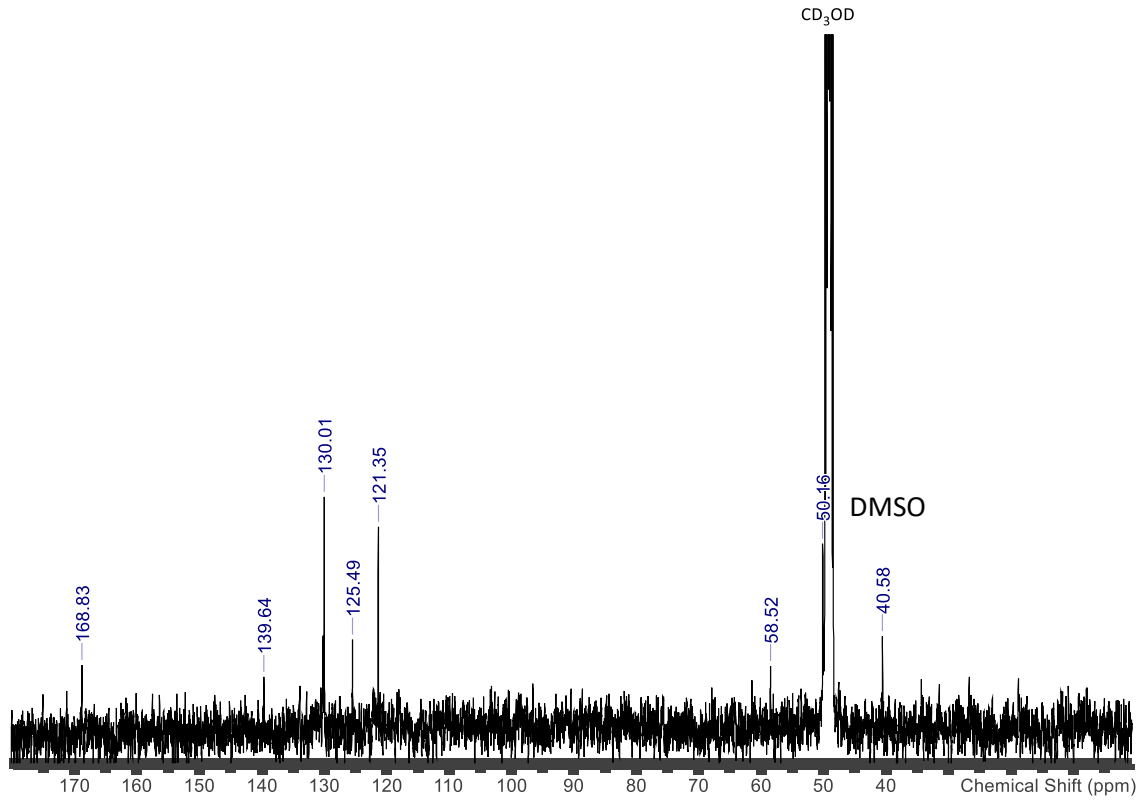

S7c: $^{19}F\{^{1}H\}$ NMR spectrum (CD_3OD) (the broad baseline is from the Teflon in the probe; * = minor $[GaF_4]^-$ impurity)

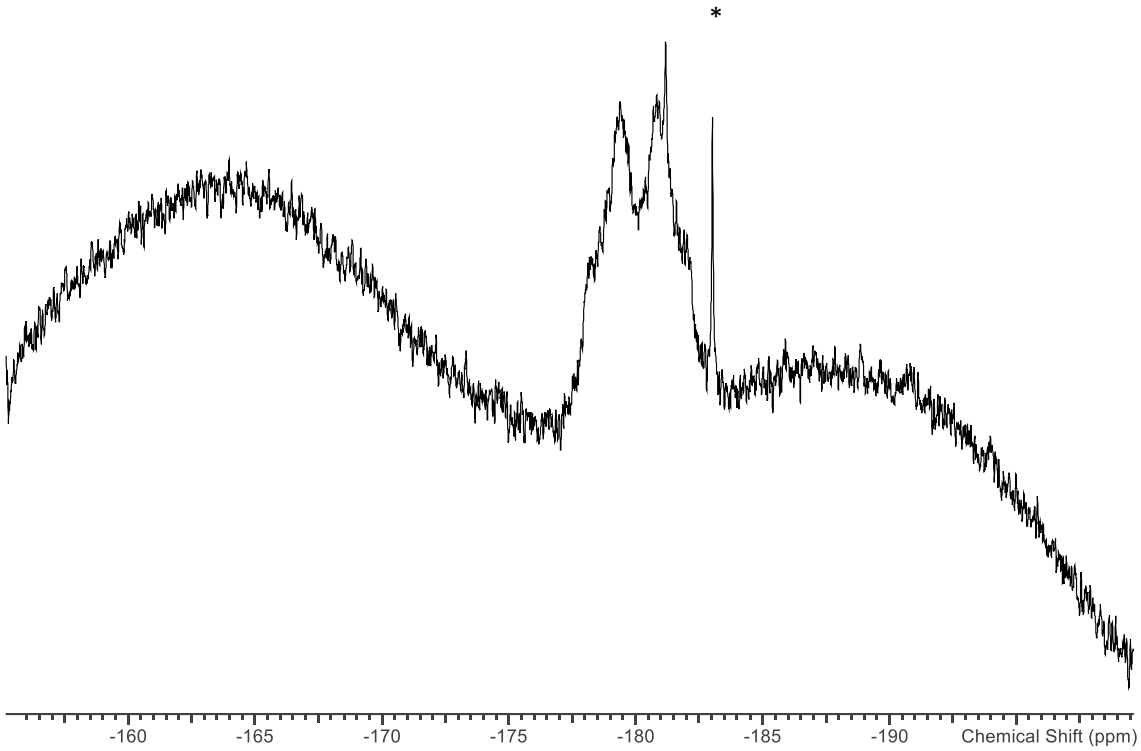

S7d: ESI^+ MS (MeOH) – top = experimental; bottom = calculated for $[GaF_2(\mathbf{L^1})]^+$

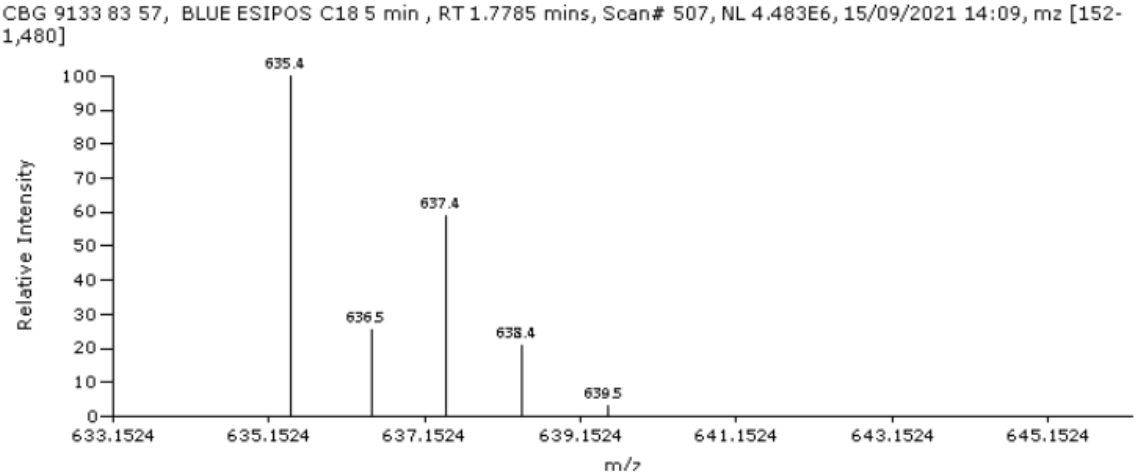

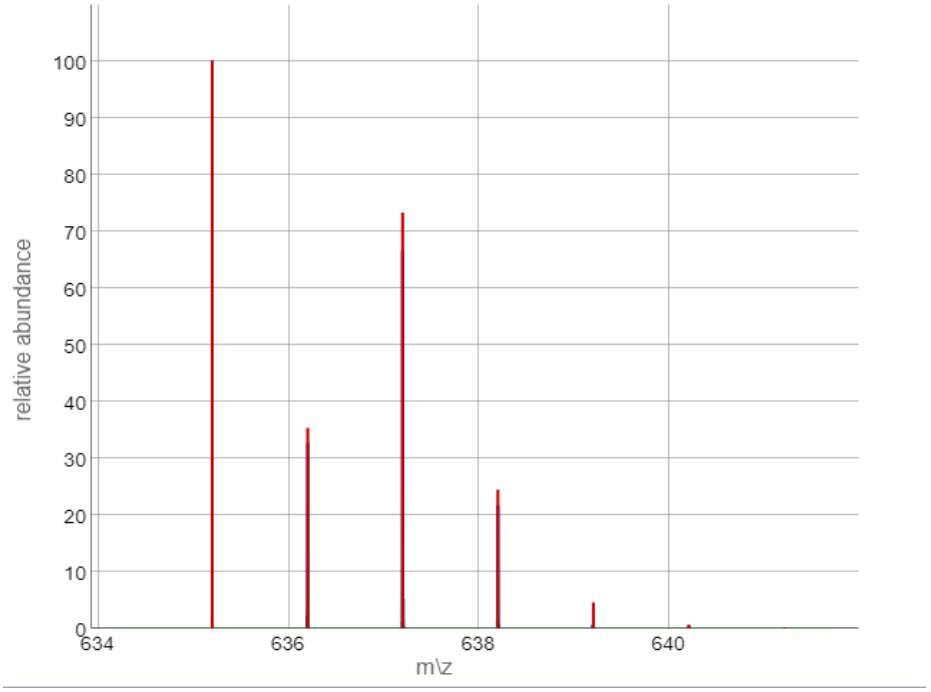

S7e: IR spectrum (Nujol)

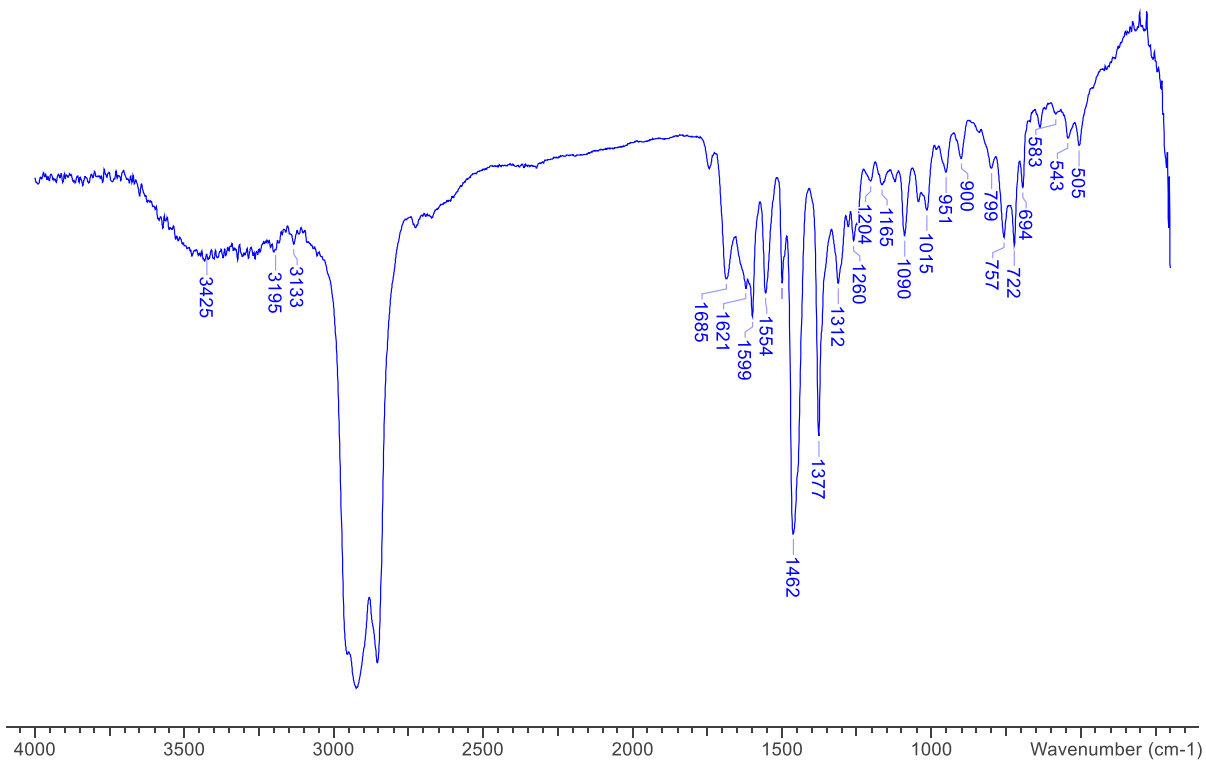

Figure S8 Spectroscopic data for [FeF_3(**L^1**)]

S8a: IR spectrum (Nujol)

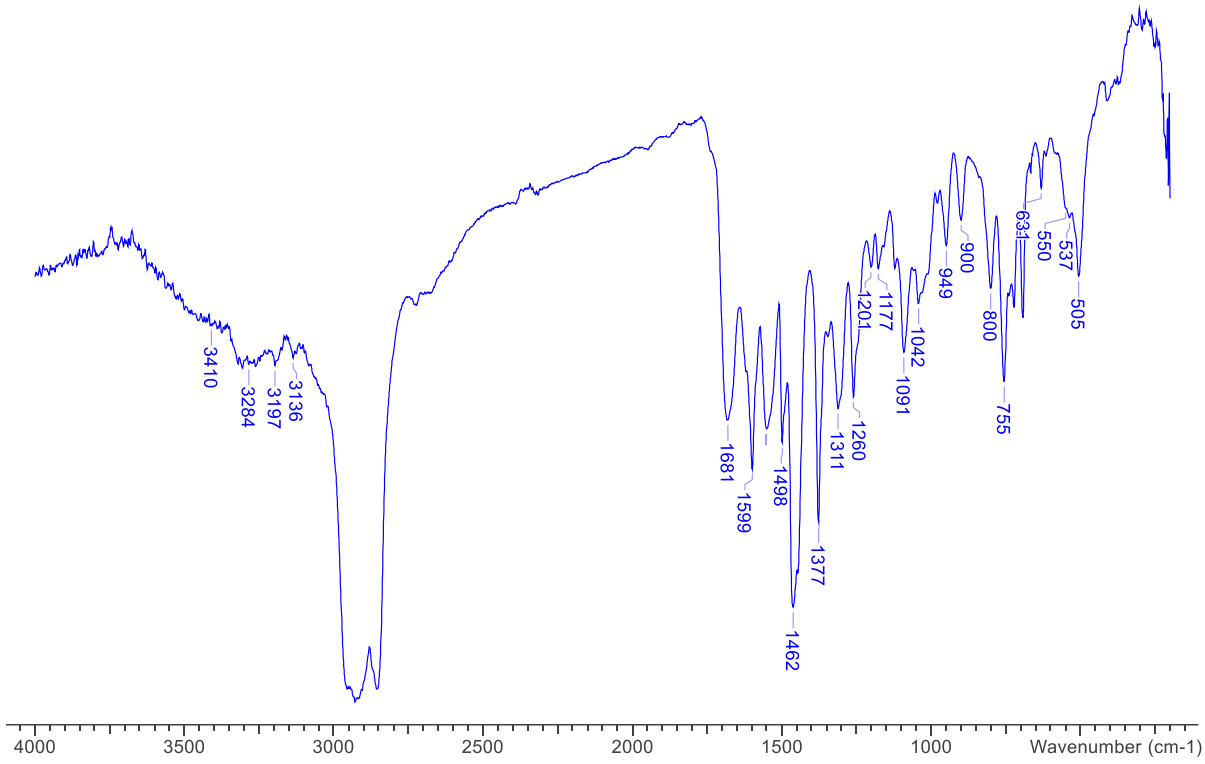

Figure S9 Spectroscopic data for [AlF_3(**L²**)]

S9a: ^{1}H NMR spectrum (CD_3OD)

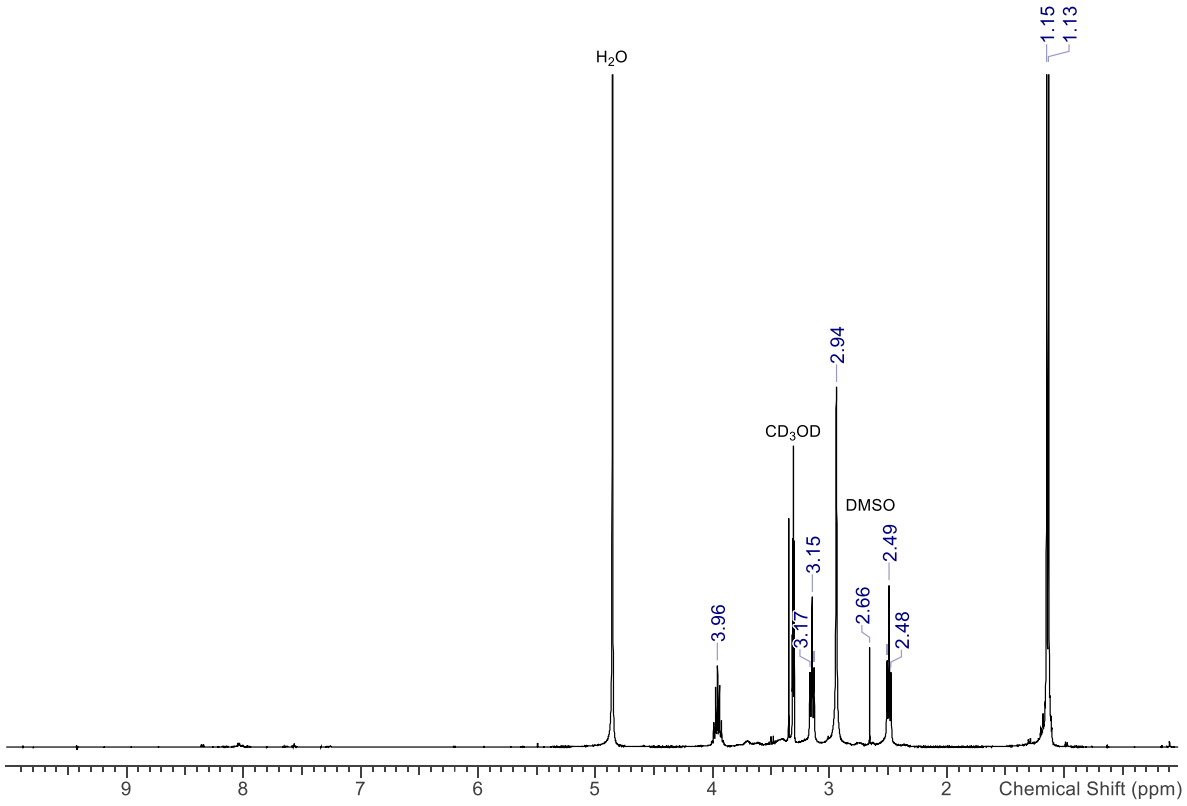

S9b: ^{1}H NMR spectrum (D_2O)

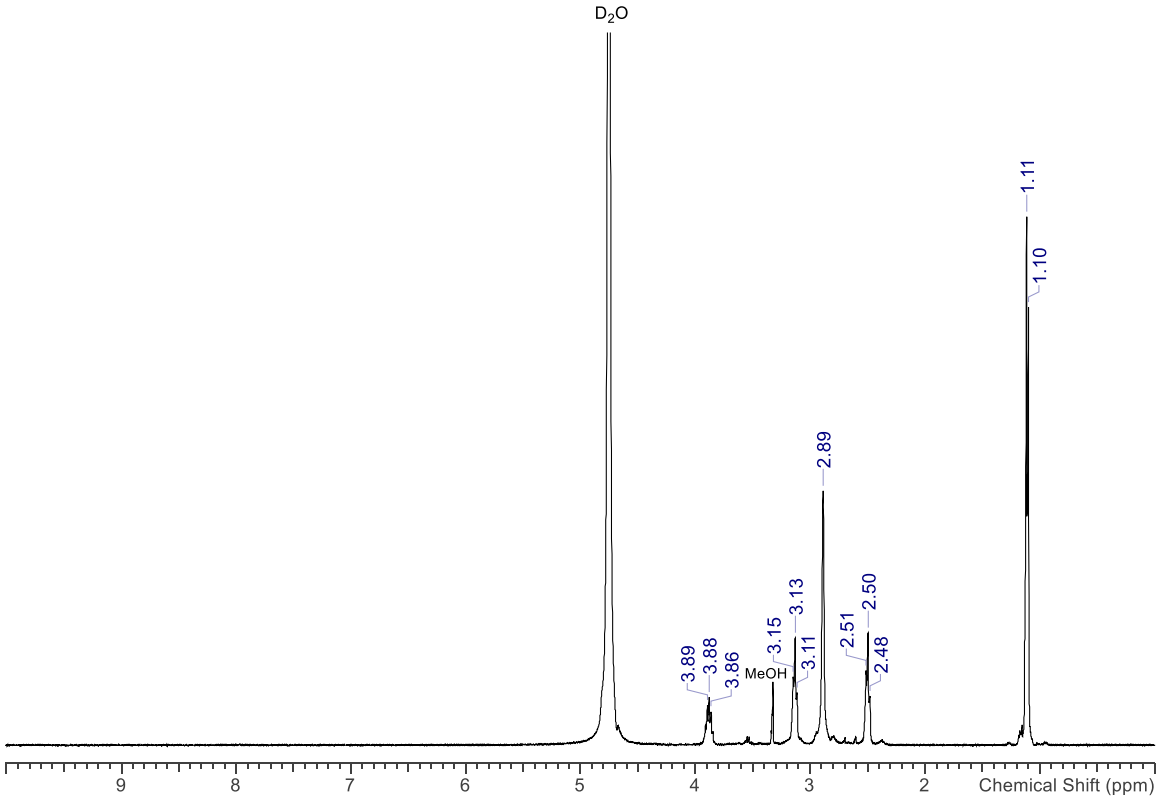

S9c: $^{13}C\{^{1}H\}$ NMR spectrum (CD_3OD)

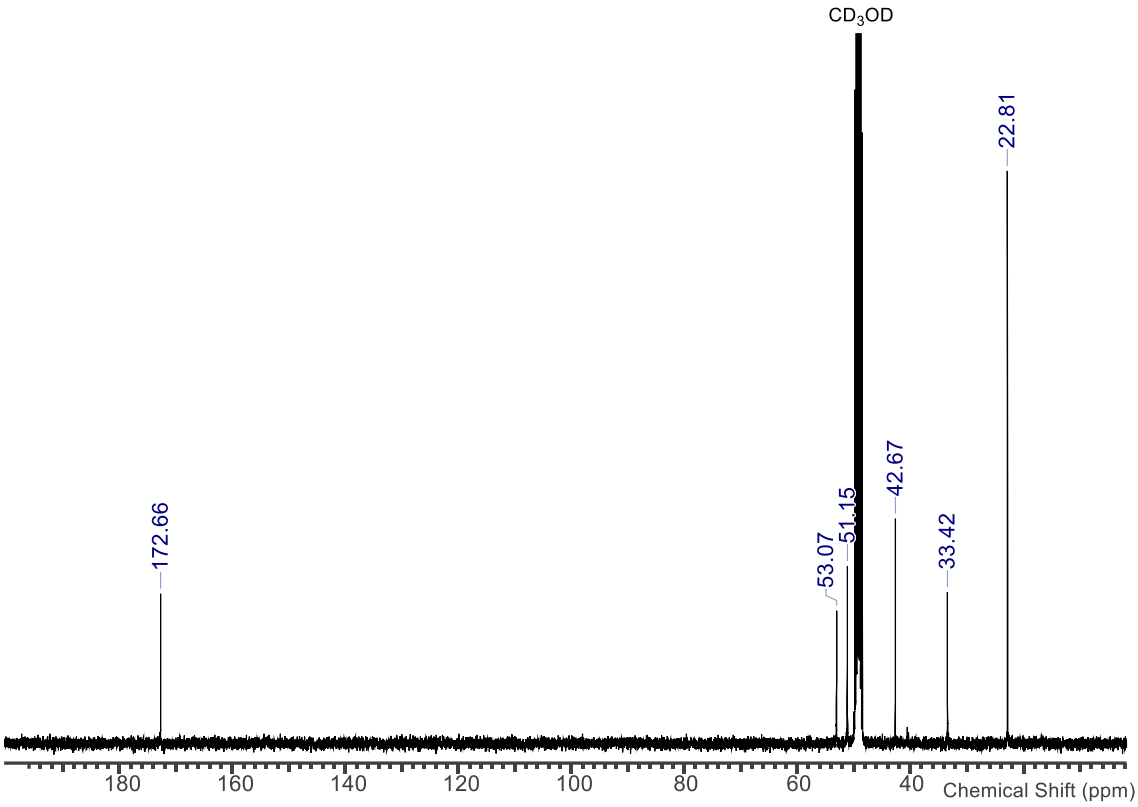

S9d: $^{13}C\{^{1}H\}$ NMR spectrum (D_2O)

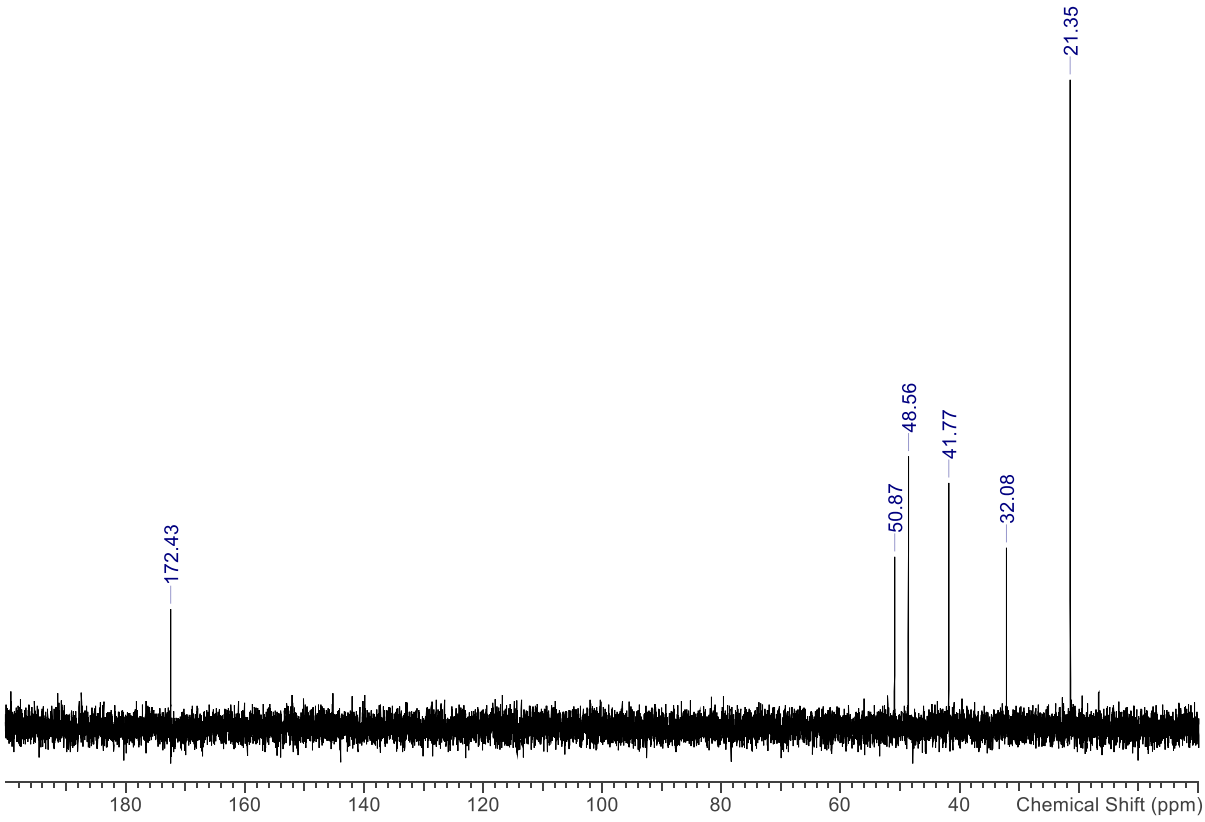

S9e: $^{19}F\{^{1}H\}$ NMR spectrum (CD_3OD) (note that the broad underlying baseline is due to the Teflon in the probe)

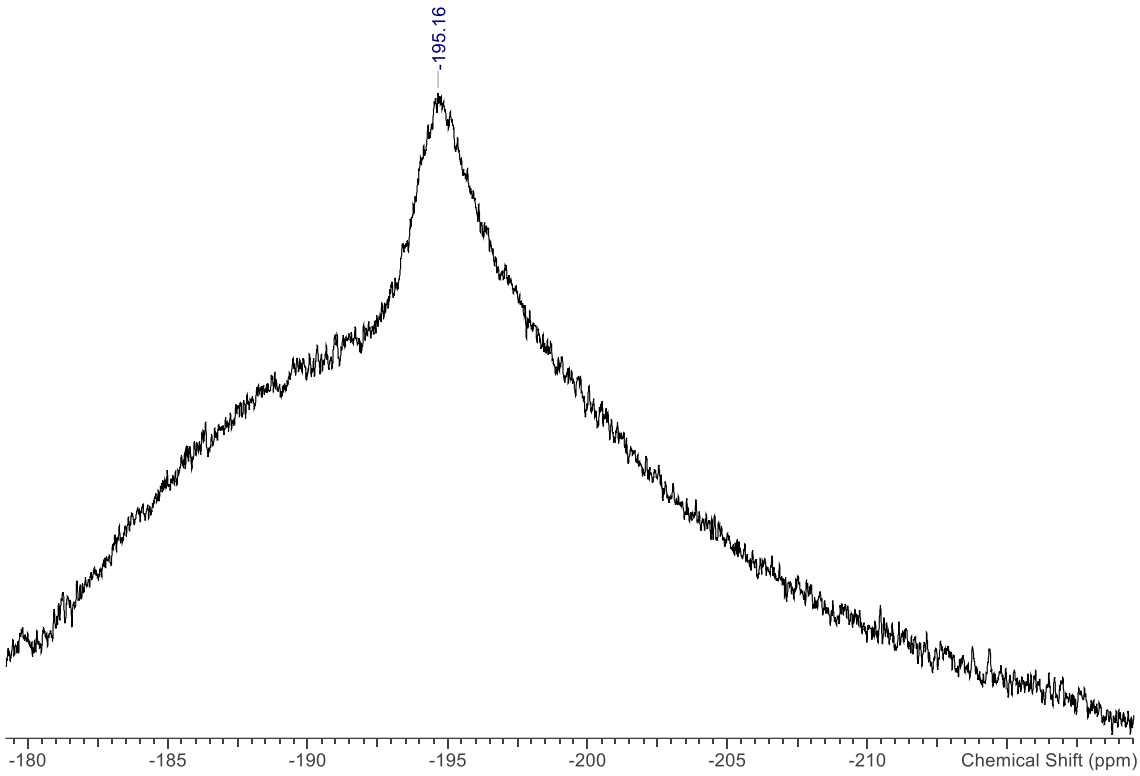

S9f: $^{19}F\{^{1}H\}$ NMR spectrum (D_2O) (note that the broad underlying baseline is due to the Teflon in the probe). The peak at -121 ppm is from some decomposition to form F^-.

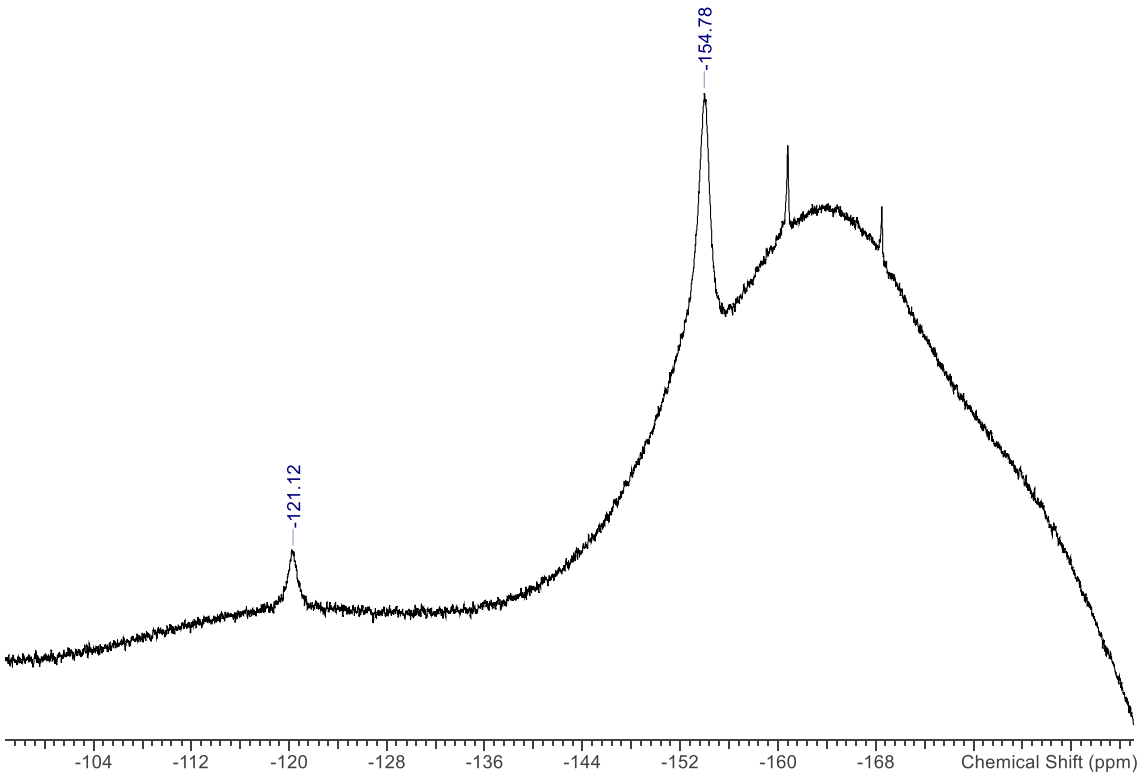

S9g: ESI$^+$ MS (MeOH) – top = experimental; bottom = calculated for [AlF_3(**L^2**) + H]$^+$

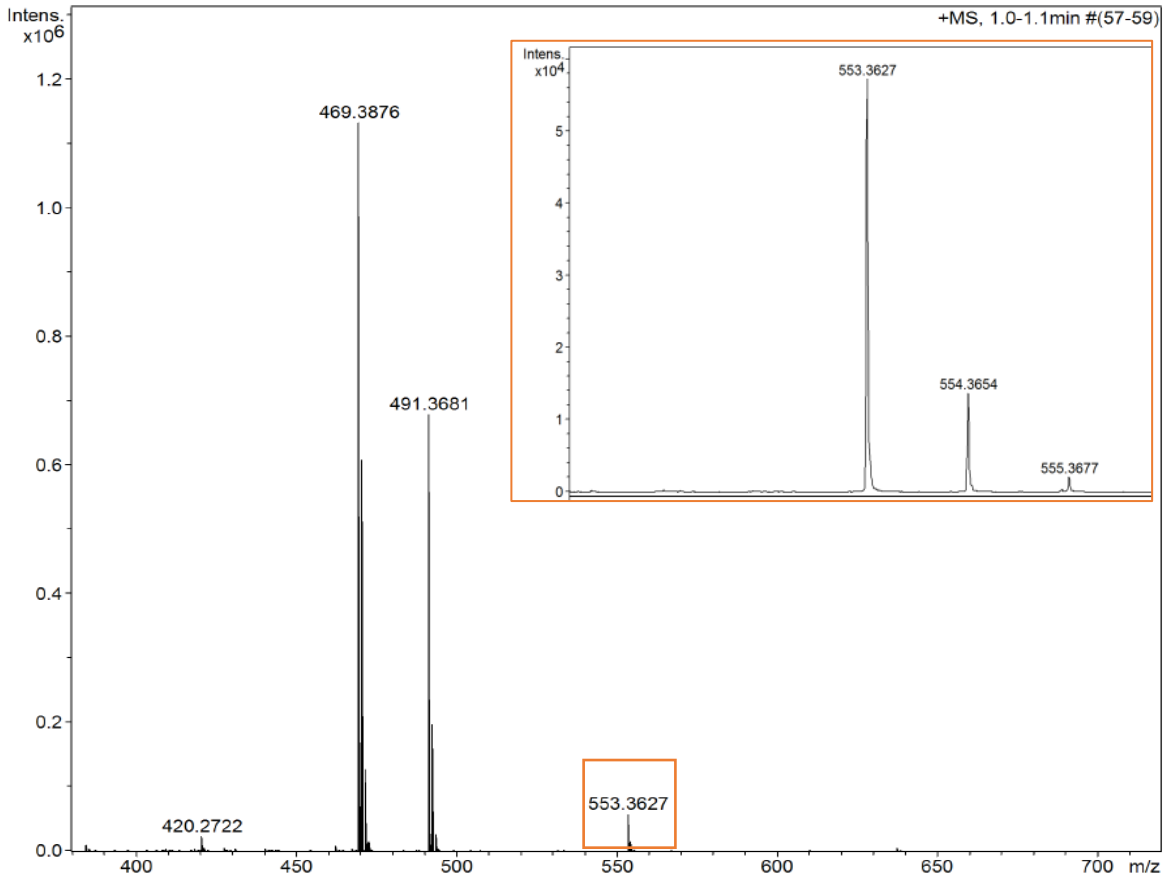

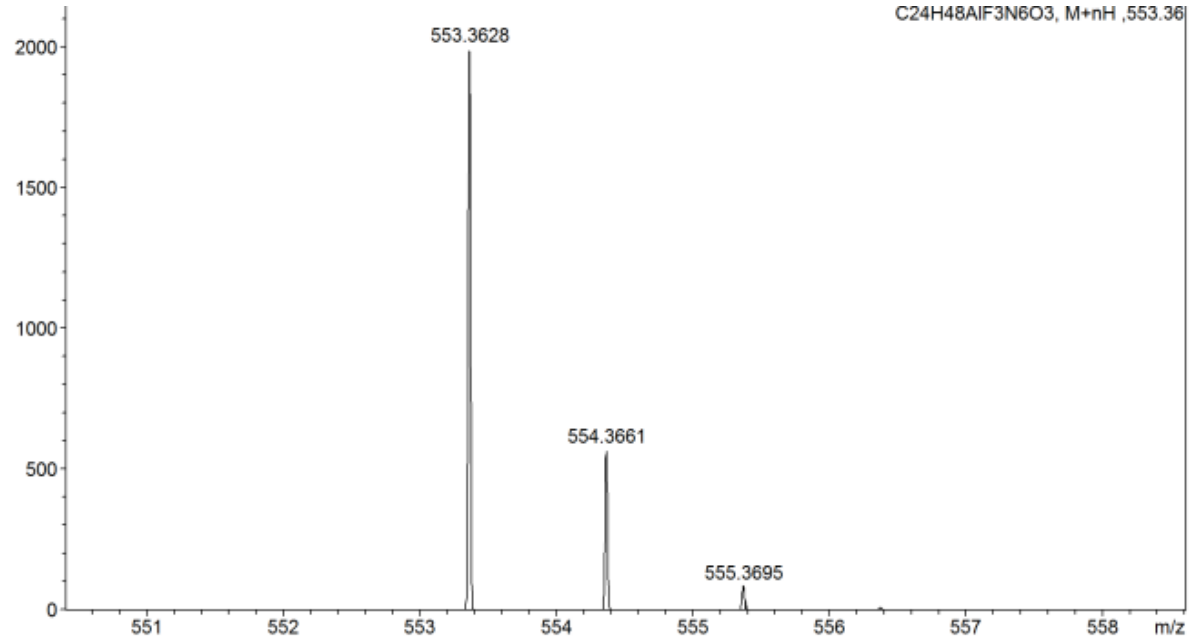

S9h: IR spectrum (Nujol)

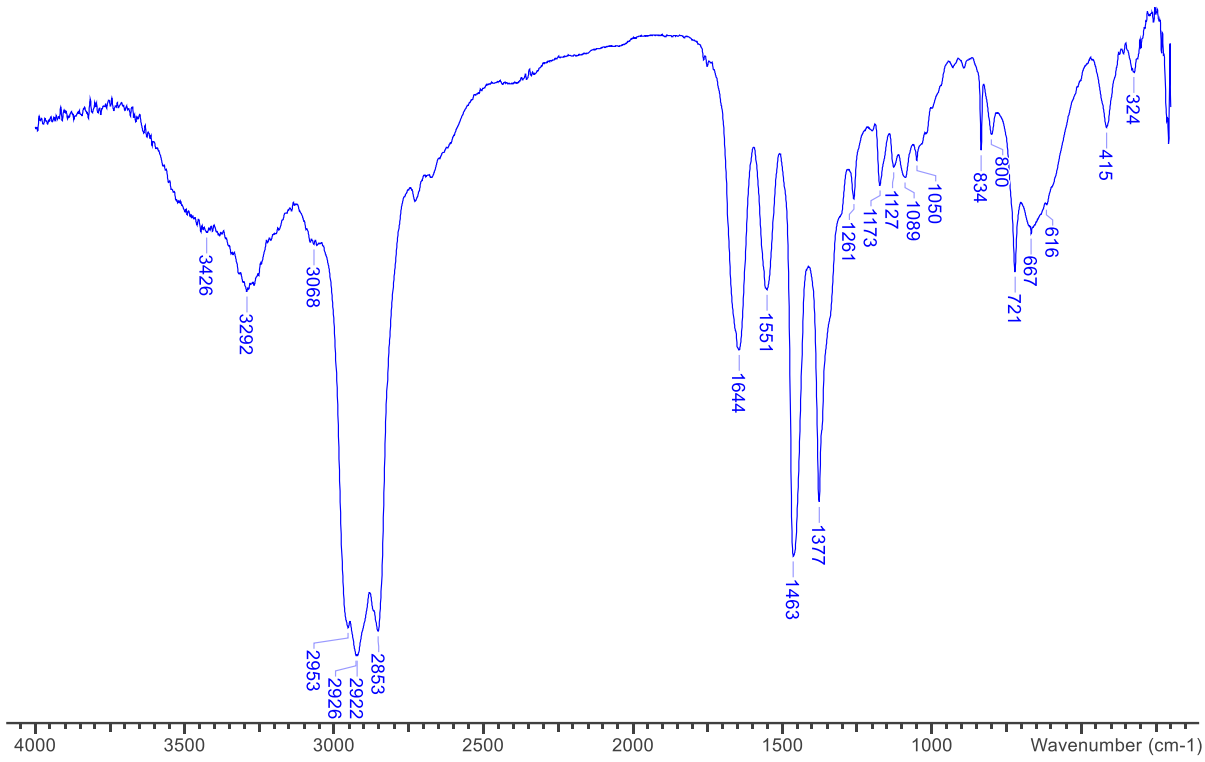

Figure S10 Spectroscopic data for [GaF_3(**L²**)]

S10a: ^{1}H NMR spectrum (CD_3OD)

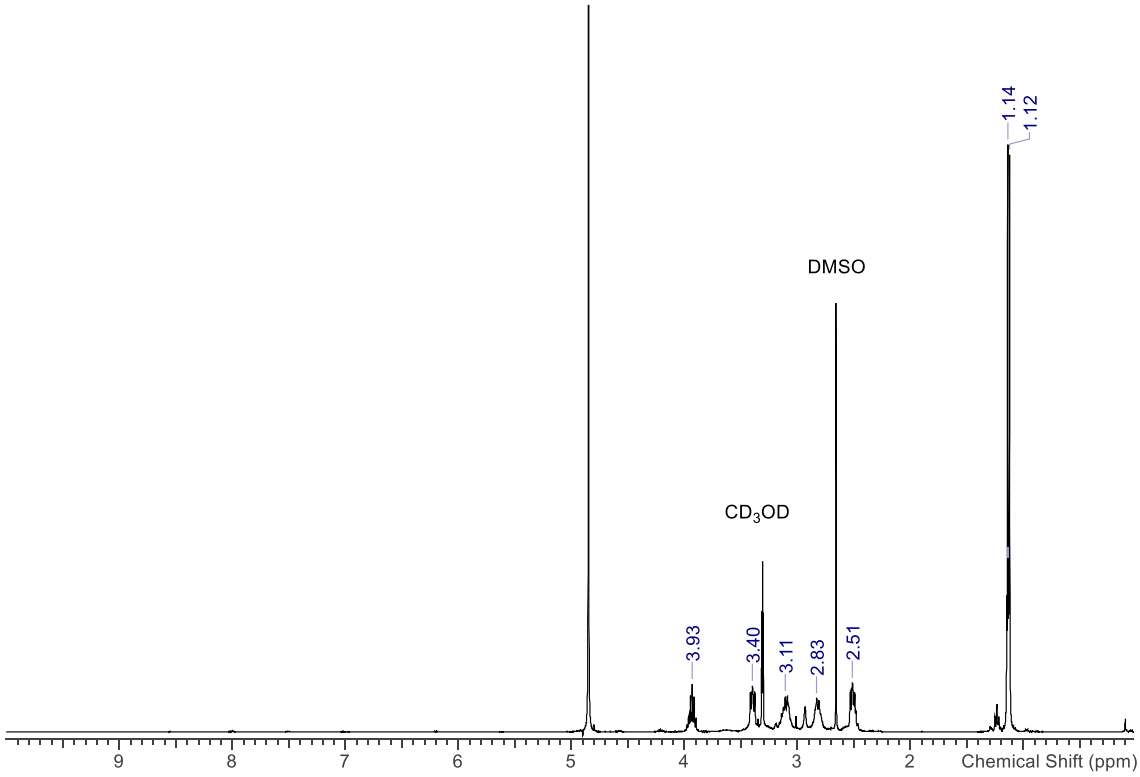

S10b: $^{13}C\{^1H\}$ NMR spectrum (CD_3OD)

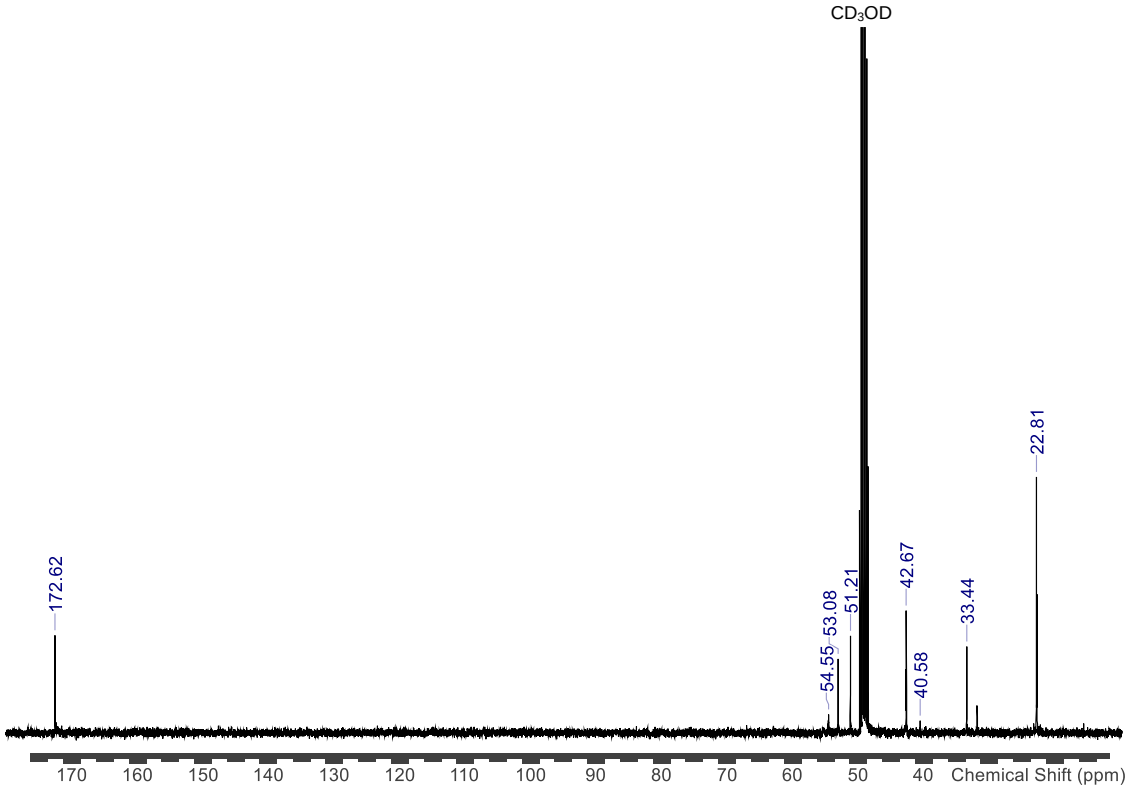

S10c: $^{19}F\{^{1}H\}$ NMR spectrum (CD_3OD)

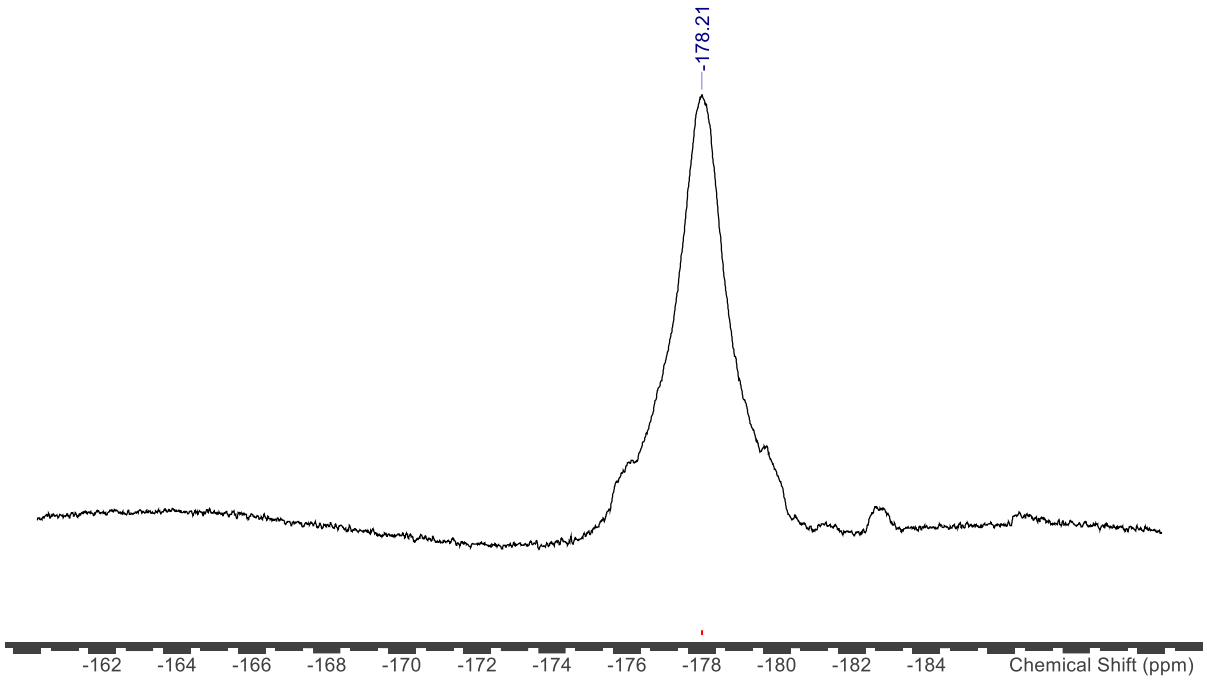

S10d: ESI^+ MS (MeOH) – top = experimental; bottom = calculated for $[GaF_2(\mathbf{L^2})]^+$

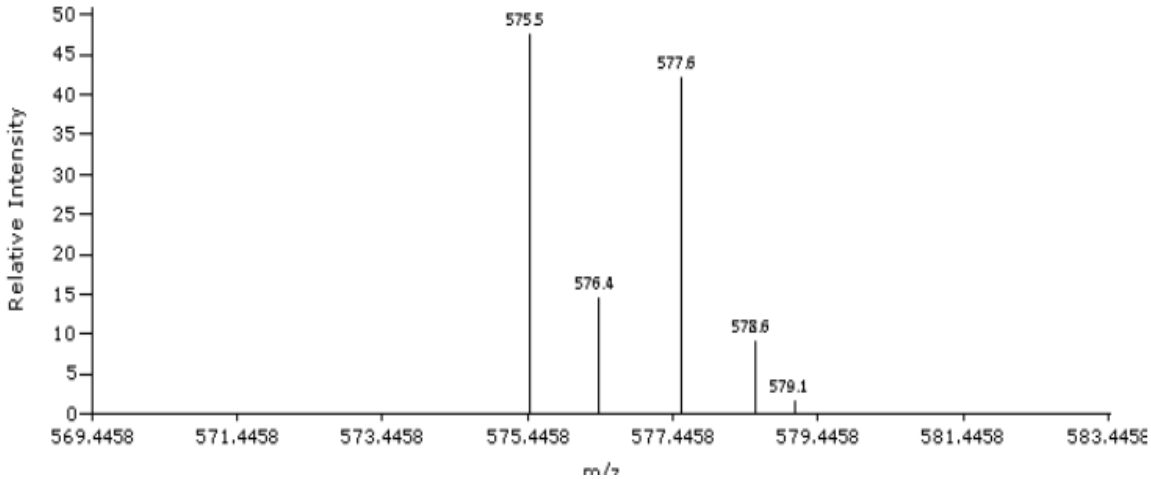

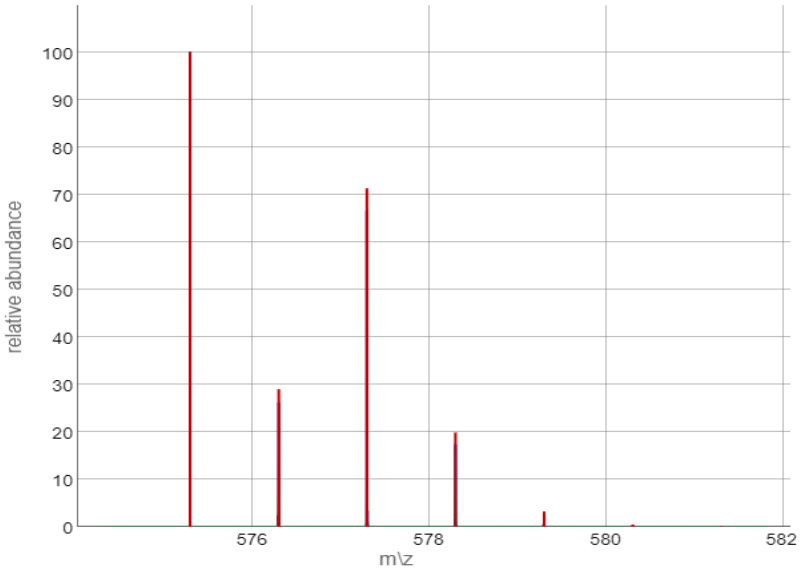

S10e: IR spectrum (Nujol)

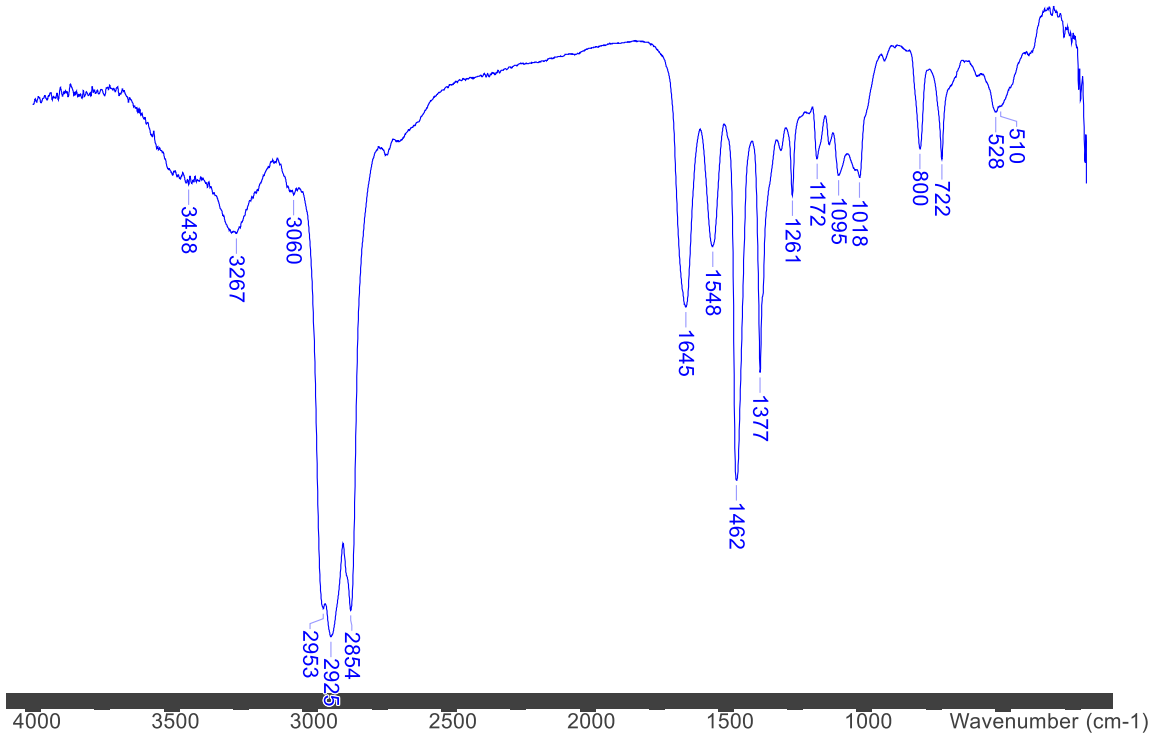

Figure S11 Spectroscopic data for product (mixture) from reaction of $[InF_3(OH_2)_2(dmso)]$ with **L²**

S11a: ^1H NMR spectrum (CD_3OD)

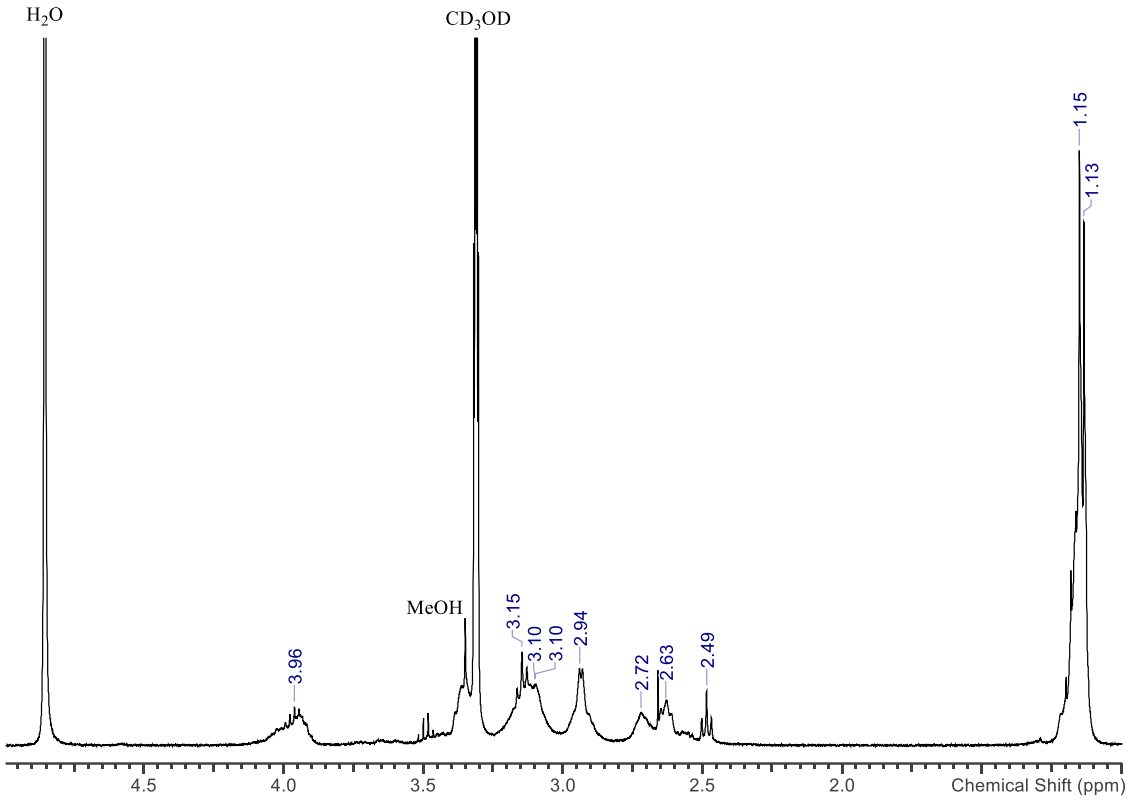

S11b: $^{19}F\{^1H\}$ NMR spectrum (CD_3OD) (the sharp singlet at *ca*. -130 ppm is F^-)

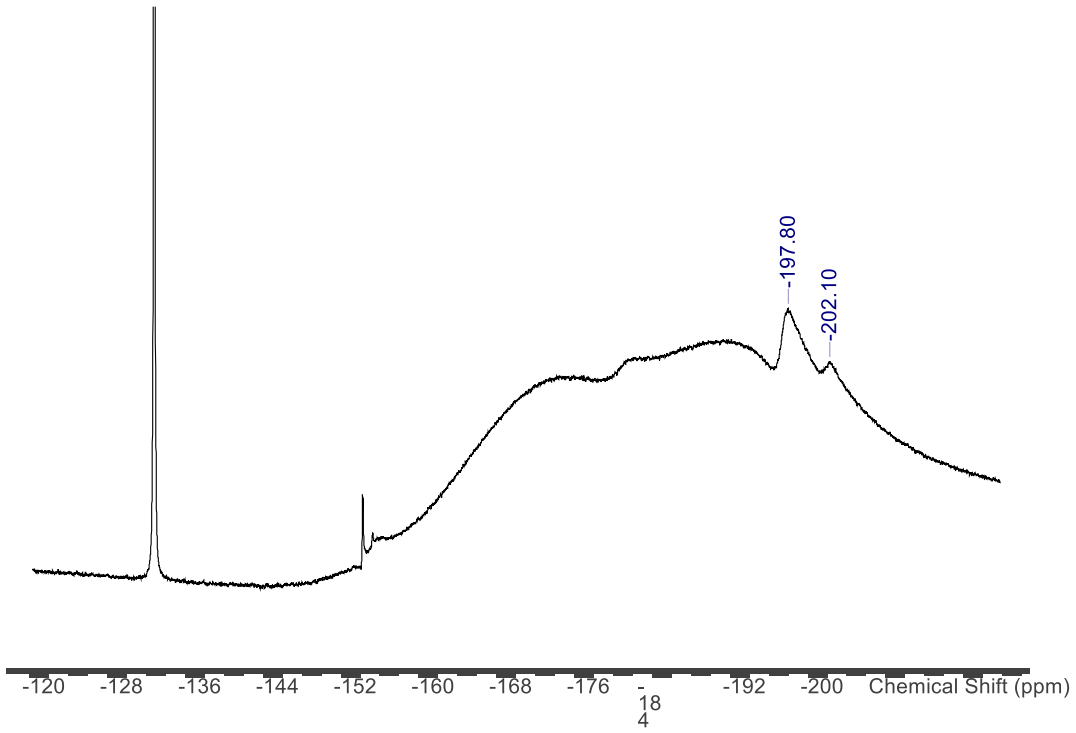

Figure S12 Spectroscopic data for [FeF_3(**L²**)]

S12a: IR spectrum (Nujol)

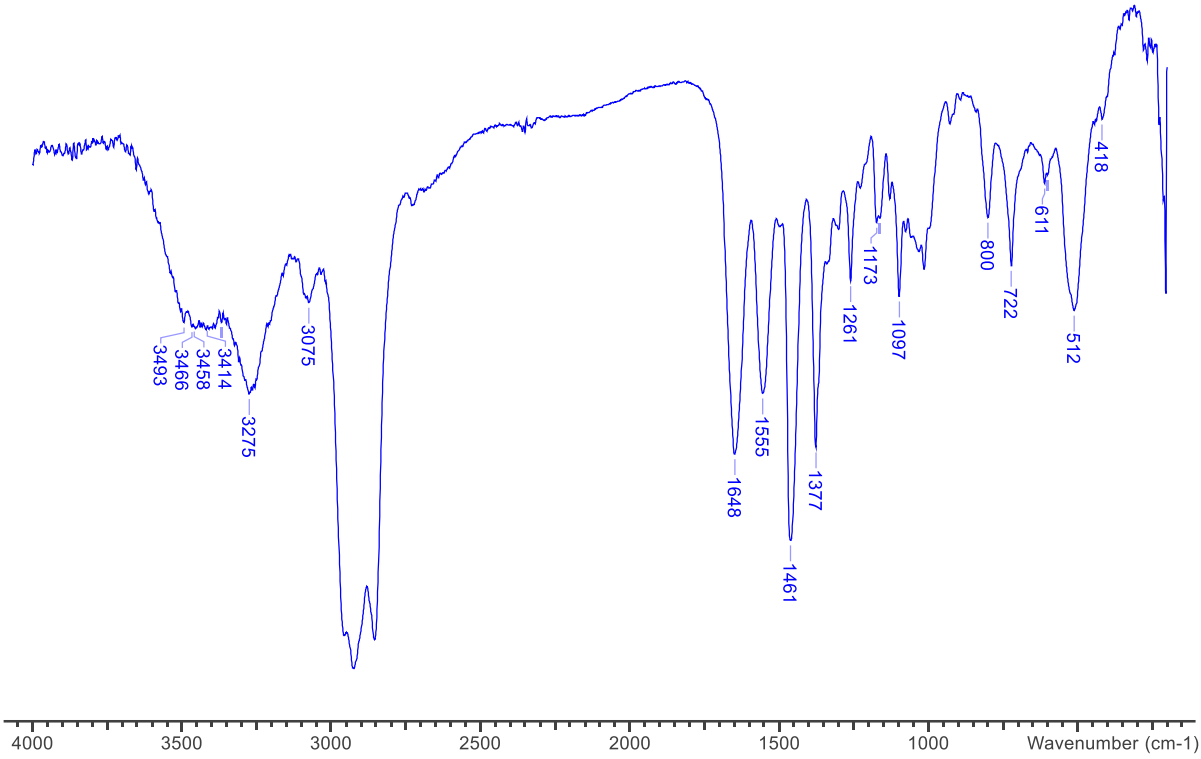

S12b: ESI^+ MS (MeOH) top = experimental; bottom = calculated for [FeF_2(**L²**)]$^+$

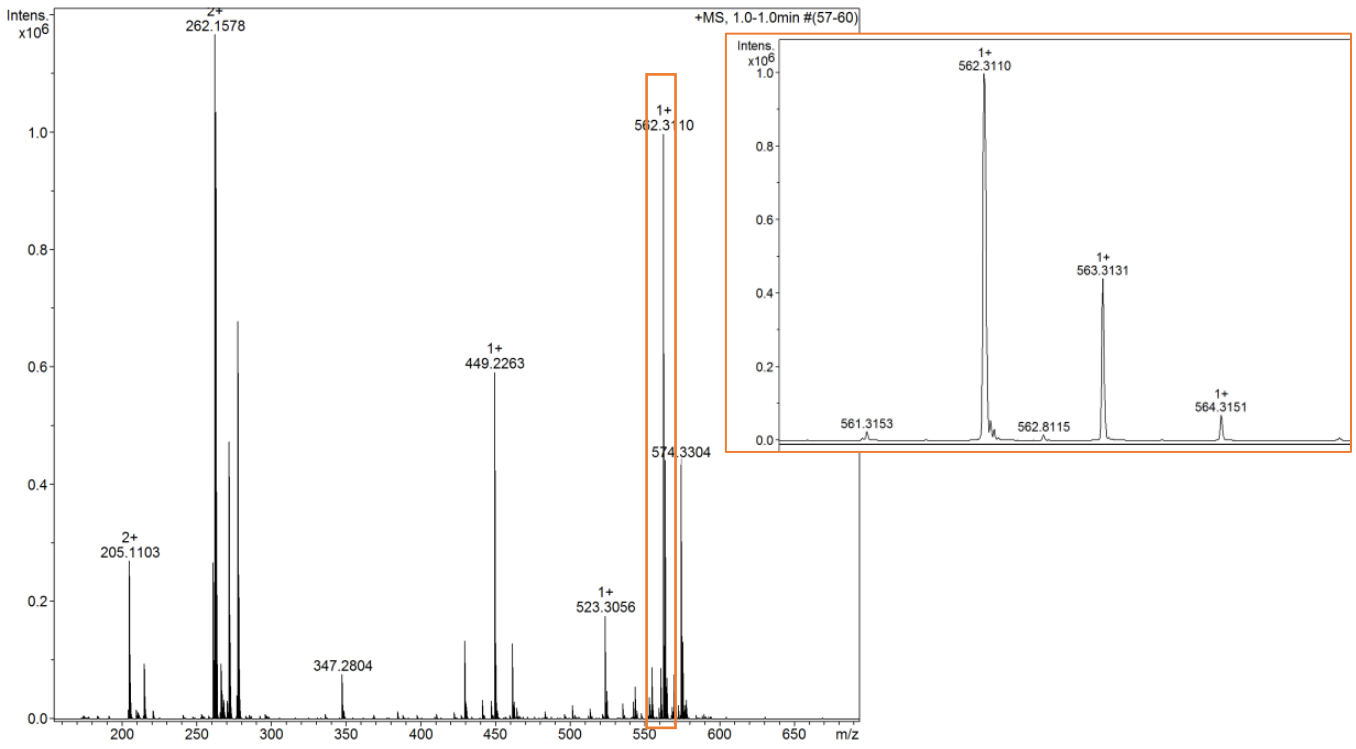

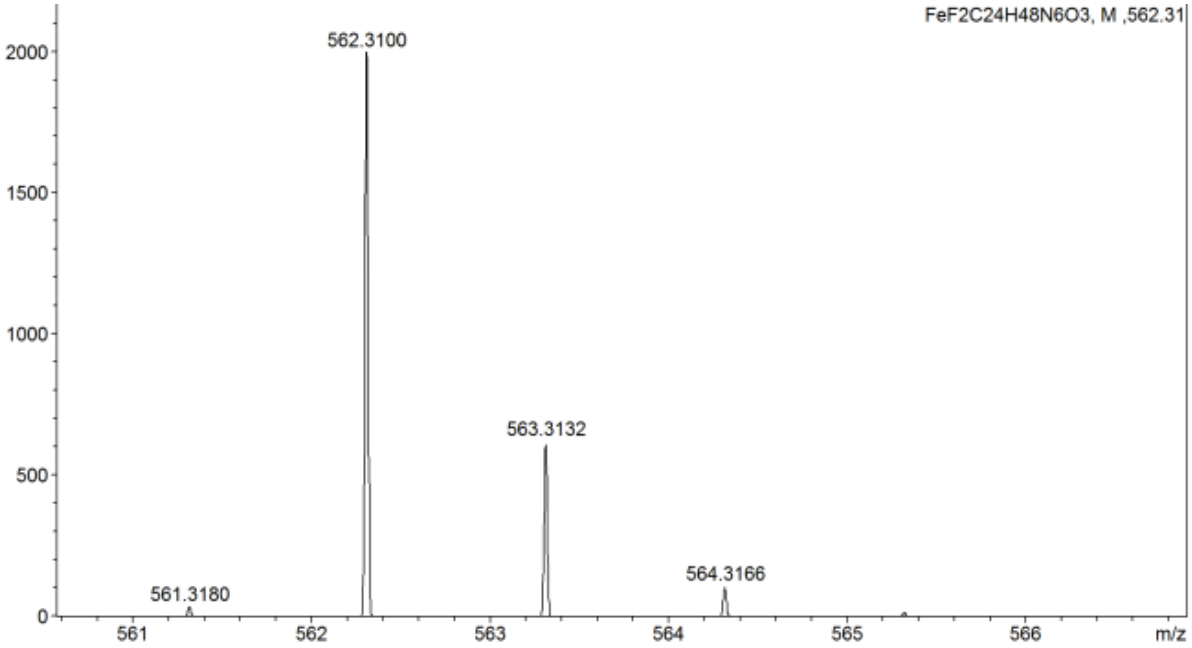
FeF2C24H48N6O3, M ,562.31
562.3100
563.3132
564.3166
561.3180
2000
1500
1000
500
0
561
562
563
564
565
566
m/z

Figure S13 Spectroscopic data for [AlF_3(**L**^{3})]

S13a: ^{1}H NMR spectrum (CD_3OD)

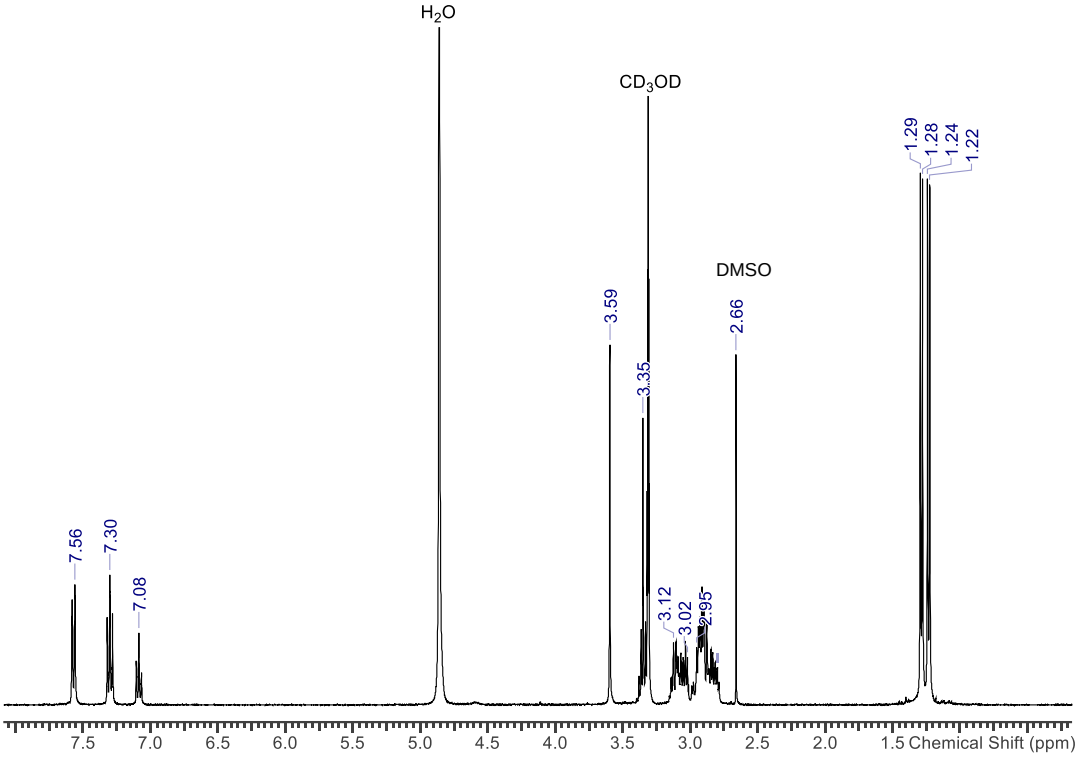

S13b: $^{13}C\{^1H\}$ NMR spectrum (CD_3OD)

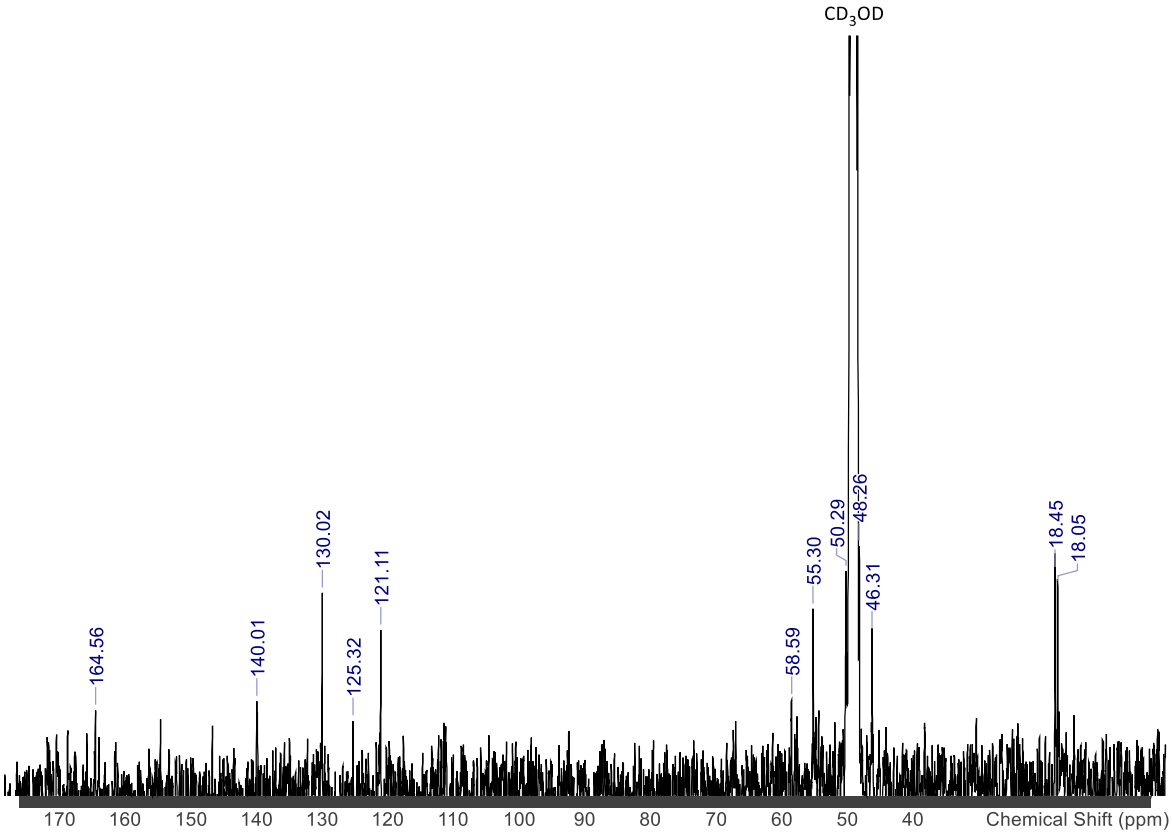

S13c: $^{19}F\{^{1}H\}$ NMR spectrum (CD_3OD) (note that the broad underlying baseline is due to the Teflon in the probe)

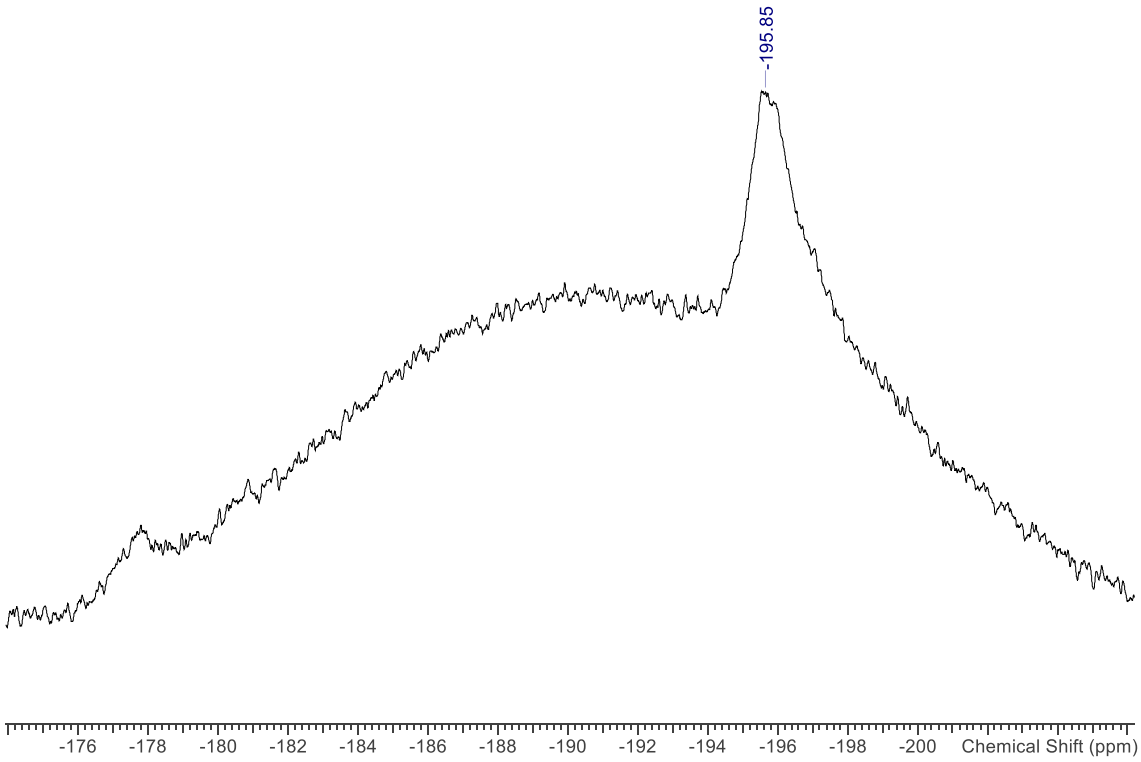

S13d: $^{19}F\{^{1}H\}$ NMR spectrum (D_2O) (note that the broad underlying baseline is due to the Teflon in the probe). (A singlet is also evident at -122 ppm due to F^-)

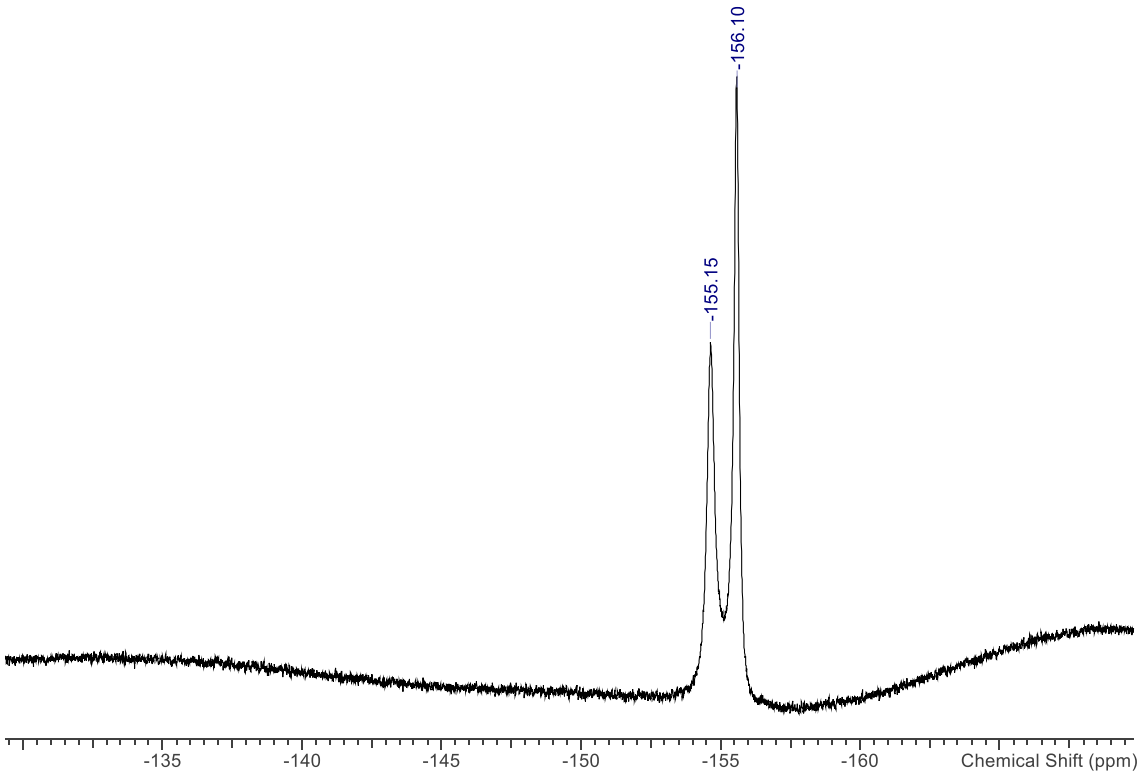

S13e: IR spectrum (Nujol)

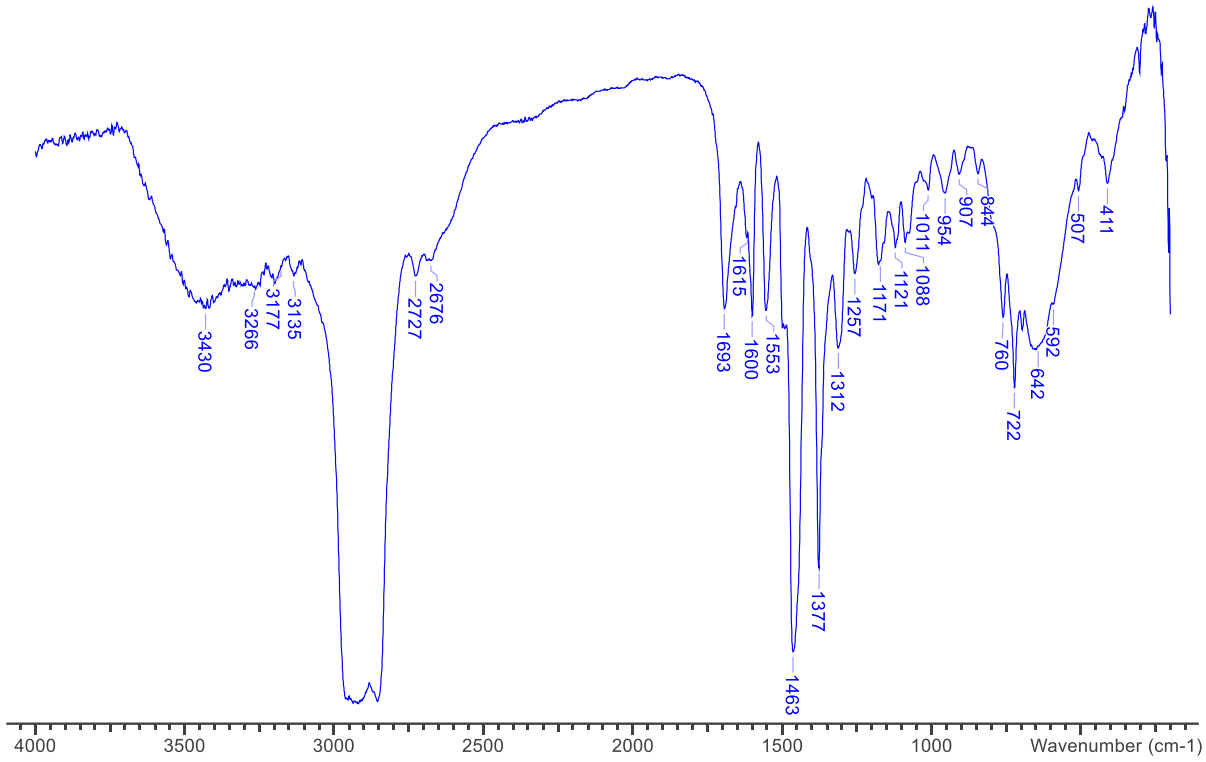

S13f: ESI^{+} MS (MeOH) top = experimental; bottom = calculated for [AlF3(L3)][H]+

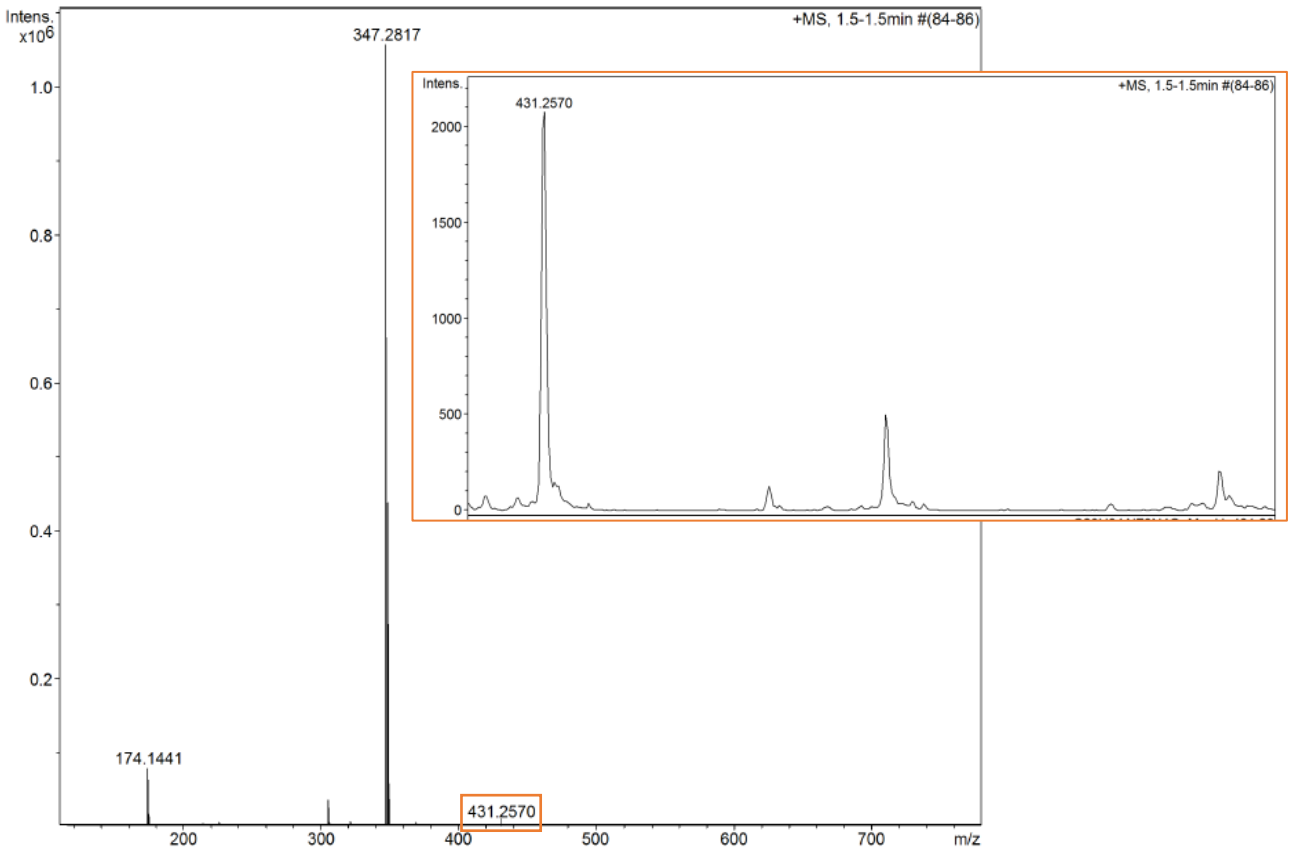

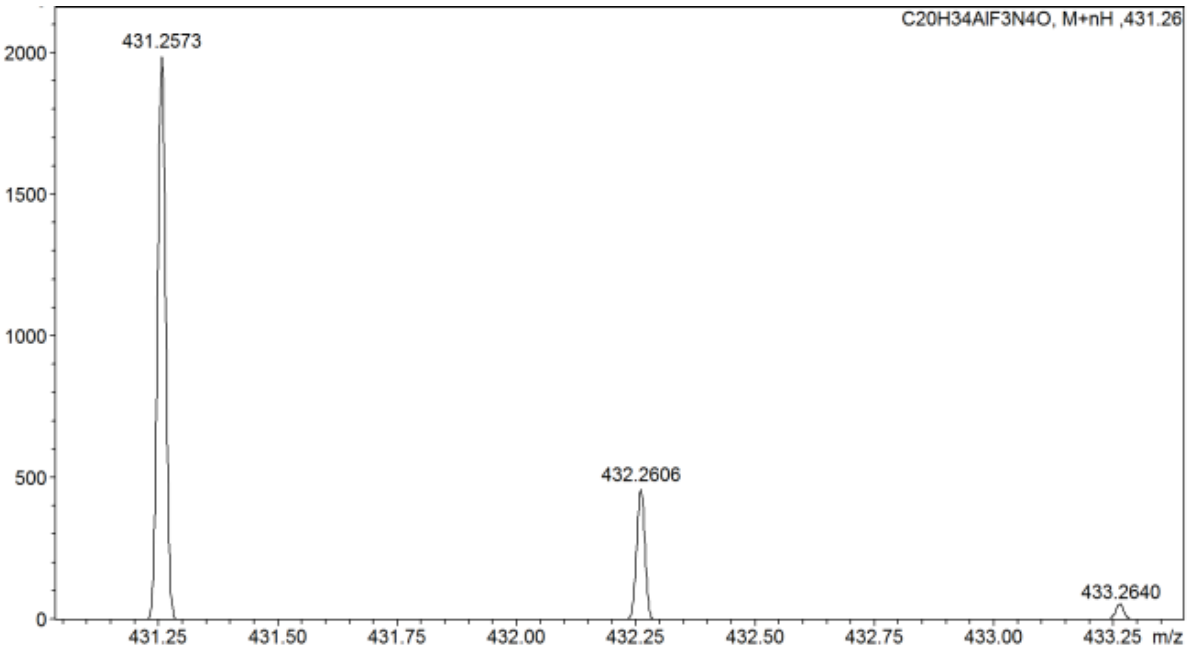
C20H34AlF3N4O, M+nH ,431.26
431.2573
432.2606
433.2640
2000
1500
1000
500
0
431.25
431.50
431.75
432.00
432.25
432.50
432.75
433.00
433.25
m/z

Figure S14 Spectroscopic data for [GaF_3(**L**^{3})]

S14a: ^{1}H NMR spectrum (CD_3OD)

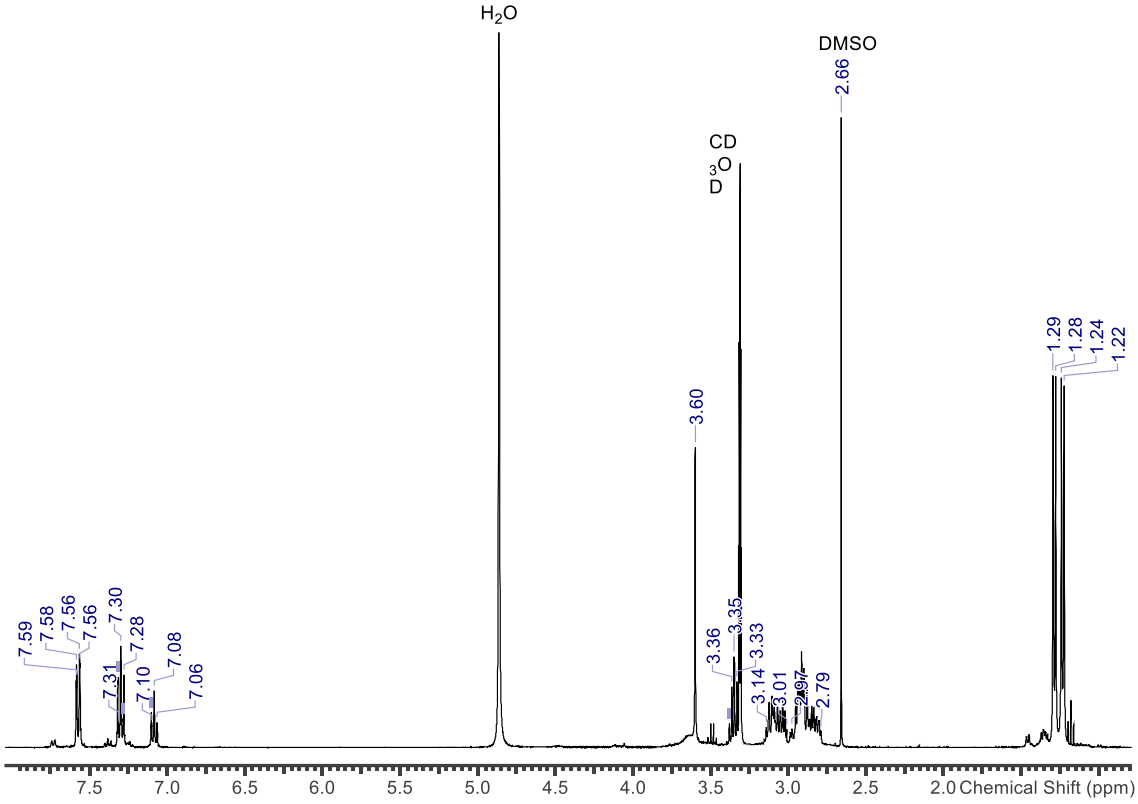

S14b: $^{13}C\{^1H\}$ NMR spectrum (CD_3OD)

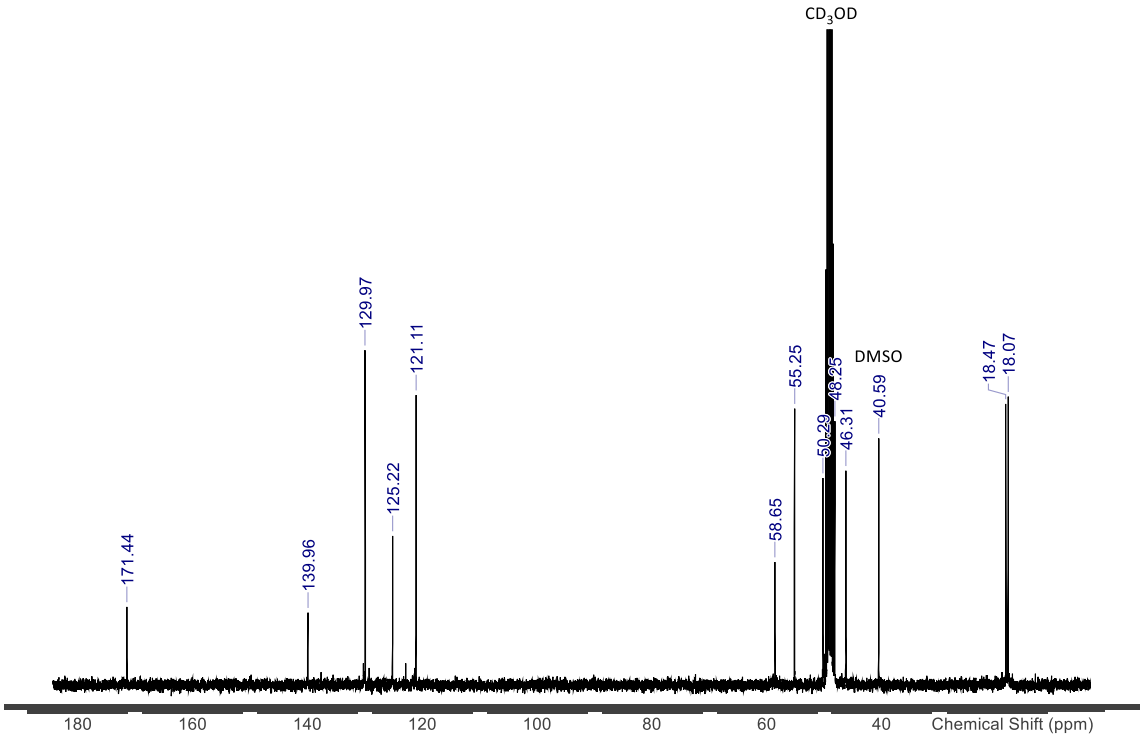

S14c: $^{19}F\{^{1}H\}$ NMR spectrum (CD_3OD) (note that the broad underlying baseline is from the Teflon in the probe). The singlet at -133 ppm is due to F^-.

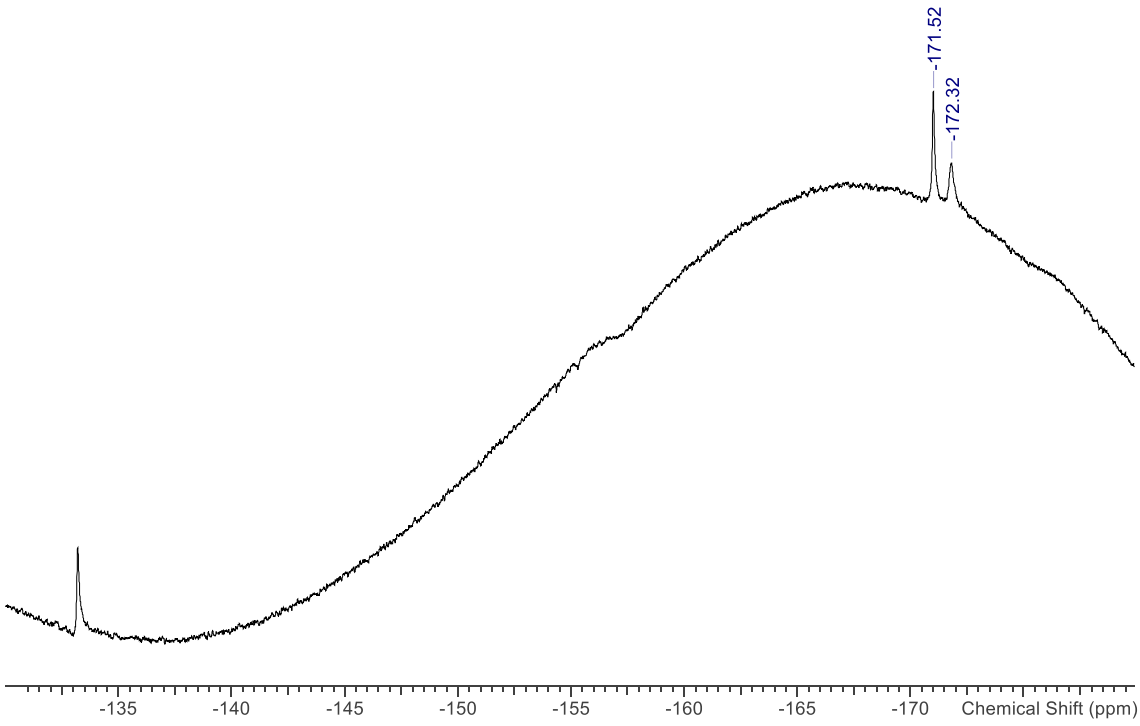

S14e ESI^+ MS (MeOH) top = experimental; bottom = calculated for $[GaF_2(\mathbf{L^2})]^+$

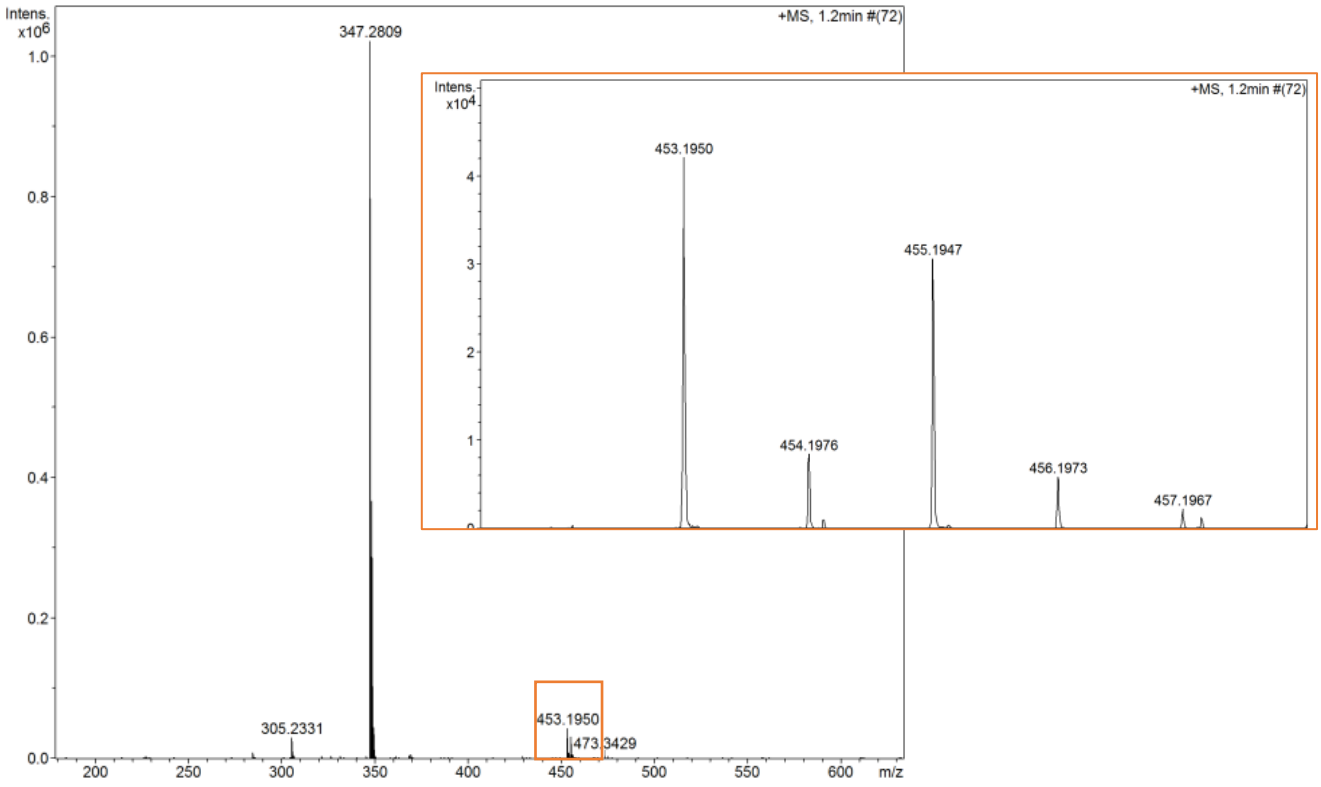

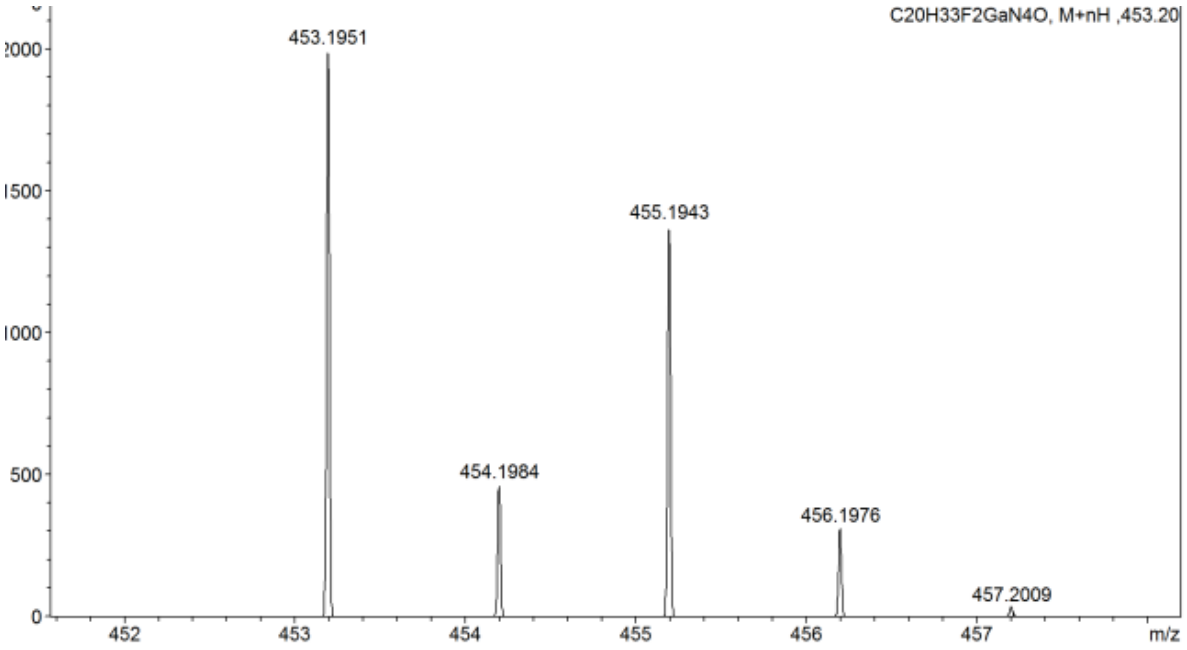

S14f: IR spectrum (Nujol)

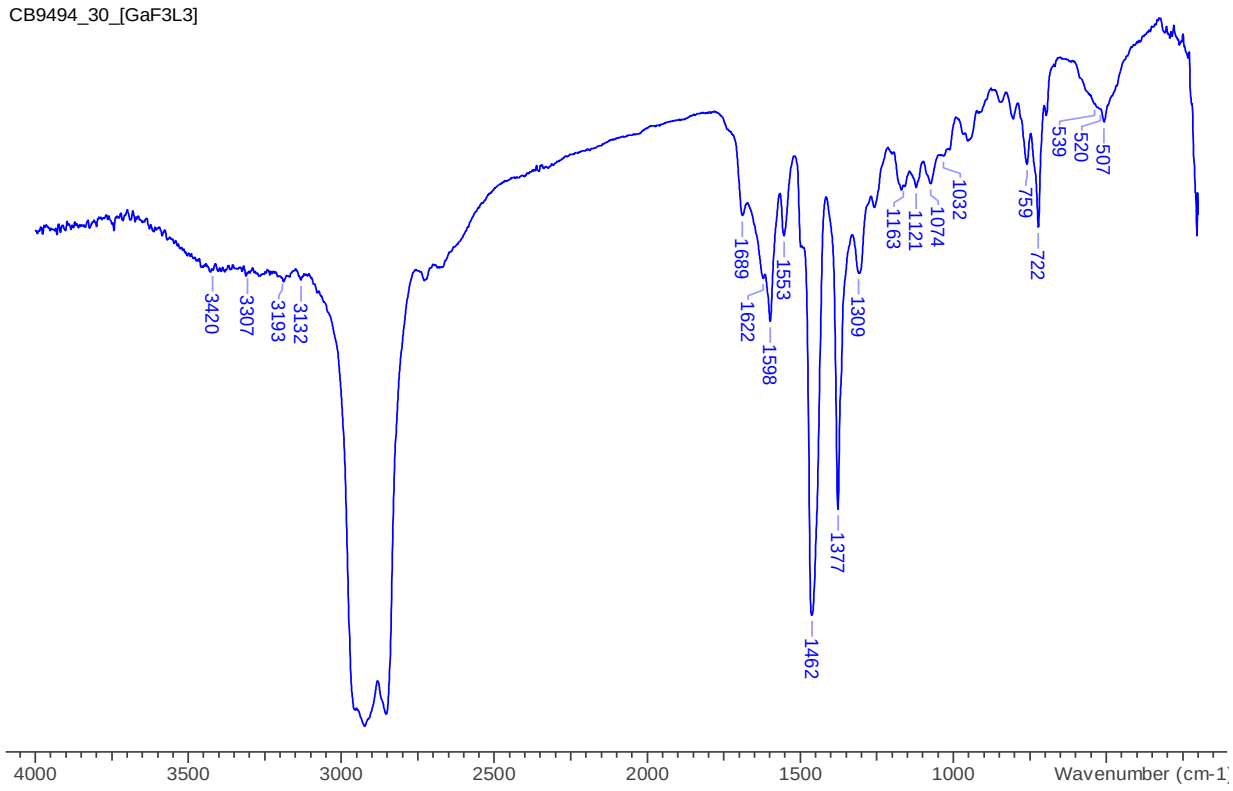

Figure S15 Spectroscopic data for [FeF_3(**L**^{3})]

S15a: IR spectrum (Nujol)

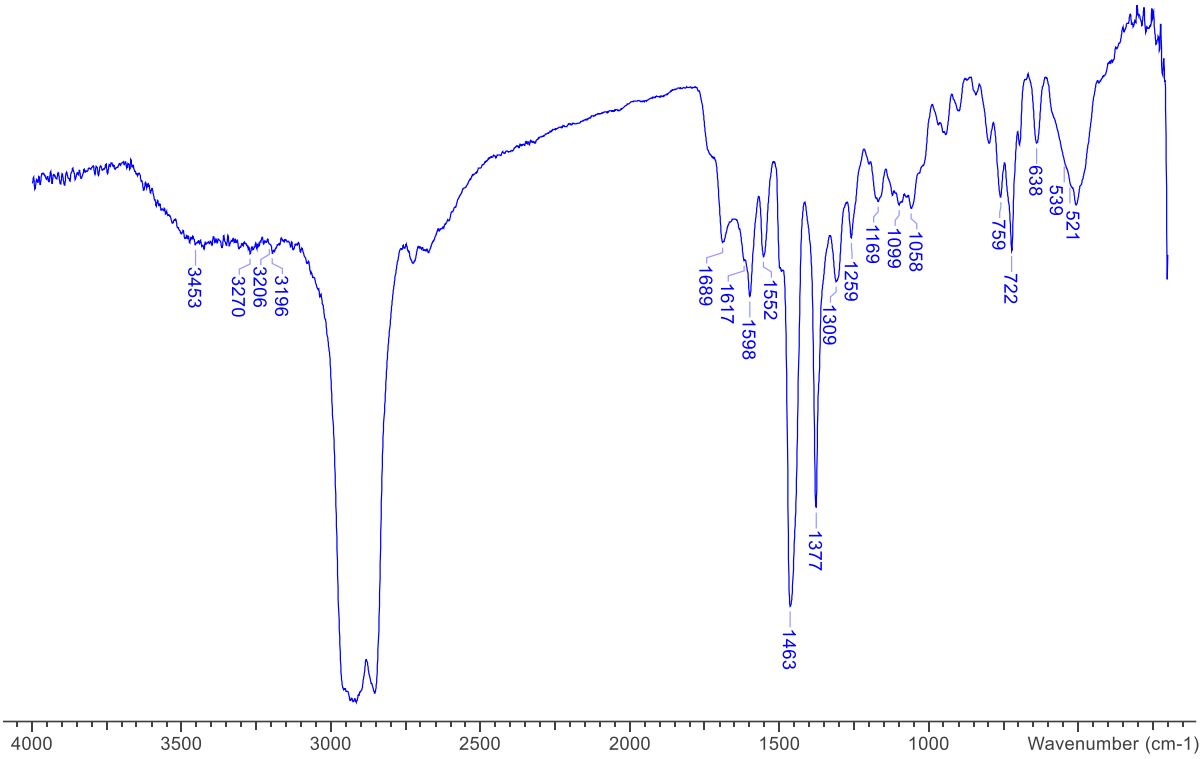

S15b: ESI$^+$ MS (MeOH) top = experimental; bottom = calculated for [FeF_2(**L**^{2})]$^+$

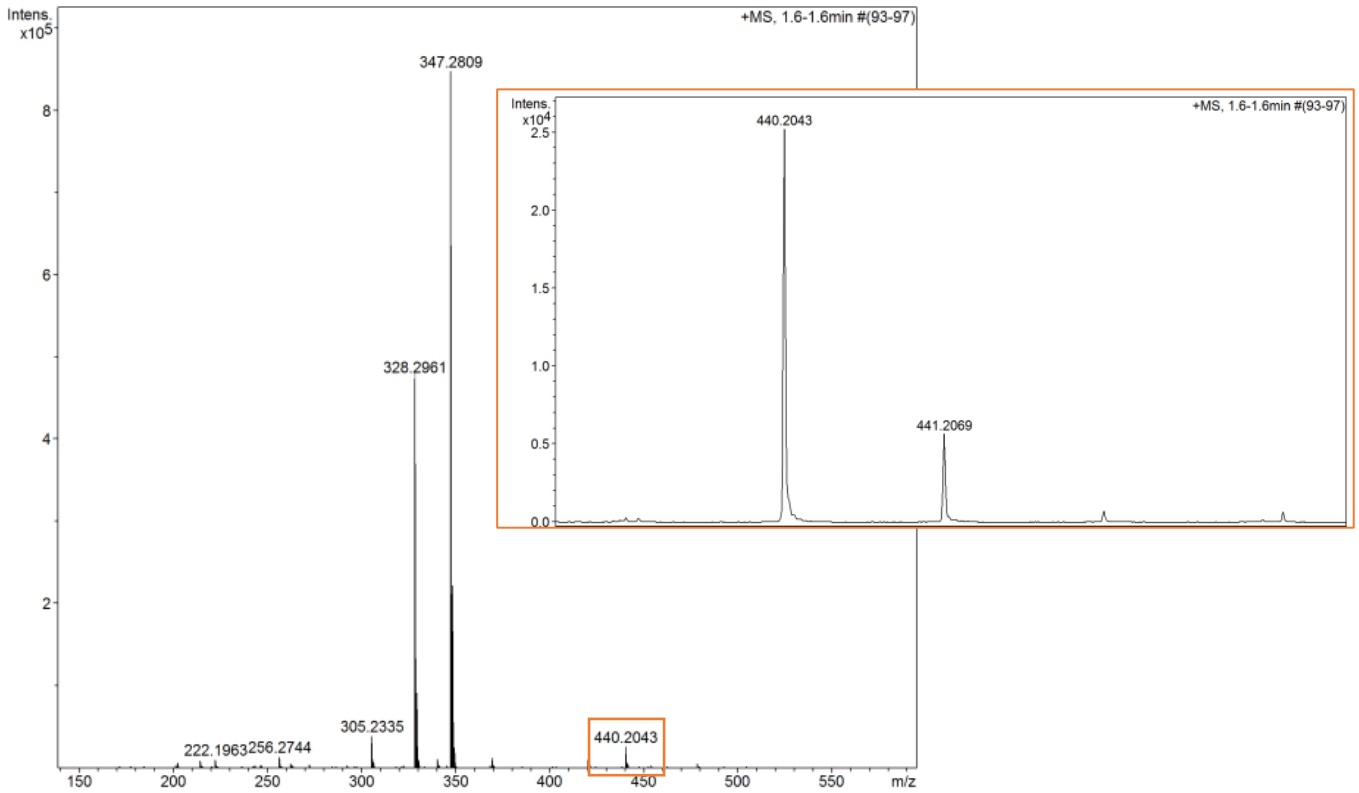

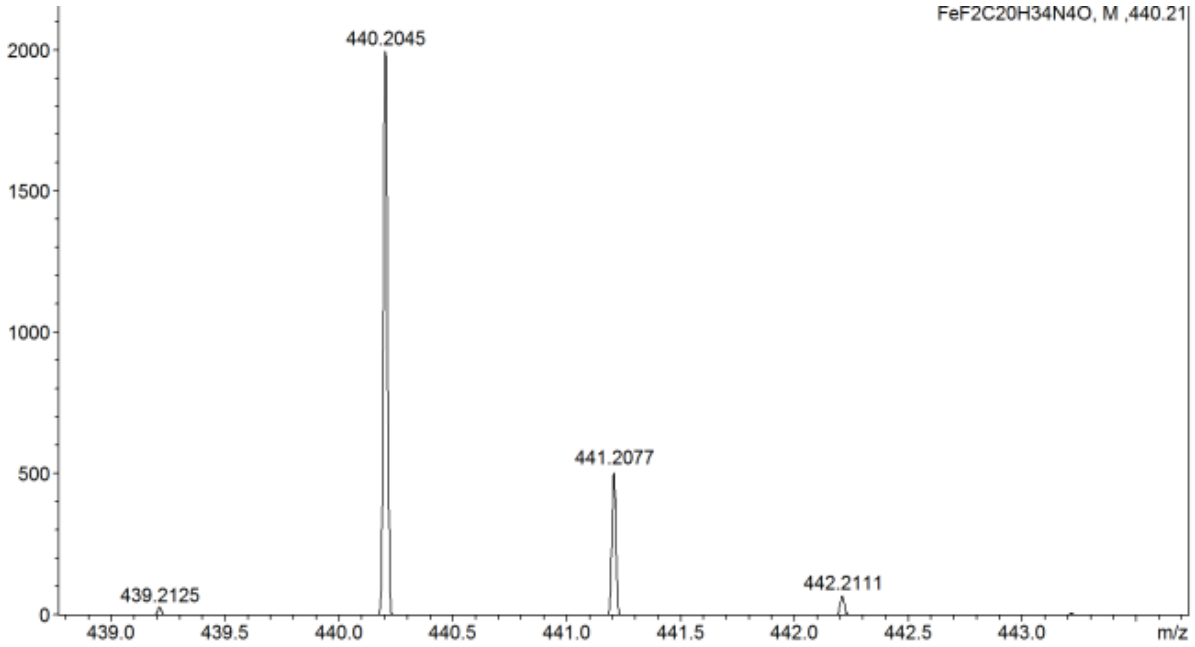
FeF2C20H34N4O, M ,440.21
440.2045
441.2077
439.2125
442.2111
2000
1500
1000
500
0
439.0
439.5
440.0
440.5
441.0
441.5
442.0
442.5
443.0
m/z

Figure S16 View of the structure of $\mathbf{L^1}\cdot HNO_3$ showing the atom numbering scheme. H atoms are omitted for clarity. Ellipsoids are drawn at the 50% probability level.

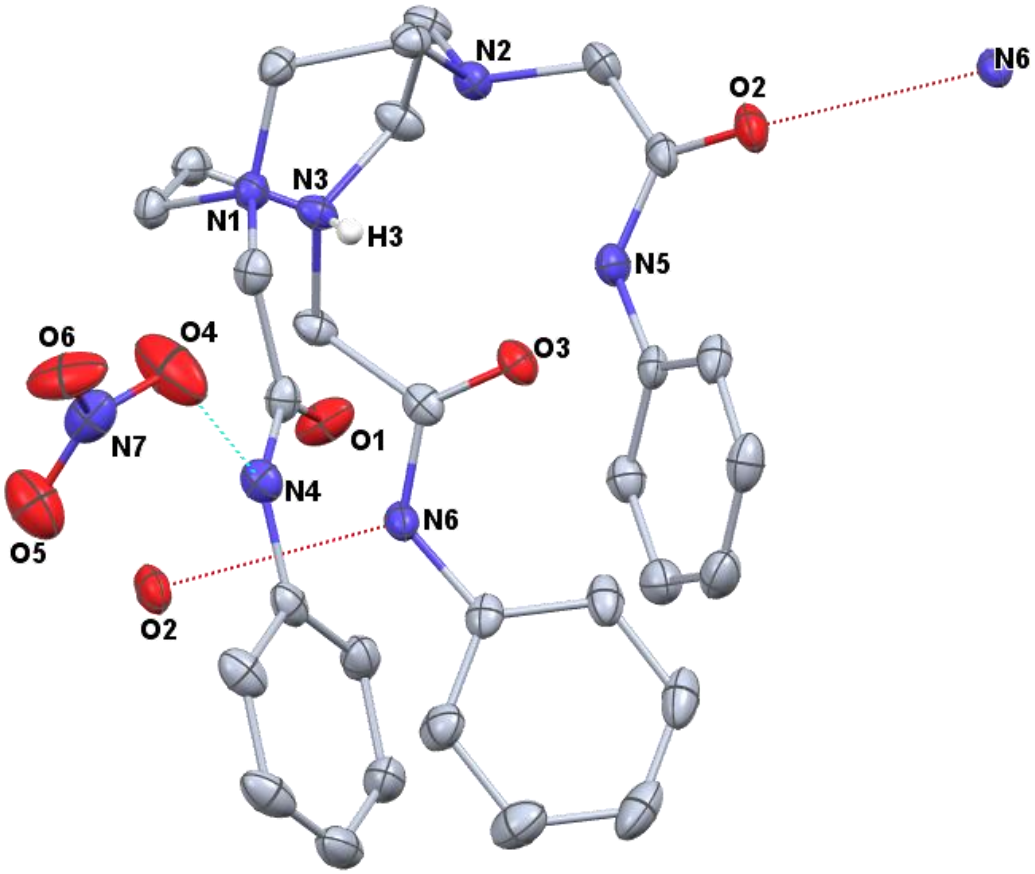

X-ray crystallography

Crystals of $\mathbf{L^1}\cdot HCl$, $\mathbf{L^1}\cdot HNO_3$, $[GaF_3(\mathbf{L^1})]\cdot 1.5MeOH\cdot 0.5H_2O$, $[InF_3(\mathbf{L^2})]$, $[GaF_3(\mathbf{L^3})]$ and $[FeF_3(\mathbf{L^3})]$ suitable for single crystal X-ray analysis were grown as described in the experimental methods. Data collections used a Rigaku AFC12 goniometer equipped with an enhanced sensitivity (HG) Saturn724+ detector mounted at the window of an FR-E+ SuperBright molybdenum (λ = 0.71073 Å) rotating anode generator with HF Varimax optics (100 µm focus) with the crystal held at 100 K, or a Rigaku UG2 goniometer equipped with a Rigaku hybrid pixel array detector (Hypix 6000 HE detector) mounted at the window of an FR-E+ SuperBright molybdenum (λ = 0.71073 Å) rotating anode generator with Arc)Sec VHF Varimax confocal mirrors (70 µm focus), with the crystal held at 100 K. Structure solution and refinement were performed using SHELX(T/S/L)97, SHELX2013, SHELX-2014/7 *via* Olex[i] or using nosphereA2[ii,iii] (for $\mathbf{L^1}\cdot HCl$, $[InF_3(\mathbf{L^2})]$, $[GaF_3(\mathbf{L^3})]$ and $[FeF_3(\mathbf{L^3})]$). Structure solution and refinement was mostly

routine, except for some disorder as follows: the structure of $\mathbf{L^1}\cdot HNO_3$ showed disorder in the NO_3^- anion, which was modelled satisfactorily with split atom occupancies. The structure of $[GaF_3(\mathbf{L^1})]\cdot MeOH\cdot 0.5H_2O$ is modulated and has disorder in two of the arms (modelled 50:50). In one part there is a lattice MeOH and H_2O bonding to the NH. One ^{i}Pr group in $[InF_3[\mathbf{L^2}]]$ is disordered; this was modelled with split atom occupancies. A solvent mask was used in the refinement of the structures of $[GaF_3(\mathbf{L^3})]$ and $[FeF_3(\mathbf{L^3})]$ and were consistent with there being 1.2 and 2.4 molecules of disordered H_2O solvent molecules per unit cell, respectively. Details are provided in the relevant cif files. The crystallographic parameters are given in Table S1 below.

Table S1 X-ray crystallographic parameters[a]

Complex	**L¹**·HCl	**L¹**·HNO_3	[GaF_3(**L¹**)] ·1.5MeOH·0.5H_2O	[InF_3(**L²**)]	[FeF_3(**L³**)]	[GaF_3(**L³**)]
Formula	$C_{30}H_{37}ClN_6O_3$	$C_{30}H_{37}N_7O_6$	$C_{30}H_{36}F_3GaN_6O_3$ ·1.5CH_4O·0.5H_2O	$C_{24}H_{48}F_3InN_6O_3$	$C_{20}H_{34}F_3FeN_4O_1$	$C_{20}H_{34}F_3GaN_4O$· 0.067H_2O
M	565.12	591.66	712.45	640.50	459.36	474.489
Crystal system	Monoclinic	Monoclinic	Monoclinic	Trigonal	Trigonal	Trigonal
Space group (no.)	$P2_1/c$ (14)	$P2_1/n$ (14)	$P2_1/n$ (14)	R3c (161)	R-3 (148)	R-3 (148)
a /Å	12.8300(3)	20.4918(5)	17.0116(5)	14.2596(2)	33.7472(5)	33.4699(7)
b /Å	23.5152(6)	14.3084(2)	12.0324(3)	14.2596(2)	33.7472(5)	33.4699(7)
c /Å	9.6411(2)	20.9037(5)	17.3324(6)	26.9863(5)	10.2893(2)	10.3165(2)
α /°	90	90	90	90	90	90
β /°	99.705(2)	107.779(3)	115.495(4)	90	90	90
γ /°	90	90	90	120	120	120
U /Å³	2867.09(12)	5836.3(2)	3202.3(2)	4752.13(13)	10148.3(4)	10008.6(4)
Z	4	8	4	6	18	18
μ(Mo-K_α) /mm^{-1}	0.176	0.096	0.927	0.796	0.711	1.280
F(000)	1201	2512	1490	2001	4383.6	4484.66
Total no. reflns	33643	65442	31373	50509	147068	31588
R_{int}	0.029	0.037	0.039	0.035	0.052	0.020
Unique reflns	8740	15028	8240	2726	5824	6970
No. of params, restraints	694, 651	820, 6	593, 92	115, 65	568, 1209	568, 6970
GOF	0.985	1.016	1.056	1.032	1.103	1.011
R_1, wR_2 [I > 2σ(I)][b]	0.038, 0.088	0.053, 0.108	0.053, 0.127	0.035, 0.094	0.028, 0.057	0.014, 0.026
R_1, wR_2 (all data)	0.057, 0.095	0.078, 0.118	0.086, 0.147	0.037, 0.096	0.037, 0.061	0.017, 0.027

[a] common items: T = 100 K; wavelength (Mo-K_α) = 0.71073 Å; θ(max) = 27.5°;

[b] $R_1 = \Sigma||F_o| - |F_c||/\Sigma|F_o|$; $wR_2 = [\Sigma w(F_o^2 - F_c^2)^2 / \Sigma wF_o^4]^{1/2}$

Radiofluorination procedure:

In a typical experiment, [GaF_3(**L**^{1})] (1–2 mg, 1.5–3 µmol. mL^{-1}) was dissolved in MeOH (0.75 mL). To this, an aqueous solution of cyclotron target water containing [^{18}F]F^- (0.25 mL, 50–200 MBq) was added. Samples were either maintained at 25 °C or heated to various temperatures up to 80 °C, for 10 – 60 mins, prior to analysis by radio-HPLC and UV-HPLC. The product peak was identified by direct comparison of the retention time (R_t) of the radiotrace and UV trace in the crude sample, to the R_t of the analytical UV-HPLC trace of the reference standard (0.1 mg [Ga$^{19}F_3$(**L**^{1})] in 100 µL MeOH and 900 µL H_2O). The % radiochemical yield (RCY) [Ga$^{18}FF_2$(**L**^{1})] was assessed by taking a ratio of the integrals of the peaks associated with [^{18}F]F^- against the peak from the radioproduct.

SPE purification protocol:

The crude reaction mixture (1 mL) was diluted with 9 mL of water and loaded onto an HLB (hydrophobic-lipophilic-balance) solid phase extraction (SPE) cartridge (Waters, P/N 186000132). This was washed with water (30 mL) to remove [^{18}F]F^-, and then the product was eluted from the cartridge with ethanol (2 mL). The eluted portion was split into two 1 mL fractions and diluted with (i) water to result in a formulated product in 90:10 H_2O/EtOH or (ii) PBS to result in a formulated product in 90:10 PBS/EtOH.

HPLC analysis:

The formulated products were analysed by HPLC at t = 0 and various time intervals up to 2 h. Purified samples were analysed on an Agilent 1290 HPLC system with an Agilent 1260 DAD UV detector (G4212B) and a Bioscan FC3200 sodium iodide PMT with a rate meter. Dionex Chromeleon 6.8 Chromatography data recording software was used to integrate the peak areas.

Analytical HPLC method for radiofluorination experiments:

Column: Agilent Zorbax 1.8 µm CB-C18 4.6 x 50 mm. Mobile phase **A** = 90% H_2O + 10% MeOH; **B** = 100% MeOH; **C** = 100% H_2O. Flow rate 1 mL min^{-1}. Gradient:

Time (mins)	% A	% B	% C
0	0	0	100
1.5	50	0	50
2	100	0	0
10	0	100	0
10.5	0	100	0
11	50	0	50
12	0	0	100
13	0	0	100

The crude products formed in the radiofluorination experiments were analysed on an Agilent 1260 Infinity II HPLC system with an Agilent 1260 DAD UV detector (G7111B) and a LabLogic Systems Ltd sodium iodide 1" PMT. LabLogic Laura radiochromatography data collection and analysis software was used to integrate the peak areas.

Figure S17 Analytical HPLC traces from stability tests of [GaF_3(**L**^{1})]

S17a Analytical UV-HPLC trace of [GaF_3(**L**^{1})] reference standard analysed on Agilent 1260 HPLC system

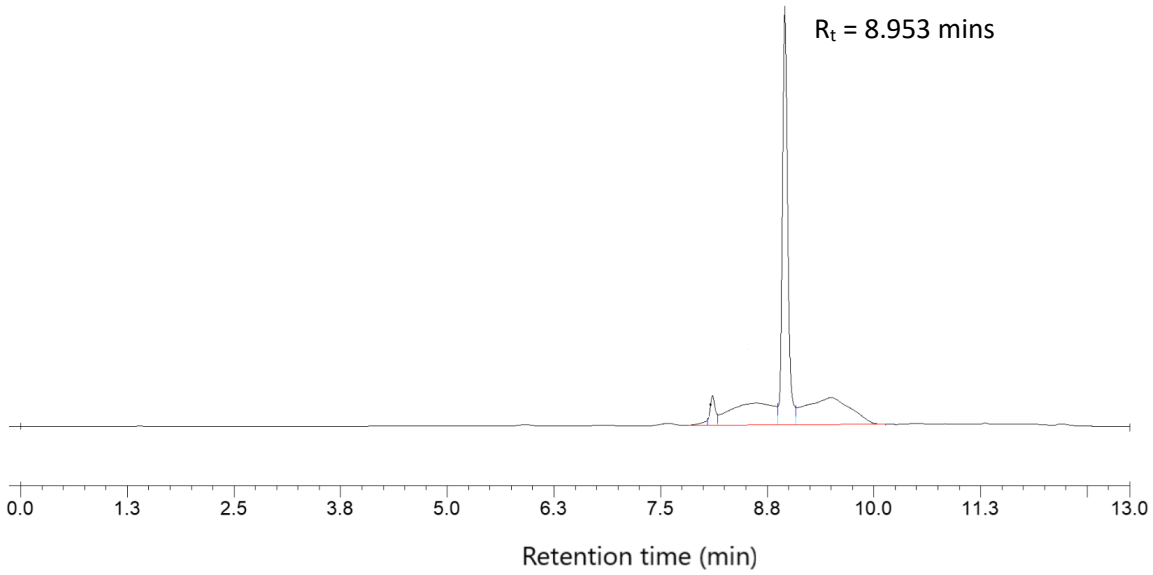

S17b Analytical UV- (top) and radio- (bottom) HPLC traces of crude [$Ga^{18}FF_2$(**L**^{1})] prior to SPE purification

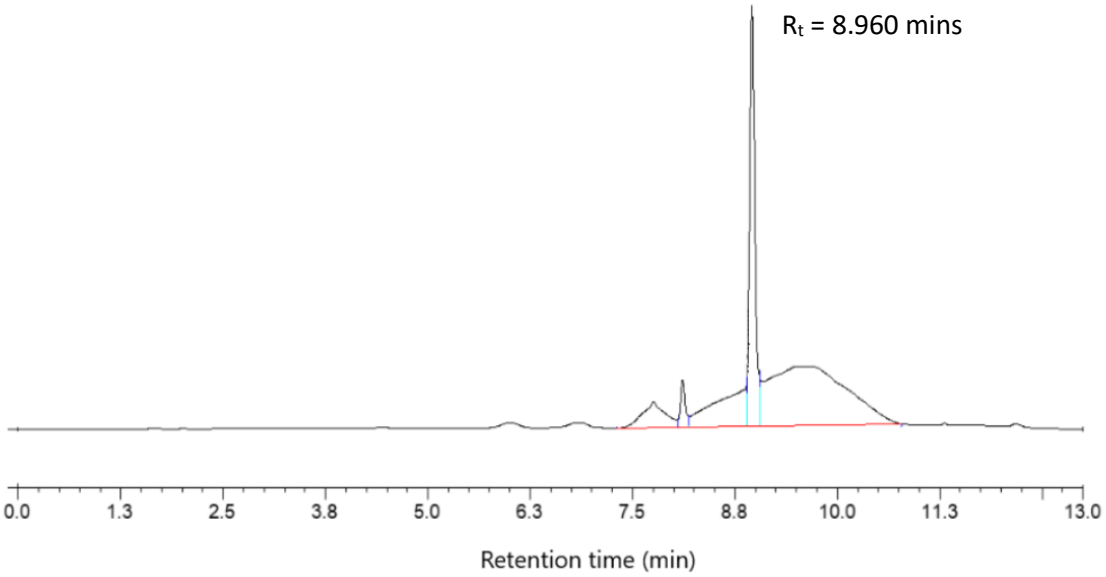

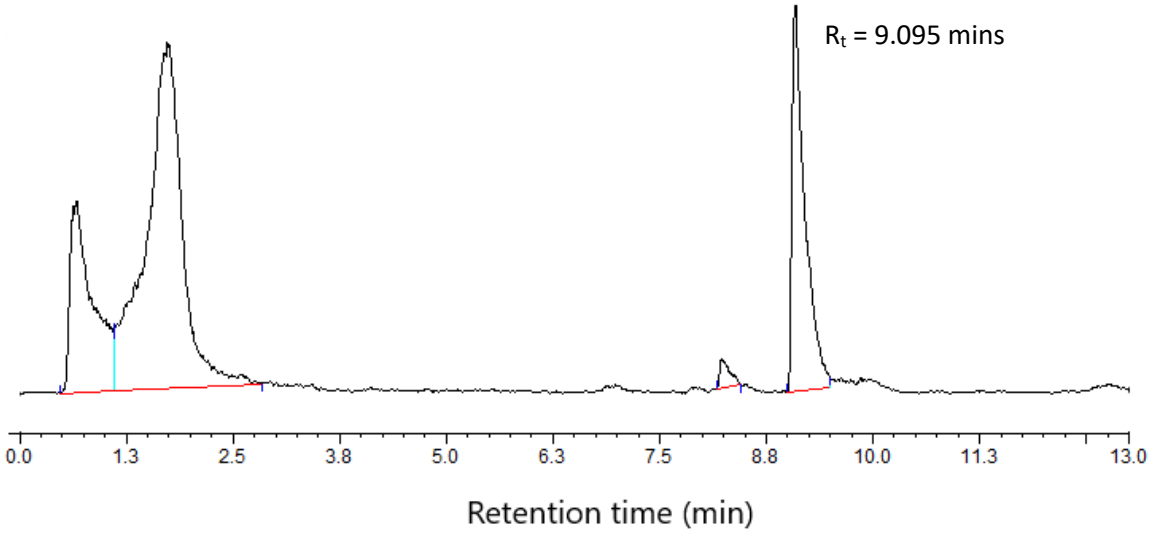

S17c Analytical radio-HPLC trace of [$Ga^{18}FF_2$(**L**^{1})] at t = 0 min. in 10:90 EtOH:H_2O

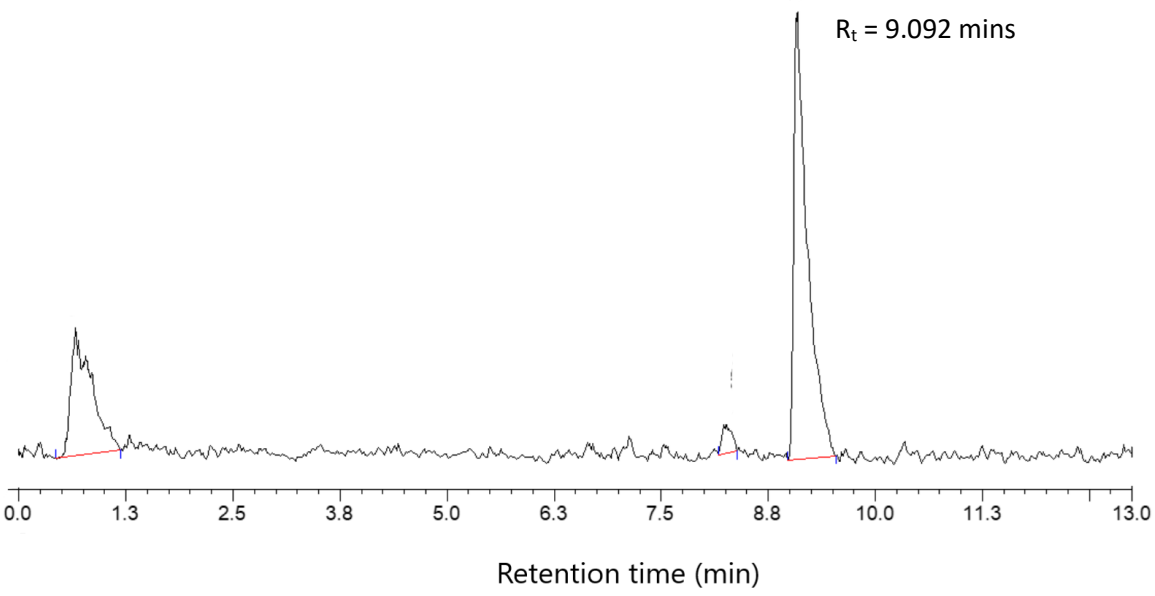

S17d Analytical radio-HPLC trace of [$Ga^{18}FF_2$(**L**^{1})] at t = 30 min. in 10:90 EtOH:H_2O

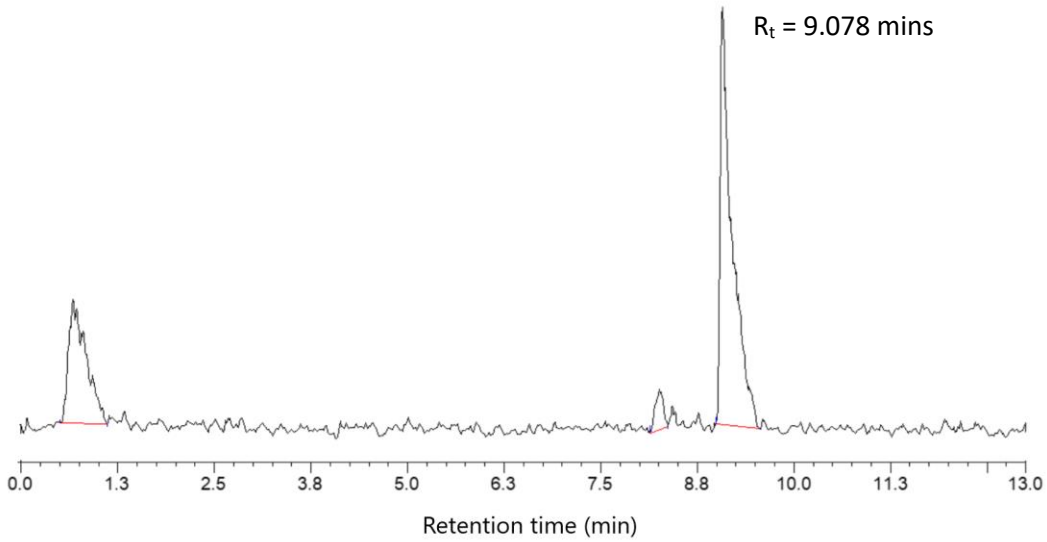

S17e Analytical radio-HPLC trace of [$Ga^{18}FF_2$(**L**^{1})] at t = 80 min. in 10:90 EtOH:H_2O

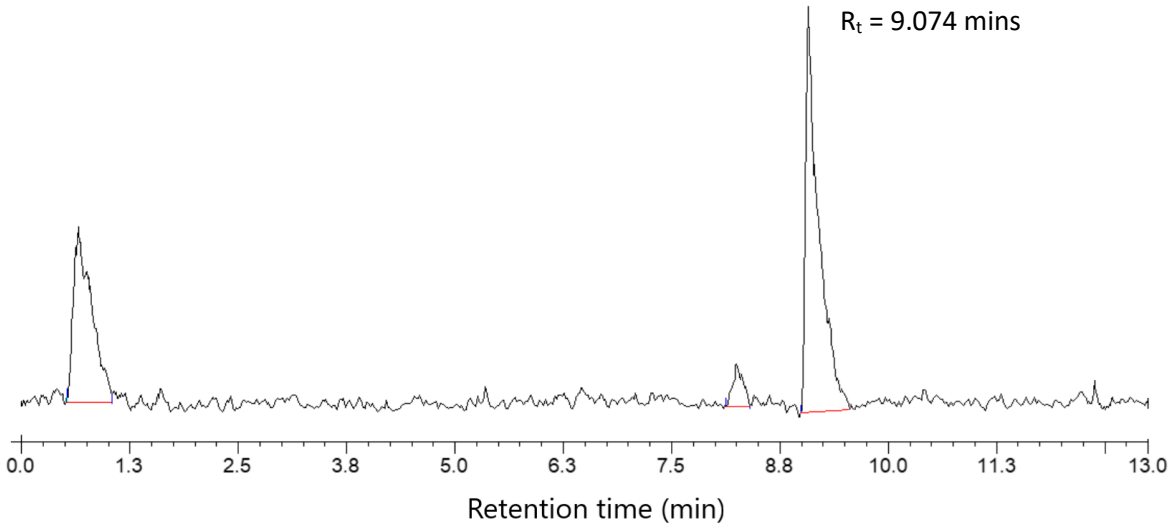

S17f Analytical radio-HPLC trace of [$Ga^{18}FF_2$(**L**^{1})] at t = 120 min. in 10:90 EtOH:H_2O

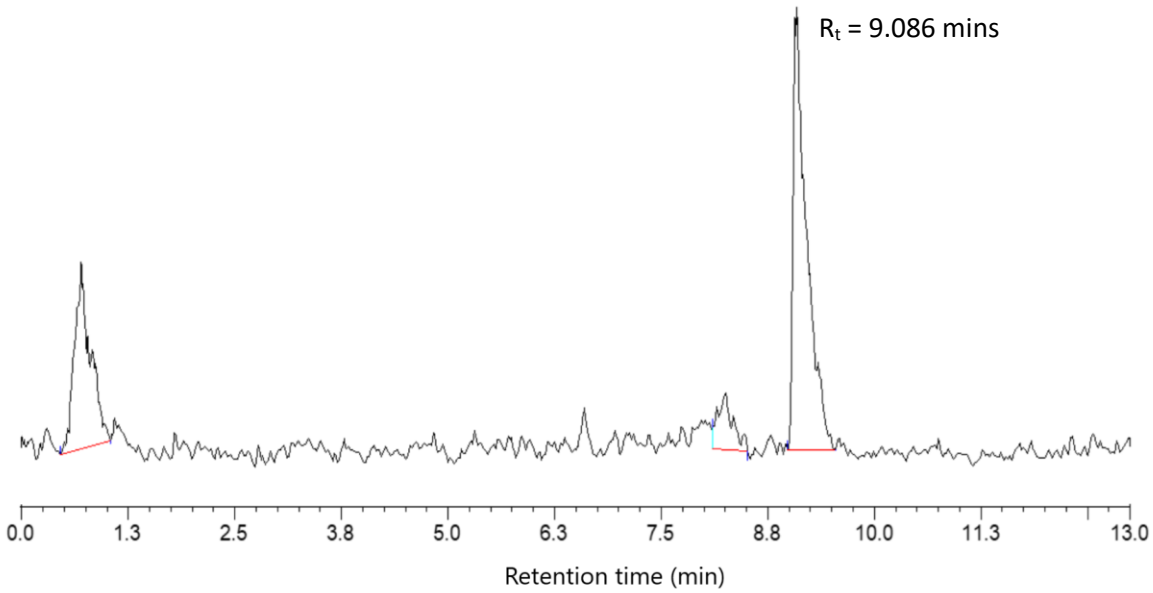

S17g Analytical radio-HPLC trace of [$Ga^{18}FF_2$(**L**^{1})] at t = 0 min. in 10:90 EtOH:PBS

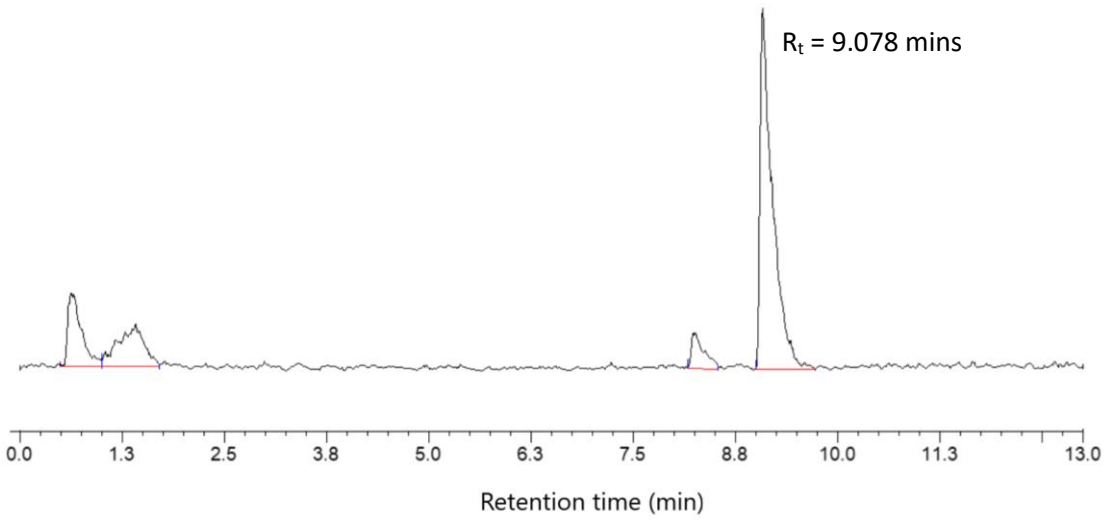

S17h Analytical radio-HPLC trace of [$Ga^{18}FF_2$(**L**^{1})] at t = 30 min. in 10:90 EtOH:PBS

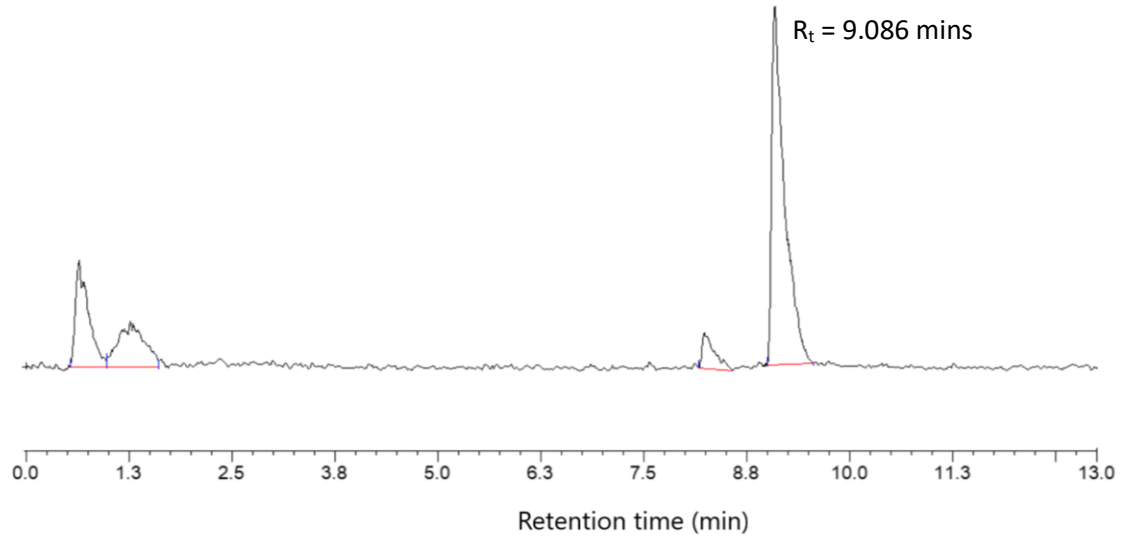

S17i Analytical radio-HPLC trace of [$Ga^{18}FF_2$(**L**^{1})] at t = 80 min. in 10:90 EtOH:PBS

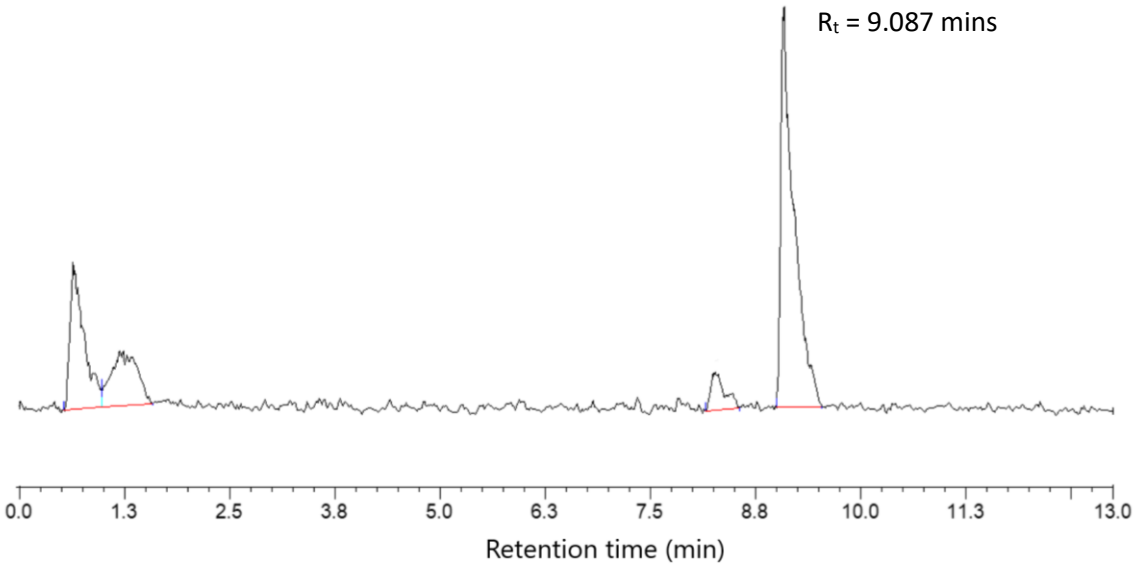

S17j Analytical radio-HPLC trace of [$Ga^{18}FF_2$(**L**^{1})] at t = 120 min. in 10:90 EtOH:PBS

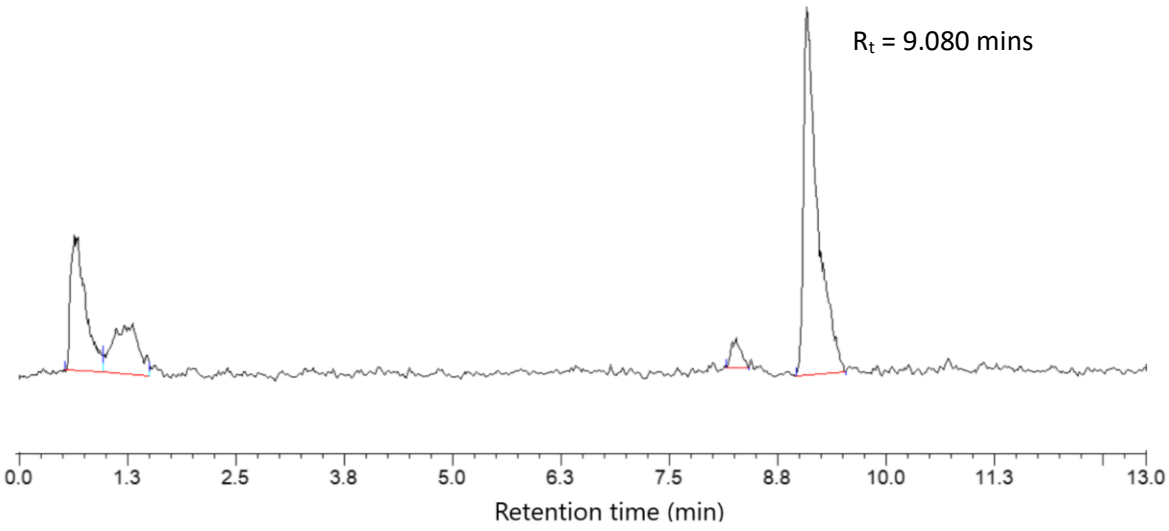

[i]. (a) G. M. Sheldrick, *Acta Crystallogr., Sect. C: Struct. Chem*., 2015, **71**, 3; (b) G. M. Sheldrick, *Acta Crystallogr., Sect. A: Found. Crystallogr.,* 2008, **64**, 112; (c) O. V. Dolomanov, L. J. Bourhis, R. J. Gildea, J. A. L. How J. A. L. Howard and H. Puschmann, *J. Appl. Crystallogr.,* 2009, **42**, 339.

[ii]. F. Kleemiss, O. V. Dolomanov, M. Bodensteiner, N. Peyerimhoff, L. Midgley, L. J. Bourhis, A. Genoni, L. A. Malaspina, D. Jayatilaka, J. L. Spencer, F. White, B. Grundkotter-Stock, S. Steinhauer, D. Lentz, H. Puschmann and S. Grabowsky. ***Chem. Sci.***, 2021,**12**, 1675.

[iii]. L. Midgely, L. J. Bourhis, O. V. Dolomanov, S. Grabowsky, F. Kleemiss, H. Pushmann and N. Peyerimhoff, *Acta Crystallogr.,* 2021, **A77**, 519.